DOCTOR OF PHILOSOPHY

Stabilised silicate and borate solutions for foliar agricultural sprays

Rixon, Tom

Award date:
2020

Awarding institution:
Bangor University

DOCTOR OF PHILOSOPHY

Stabilised silicate and borate solutions for foliar agricultural sprays

Rixon, Tom

Award date:
2020

Stabilised silicate and borate solutions for foliar agricultural sprays

A thesis submitted for the degree of Doctor of Philosophy

PRIFYSGOL
BANGOR
UNIVERSITY

Prifysgol Bangor • Bangor University

April 2020

By

Thomas Andrew Rixon

Abstract

This thesis describes the synthesis and characterisation of seven organic tetraalkylammonium hydroxide salts potentially capable of inhibiting the polycondensation of bioactive silicic acid. The preparation of the hydroxide salts $[Me_3NCH_2CH(OH)CH_2OH][OH]$ (**TAA(1)**), $[Et_2MeNCH_2CH(OH)CH_2OH][OH]$ (**TAA(2)**), $[Et_3NCH_2CH(OH)CH_2OH][OH]$ (**TAA(3)**), $[Me_2(CH_2CH_2OH)NCH_2CH(OH)CH_2OH][OH]$ (**TAA(4)**), $[Et_2(CH_2CH_2OH)NCH_2CH(OH)CH_2OH][OH]$ (**TAA(5)**), $[Me_3N(CH_2CH(OH)(OCH_2CH_2)_nOCH_2CH(OH)CH_2NMe_3][OH]_2$ (**TAA(6)**), $Me_2(CH_2CH(OH)CH_2OH)N(CH_2)_2N(CH_2CH(OH)CH_2OH)Me_2][OH]_2$ (**TAA(7)**), is reported, together with stability trials of some acidified formulations containing these salts and silicic acid. **TAA(1)** was used in formulations for controlled glasshouse pot trials of crops including potato, wheat, cabbage and tomato to test the efficacy of silicic acid formulations on plant growth. The cabbage and wheat trial results report small improvements in foliar yield (up to a 30% improvement in dry weight of stem and leaf produce in cabbage; up to a 47% improvement in wheat), while the potato and tomato results report negligible or no improvements. Assays were carried out on leaf digests of the wheat and cabbage produce to determine silicon uptake by AAS, and a small increase in Si concentration (10-25% for cabbage; 23-45% for wheat) was reported on the leaves sprayed with silicic acid prototypes.

The synthesis and characterisation of a number of novel polyoxidoborate compounds containing organic amines was also reported, due to the similarity of the cations to those used in the formulations. All of these compounds contain 6-membered B_3O_3 boroxole rings within their structures. A total of twenty-eight new non-metal cation polyborate salts are reported; of which 18 of these contain the pentaborate anion, $[B_5O_6(OH)_4]^{--}$, and one contains the tetraborate

dianion, $[B_4O_5(OH)_4]^{2-}$. The crystal structures of seventeen salts containing these polyborate anions are reported: $[Me_3N(CH_2)_2NMe_3][B_4O_5(OH)_4]\cdot 2H_2O\cdot 2B(OH)_3$ (**1a**), $[Me_3NCH_2CH_2NMe_3][B_5O_6(OH)_4]_2$ (**1b**), $[Me_3N(CH_2)_3NMe_3][B_5O_6(OH)_4]_2\cdot 0.5H_2O$ (**2a**), $[Me_3NCH_2CH{=}CH_2][B_5O_6(OH)_4]$ (**2b**), $[CH_3(C_3H_3N_2)(CH_2)_6(C_3H_3N_2)CH_3][B_5O_6(OH)_4]_2$ (**3a**), $[C_2H_5(C_3H_3N_2)(CH_2)_6(C_3H_3N_2)C_2H_5][B_5O_6(OH)_4]_2$ (**4a**), $[CH_3(C_3H_3N_2)CH_2(C_6H_4)CH_2(C_3H_3N_2)CH_3][B_5O_6(OH)_4]_2$ (**5a**), $[CH_3(C_4H_8N)(CH_2)_6(C_4H_8N)CH_3][B_5O_6(OH)_4]_2$ (**6a** and **6b**) (two polymorphs), $[C_2H_5(C_4H_8N)(CH_2)_6(C_4H_8N)C_2H_5][B_5O_6(OH)_4]_2$ (**7a**), $[C_4H_9(C_4H_8N)(CH_2)_6(C_4H_8N)C_4H_9][B_5O_6(OH)_4]_2\cdot 4B(OH)_3$ (**8a**), $[C_3H_5(C_4H_8N)(CH_2)_6(C_4H_8N)C_3H_5][B_5O_6(OH)_4]_2$ (**9a),** $[MeNHC(NH_2)NH_2]$ $[B_5O_6(OH)_4]\cdot H_2O$ (**18a**), $[Me_2NC(NH_2)NH_2][B_5O_6(OH)_4]$ (**19a**), $[Me_2NC(NHMe)N(Me)_2]$ $[B_5O_6(OH)_4]\cdot B(OH)_3$ (**20a**), $[NH_2NHC(NH_2)NH_2][B_5O_6(OH)_4]$ (**21a**), and $[C_7H_{14}N_3][B_5O_6(OH)_4]$ (**22a**). All of these compounds were characterized using spectroscopic (FTIR, multi-element NMR) and analytical (elemental analysis and thermal analysis) techniques. In the solid state, all of the reported polyborate salts form giant H-bonded anionic lattices. In some cases, cation-anion H-bonding interactions are displayed in the structures. The tetraborate (**1a**) requires two 'spacer' molecules of boric acid and water to fully incorporate the dication into the vacancies within the lattice. Of the pentaborate products, the "herringbone" and "brickwall" structures were particular prevalent in accommodating bulkier dications. Of the reported pentaborate salts, the anionic lattice in $[C_4H_9(C_4H_8N)(CH_2)_6(C_4H_8N)C_4H_9][B_5O_6(OH)_4]_2$ (**8a**) was particularly interesting, containing the unique "α,α,β,β" configuration, featuring two C(8) β-chains, with each anionic unit forming hydrogen-bonding interactions with two adjacent molecules of boric acid.

Acknowledgements

I would firstly like to offer my sincerest gratitude to my PhD supervisor, Professor Mike Beckett for his continued guidance and support not only through the duration of the project but also through my entire undergraduate studies as my personal tutor. I am extremely grateful for the opportunity you provided for me in this studentship and your continued contributions throughout my time within the department. I wish you an enjoyable, relaxing and healthy retirement after a few turbulent years.

I would also like to thank my co-supervisor, Dr. Juma'a Al-Dulayymi for his assistance in my first year of study and for helping to get this project up and running. Thanks also must be given to my research committee, Dr. Leigh Jones and Prof. Bela Paizs, who have since left the department, for their constructive feedback and guidance. I wish you the best of luck in your new ventures.

My sincerest thanks must also be extended to my company supervisor, Mr. Simon Fox, Director and Founder of Emerald Research Ltd., as well as Dr. Owen Jones, for sponsoring this KESS II funded project, as well as WEFO for providing the funding for the studentship. I would also like to thank Dr. David Shaw, Sarvari Research Trust, for his consultancy and for organising the potato trial with me, and Henfaes Research Station, Abergwygregyn, for providing some facilities. I would also like to thank the staff at the National Plant Phonemics Centre, IBERS, Aberystwyth, for carrying out the Hydroponic tomato trials; in particular Prof. John Doonan, Dr. Fiona Corke, and Mr. Alan Gay for their invaluable contributions and advice regarding these field trials.

I would also like to extend my thanks to all of the SNS technical staff for their endless assistance throughout the project. In particular, Mr Nicholas Welsby, Mr Gwynfor Davies, Mr Glynne Evans and Mr. Denis Williams for their kind support within the Chemistry family, and Mrs. Helen

Simpson, SNS for her guidance during my crop trials, as well as Ms. Sarah Chesworth, ECW for her assistance with TXRF analysis. In addition, I would like to thank Dr. Peter Horton (National Crystallographic Service, Southampton) for obtaining and refining the crystallographic data for my polyborate structures. I would also like to thank the undergraduate project students of the Beckett group over the previous three years for their contributions and helping me to broaden my knowledge in some areas of the project.

Thank you to all of the administrative staff, in particular Miss Siobhan Jones, Mrs. Tracey Roberts, and Mrs. Caroline Randall for all of their help and for putting up with my regular visits to the general office in the 'good old days'!

Thanks also to the "501 society" for keeping me sane and helping to weather the storm, namely Mr. Chester Blackburn, Mr. Kenny Chan, Mr. David Mondragon, Mr. James Cooper, Mr. Richard Froom, Dr. Mohammed Altahan, and Dr Mohammed Hussein Al-Mashhadani; as well as Dr. Paddy Murphy and Mr. Jamie Tibble for their entertaining lunchtime ramblings, and for the constructive discussions about our projects. I must also thank Dr. Lorrie Murphy and Dr. Andrew Davies for their pastoral support and advice during the project. I wish the best of luck to the rest of the Chemistry Family, who have either already moved on to new ventures or will be doing so in the near future.

Finally, I would like to thank my family for believing in me, encouraging me, and especially for putting up with me during the write-up period. Your love and support gives me the energy I needed to finish this project.

Contents

List of Figures

List of Tables

List of Schemes

List of Graphs

Chapter 1: Introduction

1.1: General Introduction

The primary concern of this thesis is to successfully prepare and characterize water-based formulations containing high levels of soluble biologically active silicon, with the intention to use them as foliar micronutrient sprays to improve the growth, development and yield of a number of agricultural crops. As silicon naturally tends to polymerise into non-biologically active moieties, it is essential that the silicon present in a spray is stable in a bioactive form, using structure-directing organic molecules that are non-toxic and do not interfere with plant metabolism.

This introduction will include a review of silicon and boron in the natural environment, and their importance to the agricultural sector, with a particular focus on water-soluble bioactive silicon. It will also explain the various analytical techniques utilized to identify the speciation and composition of any silicates present in both formulations and in digests of mature plant material. There will also be a focus on the principles of NMR spectroscopy of boron and silicon-containing species due to its high analytical importance in each synthetic chapter.

Chapter two of this thesis will be focusing on the development of some products containing stabilized bioactive silicon as a micronutrient source for both foliar sprays and as soil fertilisers. Additional nutrients such as fulvic acid, and micronutrients such as boric acid will also be explored and incorporated into formulations for their potential synergistic properties. The chapter will then explain the development of some new structure-directing molecules to be used in agriculture, and the preparation of working formulations to be used in a farming environment. The formulations will then be subjected to stability trials to identify a potential shelf-life.

The third chapter of the thesis investigates a number of practical applications for the formulations in agriculture. It will contain a literature review of completed agricultural trials making use of stabilized soluble silicon as a micronutrient. A series of crop trials carried out using the prepared formulations in glasshouses on a number of different common agricultural plant varieties will be investigated. Crop yields, observations on quality of produce, and the chemical content of organic matter will be studied.

A secondary focus of this thesis regards the preparation of a series of novel polyborate products. This expands previous work carried out by the Beckett group on polyborates templated by non-metal cations. The cations investigated are mostly organic spacer linked bis(quaternary ammonium) (2+) cations, with some additional studies on bulkier bis(imidazolium) (2+) cations and bis(pyrrolidinium) (2+) cations. A short series of *N*-methylated guanidinium cations were also studied. These compounds were characterized using NMR spectroscopy, FTIR spectroscopy and single crystal X-ray diffraction. Thermal degradation studies of these compounds will also be presented in chapter four.

The final chapter of this thesis will summarise the experimental procedures utilized, and present the experimental data for each product.

1.2: Silicon

1.2.1: Elemental Silicon and its discovery

Silicon is the second most abundant element in the Earth's crust after oxygen, with which it has a high bonding affinity. Silicon has been used in tools, glass and building materials for centuries. However, silicon was first isolated and characterised in a sufficiently pure elemental form in 1823 by Swedish chemist Jöns Jakob Berzelius.[1] This was achieved by heating potassium metal in the presence of silicon tetrafluoride, and washing away any impurities such as potassium silicide, leaving silicon as a pure amorphous solid. Prior to this discovery, a number of attempts were made to isolate elemental silicon from silica by electrolysis. Numerous other allotropes of pure silicon have since been isolated, with Henri Étienne Sainte-Claire Deville successfully isolating the common crystalline allotrope of elemental silicon in 1854.[2] This process was achieved serendipitously by electrolysing a mixture of sodium chloride and aluminium chloride, in an attempt to isolate elemental aluminium metal from the mixture.

Amorphous elemental silicon is now commonly prepared by heating silicon dioxide (sand) in the presence of carbon, in an electrical furnace, to temperatures exceeding 2,000 ^{o}C. The amorphous allotrope has been used in solar cells due to its semiconducting properties. It can be deposited as a thin film onto a number of substrates including plastics and glass. It is an environmentally friendly alternative to systems using cadmium or lead, which are considered dangerous to the environment, but is less efficient. Amorphous silicon cells have lost some relevance over recent years, as crystalline silicon cells are more efficient,[3,4] while some novel metal alloys as well as organic materials are currently seeing the most development.

To obtain a crystalline form of elemental silicon, a seed crystal is introduced to the molten silicon during the steady-cooling process. Cooling causes the crystal to grow in size and encourage further crystallisation of the molten silicon. Further modifications can then be made to the growing crystal to obtain the desired shape.[5,6] The difference between amorphous and crystalline silicon is that an amorphous allotrope has a highly disordered supramolecular structure with no uniformity. Crystalline silicon forms an organised structure with few deformities that can enhance a number of the properties found in the amorphous allotrope.

Elemental silicon has extremely high melting and boiling points (1,414 ^{o}C and 3,265 ^{o}C respectively). These values are only exceeded by elemental boron among the metalloid and non-metal elements. As the temperature requirements are so high to form elemental silicon from silica and carbon, it is extremely rare to find in the Earth's crust, despite the high natural abundance of silicon-containing minerals.

In 1907, Henry Noel Potter successfully reduced SiO_2 to SiO by reducing the silicon dioxide in the presence of carbon in an electric furnace.[7] This work expanded on a previous study by Clemens Winkler in 1890,[8] which used a similar principle without success. The conventional combustion furnaces of that era were not hot enough to isolate the monoxide form, which required temperatures exceeding 1,700 ^{o}C. This was the first recorded instance of a reaction involving both silicon and carbon, and the basis for the complete reduction of SiO_2 to elemental Si using the high temperature electrical furnaces according to **Scheme 1.1**:

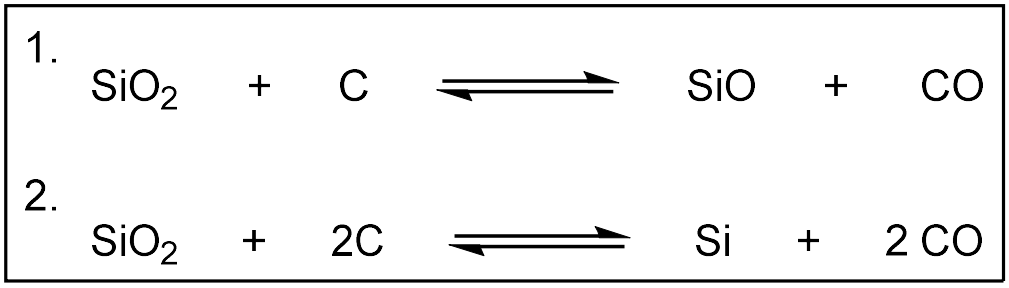

Scheme 1.1: SiO (1) and elemental Si (2) are both isolated at high temperature in the presence of pure carbon.

Isolating the crystalline elemental form of silicon is essential for its use in electronic devices; a major industrial application for the element in the late 20th and early 21st century.[9] Silicon is a unique element in that it exhibits semiconducting properties, but is also commercially available due to its high natural abundance. The semiconducting properties make it able to conduct electricity under certain conditions, but it can become a capable insulator when those conditions are changed. Crystalline silicon can be doped with other materials to modify its conducting properties.[10,11]

1.2.2: Silicate minerals

Most of the Earth's naturally occurring silicon resources are either found as metal silicates or as silicon dioxide (silica) polymers, as part of mineral rocks or sand.[12] These forms are extremely robust and are generally used as construction materials due to their extreme thermal stability, high abundance, and the lack of need to chemically process them from their raw materials. Naturally occurring metal silicates form large polymeric systems, consisting of $[SiO_4]^{4-}$ tetrahedral repeat units, wherein the Si atom sits inside each tetrahedron, and the O atoms occupy the each of the four vertices of the tetrahedron. An example repeat unit is shown in **Figure 1.1**. In the majority of cases, the O vertexes are shared with adjacent repeat units. This is known as an oxygen bridge.

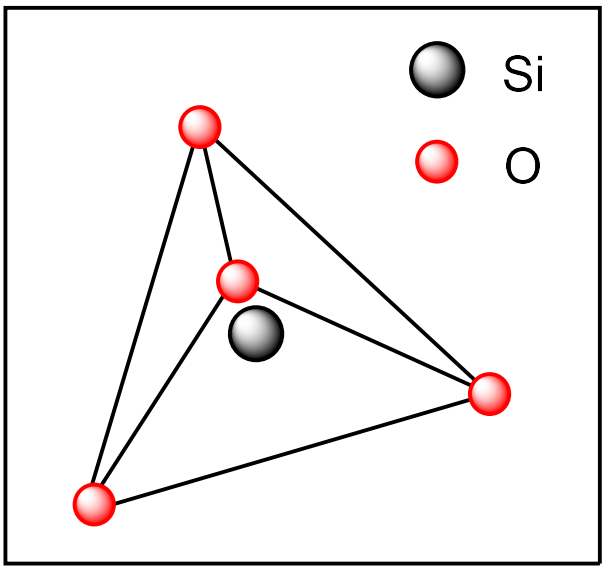

Figure 1.1: Primary structure found within naturally occurring silicate minerals.

In order to counterbalance the strong negative charge of each SiO_4 tetrahedra, interstitial metal cations are present in the structure. In some structures, a small proportion of the silicon atoms can be replaced by metals such as aluminium.[13,14] Although aluminium is normally trivalent, it still sits in the hole between the four oxygen bridging atoms as an AlO_4^{5-} tetrahedron, and therefore requires a further 1+ cation to balance the charge. Metal cations often sit in vacant spaces between the tetrahedral units, which contributes to an overall neutral molecule. Natural silicate minerals are classified into seven key groups, presented in **Table 1.1**.

Table 1.1 The seven main categories of naturally occurring silicate minerals including schematic examples.[15]

Classification	Extended Structure	Chemical Formula	Mineral Examples	Schematic Example
Nesosilicate	Isolated Tetrahedra	$[SiO_4]^{4-}$	Olivine, $MgFeSiO_4$	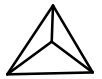
Sorosilicate	Tetrahedral Dimer	$[Si_2O_7]^{6-}$	Epidote, $Ca_2(Al_2,Fe)(SiO_4)(Si_2O_7)O(OH)$	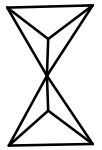
Cyclosilicates	Ring systems	$[Si_nO_{3n}]^{2n-}$	Tourmaline series: Beryl, $Be_3Al_2Si_6O_{18}$.	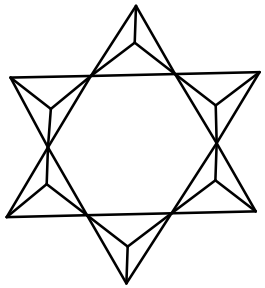
Inosilicates	Single chains	$[Si_nO_{3n}]^{2n-}$	Pyroxene series: Orthopyroxenes, $(Mg,Fe)SiO_3$ Clinopyroxenes, $Ca(Mg,Fe)Si_2O_6$	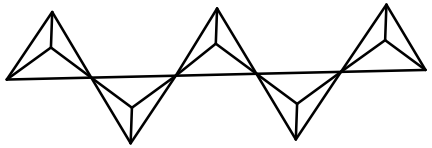

Table 1.1 (continued):

Classification	Extended Structure	Chemical Formula	Mineral Examples	Schematic Example
Inosilicates	Parallel double-chains	$[Si_{4n}O_{11n}]^{6n-}$	Amphibole group Tremolite - Ferroactinolite series, $Ca_2(Mg,Fe)_5Si_8O_{22}(OH)_2$	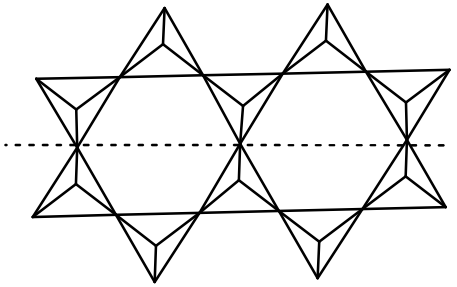
Phyllosilicates	Layered Sheets	$[Si_{2n}O_{5n}]^{2n-}$	Micas and Clays Including biotite, $K(Mg,Fe)_3(AlSi_3)O_{10}(OH)_2$	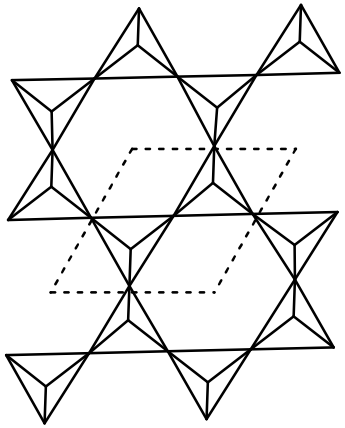
Tectosilicates	Complex 3D Networks	$[Al_xSi_yO_{(2x+2y)}]^{x-}$	Quartz, feldspars, zeolites	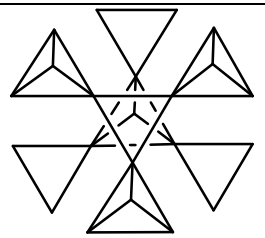

Polymeric quartz minerals are among the most abundant, consisting of extensive SiO_2 networks with no templating metal. Quartz is the main constituent of common sand, and is extremely insoluble in water (*ca.* 6 ppm is the saturation point).[16] As it usually forms large crystals, only the outermost layer has any likelihood of dissolving in water. All crystalline species are found to have similarly low solubility in untreated water. Amorphous silica and hardened silica gels have slightly higher solubilities, but still require alkaline solution (> pH 9) to dissolve in larger quantities.[17] Some silica species can be defined as bioactive, but these smaller silica particles are amorphous in nature. They are only defined as bioactive on the grounds that they can pass through a membrane filter; which would reasonably model the uptake through a cell membrane in natural applications.[16] These SiO_2 species are completely surrounded by a shell of Si-OH bonds, making them susceptible to hydrogen bonding interactions.

1.2.3: Silicate Glasses

Silica can be processed in a hot furnace to form amorphous quartz-based glasses.[18] Most glasses contain additional metal oxides, which alter their properties. The composition of the glass can affect its rate of thermal expansion, as well as its resistance to high temperatures and thermal conductivity. Borosilicate glasses, designed to withstand high temperatures, can also be produced by addition of B_2O_3 to the molten mixture.[19] These glasses have a much lower coefficient of thermal expansion than the traditional soda lime glass used in windows. Aluminosilicate glasses are also common,[18] and contain approximately 10-25% Al_2O_3. Aluminosilicate glass is used for fibreglass and is more resistant to erosion and long term weathering.

1.2.4: Silicon in solution

Silicon can also occur in solution in some cases. Sodium metasilicate (Na_2SiO_3), also known as waterglass, is water-soluble.[18] Waterglass is produced by reacting silica with a hot solution of sodium hydroxide according to **Scheme 1.2:**

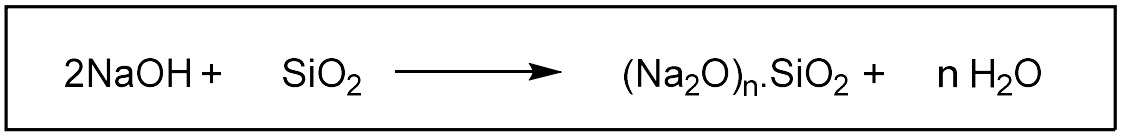

Scheme 1.2: Synthesis of a waterglass solution.

Waterglass is highly soluble and forms alkaline solutions when dissolved. These sodium silicates remain stable in both neutral and alkaline solutions. When dissolved in acidic solutions, or in the presence of elevated levels of metal salts, the silicate ions react with dissociated protons in solution to form silicic acids, which will be discussed in further detail later in this thesis.

1.2.5: Colloidal silicon and suspensions

Colloidal solutions of silicon are also possible. A colloidal solution occurs when an insoluble or partially insoluble particles remain homogeneously suspended in solution.[20] This differs from an insoluble precipitate that prefers to accumulate either on the meniscus or at the bottom of a solvent. Colloidal silica particles are amorphous and usually spherical in shape, and they tend to form when alkali silicates such as waterglass are partially neutralised to a less alkaline state. These are known as silica sols. If the pH of the solution drops below neutral, the sols will begin to harden and eventually form silica gels.

Colloidal silicon suspensions have a number of applications, and disperse through solutions in a similar manner to silica nanoparticles. The particle size can be controlled by adjusting the concentration of the suspension. Silicon dioxide is widely regarded safe for human consumption due to its biological inertness. Therefore, it is largely used in the pharmaceutical industry in the production of tablets, due to its ability to redissolve to soluble silicic acid from its powdered form when exposed to stomach acid. It can also improve the flow of powders that adsorb to it.

1.2.6: Silicic Acid

Silicic acid, $Si(OH)_4$ is a weak acid with a pKa of 9.47 at a concentration of 0.6 mol L^{-1}, and can donate a further proton with a second pKa of 12.65. It can form when sparingly soluble solid silica is placed in water according to **Scheme 1.3**.[21,22]

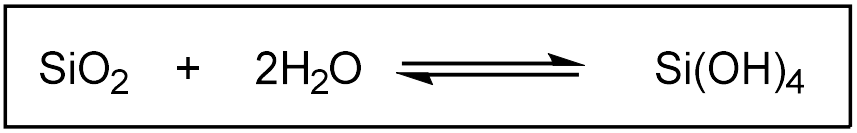

Scheme 1.3: Silicic acid forms in equilibrium from silica in solution. The equilibrium strongly favours SiO_2, therefore silicic acid only exists at very low concentrations in these conditions.

Silicic acid can be produced in larger quantities by acidifying an alkaline silicate solution (i.e. waterglass). In a proton-rich acidic environment, the metal cations are stripped from the silicate and replaced by protons, to form silicic acid in solution with a metal salt (**Scheme 1.4)**.

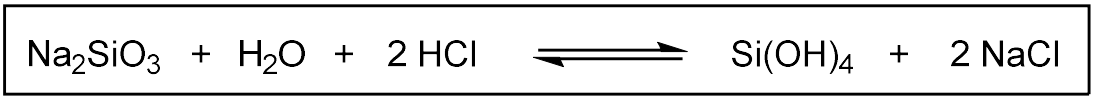

Scheme 1.4: Silicic acid formation in acidic conditions.[23]

In this acidic state, silicic acid readily polymerises *via* polycondensation mechanisms.[22,24,25] The resulting oligomers continue to polymerise and cross-link, resulting in large polymers. These polymers are the beginnings of the formation of silica gel, which eventually hardens. In our oceans, this condensation polymerisation/ hydrolysis process between monosilicic acid and silica oligomers is in equilibrium. This equilibrium favours polycondensation when the concentration of silicic acid exceeds 2 mM.[26] This means that supersaturated solutions of silicic acid are not possible in standard conditions. Silicic acid cannot be isolated as a solid or crystalline product.

1.2.7: Small silica molecules and the formation of polymeric silica

While silicic acid remains stable at low concentration in solution, exceeding the solubility limit of amorphous silica causes the polycondensation processes to begin. Initially, monomers react to form dimers,[27] releasing a molecule of H_2O, and polymerise further into cyclic species. The cyclic species continue to grow into larger particles. These oligomeric particles serve as a nucleating sites for further polymerisation and causes aggregates to form stable particles. These eventually coalesce to form a gel.[28] The process of polymerisation favours the formation of as many Si-O-Si bonds as possible, therefore there is a rapid formation of cyclic silica species from silicic acid. The formation of cyclic systems preferentially attracts further monomers of silicic acid to bind to them, to form oligomeric species.

As the silicic acid concentration begins to decrease towards the limit of saturation, the smaller silica oligomers redissolve into solution, reforming silicic acid. The newly formed silicic acid then redeposits onto larger silica particles. This process is called Ostwald Ripening.[29,30] Eventually, the particles reach the size of amorphous silica and begin to exhibit an overall negative charge. This causes repulsion between the silica particles. To counterbalance the newly formed negative charge, positive ions provided by metal salts in the solution are collected to form an overall neutral molecule. This prevents the repulsion of the negatively charged molecules - encouraging further polymerisation - and the eventual formation of extensive networks (MW >100,000) that harden to form silica gel.

By providing positively charged, sterically hindering organic cations to a solution of silicic acid, the polymerisation process may be inhibited.[26,31–37] While metal cations would sit within the lattice and facilitate further growth of the molecule, the use of a bulky non-metal cation would provide a sterically hindering barrier that prevents agglomeration and expansion of these silicate networks. This would result in a stable solution containing silicic acid and/or small oligomeric species, and would prevent the formation of silica gels.[38] These species would be small enough in diameter to remain soluble for an extended shelf-life, and may be small enough to pass through a membrane to enter cells as a micronutrient.

1.3: Analysis and characterisation of silicon – based species

Analysis of silicon-containing compounds can be carried out in a similar way to traditional organics. Analytical methods tend to fall either into qualitative methods, which identify the type of silicon speciation present in the sample, or quantitative methods that identify how much silicon is present with no regard to the bonding environment or chemistry **(Table 1.2).**

Table 1.2: A summary of some analytical techniques for silicon-based materials.

Analytical Method	**Aspect Studied**	**Quantitative?**	**Qualitative?**
Atomic Absorption Spectroscopy	Silicon concentration in liquid samples	Yes	No
Inductively coupled plasma – optical emission spectroscopy (ICP-OES)	Multi-element concentration in liquid samples	Yes	No
Inductively coupled plasma – mass spectrometry (ICP-MS)	Multi-element concentration in liquid samples based on mass of ionised elements.	Yes	No
Nuclear Magnetic Resonance (NMR) Spectrocopy	Structure based on the bonding environments for individual silicon nuclei	Yes, with isotopically enriched samples. (>95%)	Yes

Table 1.2 (continued):

Analytical Method	**Aspect Studied**	**Quantitative?**	**Qualitative?**
Fourier Transform Infrared Spectrocopy (FTIR)	Types of bonding between silicon and adjacent atoms based on vibrations	No	Yes
UV-Visible Spectrophotometry	Concentration of silicon in solution.	Yes	No
X-Ray Fluorescence	Concentration of silicon in finely ground powdered solids.	Yes	No

1.3.1: Atomic Absorption Spectrocopy[39]

Atomic absorption spectroscopy (AAS), is carried out on liquid samples containing dissolved silicon.[40,41] A small volume of dilute sample is drawn from the sample and atomised in a flame, and the subsequent atomisation causes a colour change to the flame. In order to get a reliable quantitative result, a monochromatic lamp is used as a light-source. These are unique to each element tested,[42] as the method can only be used to determine one element at a time. The absorption of light at a specific wavelength is observed, and used to calculate the concentration of silicon, based on the Beer-Lambert Law **(Equation 1.1)**.

Equation 1.1: $$A = \varepsilon C \ell$$

This law dictates that absorbance of light is directly proportional to the concentration of the absorbing species when light is passed through a liquid sample of path length ℓ. The size of the absorbance gradient relative to concentration is unique to the species. This is expressed as the molar extinction coefficient. This coefficient is unique to a certain wavelength of light, and can be obtained experimentally. To find this constant experimentally, a calibration curve

is constructed to cover at least half of the working range of the device (0.003-4 ppm for silicon). AAS can be used to determine the concentration of one of over 70 different elements in solution.

1.3.2: Inductively coupled plasma – optical emission spectroscopy (ICP-OES)[39]

In a similar process to AAS, liquid samples containing silicon can be injected into a superheated plasma, of temperatures exceeding 8,000 ^{o}C. At this temperature, all elements become thermally excited and emit light at a wavelength unique to the element. This means that a sample containing multiple elements can be injected into the plasma and multiple elemental concentrations can be determined simultaneously,[43–45] provided there are no competing elements that cause interference with each other. The emitted light is collected by the spectrophotometer, and passed through a diffraction grating to separate the different wavelengths. This produces a spectrum that can be individually quantified by spectral intensities. Similarly to AAS, approximately 70 different elements can be tested, however they can be tested simultaneously. The limit of detection is approximately 0.5 ppm but the working range is considered larger than that of an AAS.

1.3.3: Inductively coupled plasma – mass spectrometry (ICP-MS)[46]

ICP-MS uses the same plasma to heat liquid samples to their excitation state. Another characteristic of the plasma heat source is that it is ionised. This encourages the ionisation of the analyte species upon injection into the plasma. These ionised molecules are then introduced to a mass analyser, and separated based on their mass-to-charge ratio. It is then possible to determine the concentration of individual masses based on the frequency of “hits” for each recorded mass.

ICP-MS is extremely sensitive, and has a limit of detection in the parts per billion for numerous elements. However, the significant drawback to ICP-MS is that most small silicate species can suffer from interference from small organic molecules, and this raises the limit of detection to a few parts per million. ICP-MS is rarely used in complex biological samples, but is more commonly used in measuring isotopic ratios in silicon-rich samples.[47]

1.3.4 : Nuclear Magnetic Resonance (NMR)[48]

Silicon-containing compounds can be identified in some cases by nmr spectroscopy. Si can occur as numerous isotopes, but only three isotopes are stable and won't undergo spontaneous radioactive decay in "normal" timescales **(Table 1.3)**. In order to be NMR-active, an element must have at least one isotope that is spin-active. Spin active isotopes contain odd numbers of protons and/or neutrons. This spin is essential for the atoms to align themselves when exposed to a magnet in the spectrometer when undergoing NMR spectroscopy.

Table 1.3 Naturally occurring silicon isotopes

Isotope	Spin	Relative abundance / %
^{28}Si	0	92.2
^{29}Si	½ +	4.69
^{30}Si	0	3.09

Of the naturally available silicon isotopes, ^{29}Si is the only NMR-active isotope available. It has a relative abundance of less than 5%. It is possible to obtain samples of SiO_2 that are isotopically enriched.[34,49–51] Often, isotopes are separated using gas centrifugation of SiF_4. The rare isotopes are separated from the ^{28}Si and then reduced to form polycrystalline Si, which can be processed further into other compounds. It is also possible to separate isotopes by magnetic mass separation or ion exchange. As these processes are complicated and not readily available, isotopically enriched silicon is extremely expensive to obtain. This means that using NMR spectroscopy as a method of quantifying silicon in solution can be very expensive. It is therefore preferable to use NMR spectroscopy as a qualitative analysis to identify the speciation of silicon in a sample and use a different method to determine the concentration.[51–56] It is common to analyse silicate speciation both in the solid state and in solution using NMR spectroscopy.

Depending on the spin number, atoms can orientate themselves numerous ways in a magnetic field. If a nucleus has a spin of I, it will have $(2I + 1)$ possibilities in which it can orientate itself in the magnetic field. A ^{29}Si nucleus has a spin of $I = + ½$. Therefore, it has two possible orientations; $M_I = + ½$ and $-½$. These orientations or spin states exhibit different energy levels when exposed to a magnetic field. The majority of nuclei will typically inhabit

the lower energy level as the Boltzmann distribution dictates, and upon exposure to the magnetic field jump to the higher energy level state. In the case of silicon, this results in a change of +1 to its spin state, as it passes from $M_I = – ½$ *to* $M_I = + ½$.

The energy difference between these spin states is a function of the magnetic field strength used in the spectrometer, B_0, and the gyromagnetic ratio of the nucleus, γ, which is a unique value to the nucleus tested. Different elements have different gyromagnetic ratios, and therefore would all react differently to the same magnetic field. It is therefore required to tune the radio frequency of the magnet to sufficiently excite the nucleus studied.

When a sample is loaded into the magnet, it is exposed to rapid pulses of radio waves, exciting the nuclei to their higher energy excited state. Between pulses, the nuclei are allowed to revert back to the lower energy level, releasing energy. This period is called the relaxation time, and certain nuclei may require longer relaxation times than others. This significantly varies the duration of NMR spectroscopy experiments between different nuclei. The process of allowing this relaxation is known as the free induction decay (FID). Many FID cycles are repeated and added together.[57]

More pulses result in a higher signal to noise ratio and a more reliable spectrum. This occurs at the cost of lengthening the time of the experiment. In a sample that isn't oversaturated with analyte, the signal to noise ratio is doubled when the number of scans is increased fourfold. This means that a spectrum obtained on $n = 2^5$ scans will have double the signal to noise ratio of a spectrum obtained on $n = 2^3$ scans. As the number of scans reaches a high amount, it becomes difficult to clean the signal to noise ratio any further without drastically

raising the experiment time, particularly when the relaxation time between pulses is long. A full scan cycle can range from milliseconds to several seconds, with the full duration of the experiment known as the acquisition time (t_{aq}), which can vary dramatically between the nuclei tested.

Resultant signals from a typical NMR spectrum are expressed as chemical shifts. These are resonant frequencies that occur relative to internally calibrated standard molecules. The standards are set at $\delta = 0$, and nuclei within the analyte molecules will resonate at slightly different frequencies to the standards. The elements studied in this thesis, ^{1}H, ^{13}C and ^{29}Si are all referenced to tetramethylsilane (TMS), the signals from which are not present in any output spectrum. A fourth element, ^{11}B is also studied, and referenced against boron trifluoride diethyl etherate, $BF_3{\cdot}OEt_2$. NMR spectroscopy of any compound typically results in either an upfield (negative), or downfield (positive) chemical shift. This shift is expressed with the units part per million (ppm). In our experiments, all ^{1}H signals occur between +0 and +10 ppm, and all ^{13}C signals occur between +0 and + 200 ppm, ^{29}Si signals occur at -60 to -120 ppm, and ^{11}B signals between +19 and -1 ppm.

1.3.5: Q^n notation of silicon environments and their chemical shifts

The different bonding environments of each silicon atom can be differentiated based on the number of adjacent Si-O-Si bridges (up to a maximum of 4 per atom).[15] "Q^0" denotes a silicon atom that is not bridged to any further silicon atoms through oxygen atoms. "Q^1" denotes a silicon bridged to one additional silicon atom *via* oxygen. Q^1 silicon is often dominant in small dimeric silicate species, or at the terminus of a short chain of oligomeric silica. "Q^2" silicon is bonded to 2 additional silicon atoms *via* oxygen atoms, and is often present in the middle of

long chains or as part of a cyclic structure. "Q^3" and "Q^4" silicon atoms are bonded to 3 and 4 additional silicon atoms *via* oxygen bridges respectively, and are dominant in polymeric species, where Q^3 silicon is present at the surface of a mineral, and Q^4 represents the bulk of the mineral's structure. Each type of silicon environment in this series will display different chemical shift in ^{29}Si NMR spectra, due to the different bonding environments. The signal shifts upfield approximately 10 ppm for Q^n as n increases from 0 to 4.

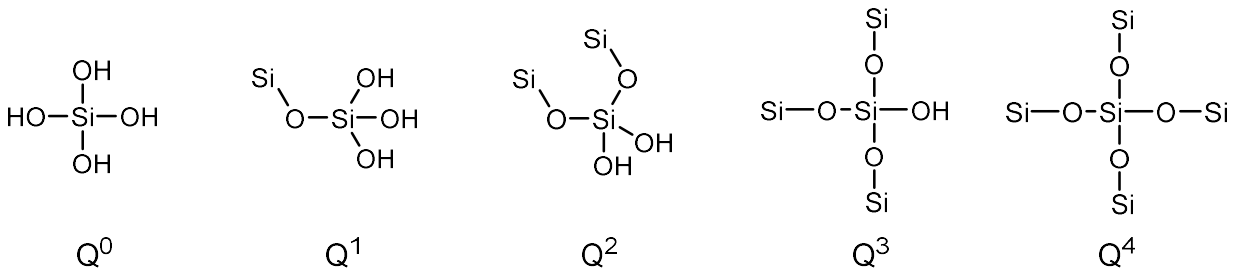

Figure 1.2 The Q_n series of silicon environments in silicates

Pure $Si(OH)_4$ contains 100 % Q^0 silicon, and can be easily identified with a single peak in ^{29}Si NMR at approximately –67 ppm in a spectra ran in D_2O referenced to TMS at 0 ppm. Unfortunately, ^{29}Si NMR is an impractical method of quantifying the distribution of silicon species in a dilute solution, as the natural abundance of the only NMR active stable isotope (Si-29) is under 5%. Si-29 enriched samples are extremely expensive to obtain and do not represent a cost-effective method of analysis. This issue is amplified further by the presence of background noise caused by the quartz or borosilicate glass NMR tubes Q^4 region of the spectra.

1.3.6: Analysis of soluble small silicate species

Many small molecule silicate anions (containing 10 or less Si atoms) have been identified in solutions containing silicates. These small molecules are generally termed as silica oligomers,

and are all defined as water-soluble, due to their ability to pass through a dialysis membrane, unlike colloidal or polymeric silica. As previously stated, the Q^n number has a strong influence on the chemical shift of the silicon atom studied. However, some additional factors such as bonding angles and ring strain can also influence the chemical shifts. In **Table 1.4**,[15] the chemical shifts are presented for a number of small soluble silicate molecules. Silicon atoms are shown by a black dot, while oxygen atoms are omitted, but would be present along the connecting lines.

The quoted chemical shifts were obtained by using isotopically enriched silica (>95% ^{29}Si). Most spectra were obtained using 1.4 M solutions of potassium silicate with a K/Si ratio of 1. Altering the M/Si ratio and the concentration can alter the size ratios of Q^1,Q^2 and Q^3 signals within spectra, due to larger species dominating at higher Si concentrations. Low M/Si ratios tend to be more polymeric in nature. Reducing the M/Si ratio tends to also cause a broadening of signals within the spectra.

Table 1.4 Small silicate species and their chemical shifts[15]

Silicate Species	**Structure[a]**	**Q^n site**	**δ (ppm)[b]**
Monomer		Q^0	-71.3
Dimer		Q^1	-79.81
Linear trimer		Q^1 Q^2	-79.34 -88.22
Cyclic trimer	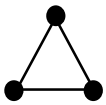	Q^2	-81.43
Linear tetramer	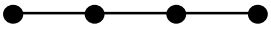	Q^1 Q^2	-79.55[c] -87.47[d]
Cyclic tetramer	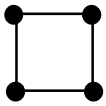	Q^2	-87.29
Monosubstituted cyclic trimer	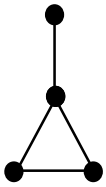	Q^1 Q^2 Q^3	-79.22 -81.08 -89.39[c]
Bridged cyclic tetramer	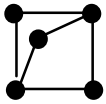	Q^2 Q^3	-85.50 -93.24
Monosubstituted cyclc tetramer	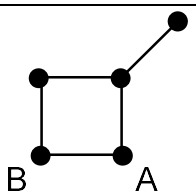	Q^1 Q^2(A) Q^2(B) Q^3	-79.16 -87.06[d] -87.38[c] -95.29

Table 1.4 (continued):

Silicate Species	**Structure[a]**	**Q^n site**	**δ (ppm)[b]**
Bicyclic pentamer	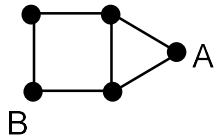	Q^2(A) Q^2(B) Q^3	-81.16 -87.58 -88.41
Prismatic hexamer	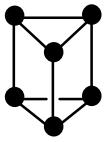	Q^3	-88.38
Tricyclic hexamer 1	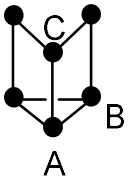	Q^2 Q^3(A) Q^3(B) Q^3(C)	-87.42 -87.94 -88.81 -96.04
Tricyclic hexamer 2a (cisoid)	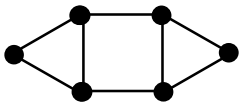	Q^2 Q^3	-81.80 -88.10[c,d]
Tricyclic hexamer 2b (transoid)	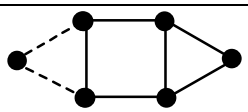	Q^2 Q^3	-82.11 -89.15
Doubly bridged cyclic tetramer	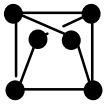	Q^2 Q^3	-85.87 -92.74
Pentacyclic heptamer	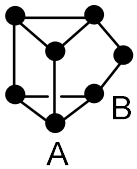	Q^2 Q^3(A) Q^3(B)	-- -90.23 -89.23

Table 1.4 (continued):

Silicate Species	**Structure[a]**	**Q^n site**	**δ (ppm)[b]**
Cubic octamer	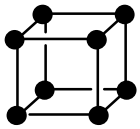	Q^3	-98.61
Hexacyclic octamer	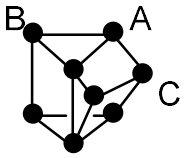	Q^3(A) Q^3(B) Q^3(C)	-89.02 -91.82 -98.01
Prismatic decamer	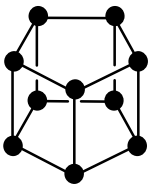	Q^3	-98.45[e]

a Silicon atoms are marked by a black dot, oxygen atoms are not present in the diagrams.

b Values were obtained from 1.4 M potassium silicate solution with a K/Si ratio of 1,[58,59] unless otherwise stated

c Tentative assignment

d Value obtained using 0.63 M potassium silicate solution with a K/Si ratio of 1.5 (G. Engelhardt, D Hoebbel, unpublished work)

e Value was obtained using a 2.5M solution of tetraethylammonium silicate (TEA), with TEA/Si ratio of 1. The Si was 29Si enriched.

There are no Q^4 silicon environments presented in **Table 1.4**. Species containing Q^4 silicon tend to be mixtures of large polymeric networks, thus are hard to isolate as pure samples. These Q^4 groups crosslink in a complicated manner that gives rise to many signals between -100 and -120 ppm in ^{29}Si spectra. This results in a broadening of the signals. This broadening effect is further enhanced by the presence of Q^4 silicon in both the NMR probe and the sample tubes, which contain quartz, making accurate structural assignments for polymeric silica impossible.

1.3.7: Fourier transform infrared spectroscopy (FTIR)[60]

Fourier transform infrared spectroscopy is an analytical tool that can be used to identify functional groups present on either solid, liquid or gaseous analytes. A broad spectrum of infrared radiation is fired through a sample, and the absorbance of the light is measured across every wavelength in the predetermined range of the machine. Absorbance spikes occur at certain wavelengths as a result of vibrating bonds within the molecule. The raw signals are processed using a fourier transform program, drawing up a spectral blueprint that is unique to each compound. FTIR spectroscopy is used primarily to support NMR spectroscopy, and any other analysis that is important for determining the molecular structure of an unknown compound.

In the analysis of silicates, most absorption bands occur between 400 cm^{-1} and 1000 cm^{-1},[54,61] these bands are produced as a result of stretching, bending and rotation of the Si-O bonds in the silica structure. $Si(OH)_4$ has been found to exhibit two key bands; an symmetric Si-O stretch at *ca.* 939 cm^{-1} and a signal referring to the movement of Si-O-H at 1090 cm^{-1}. However, these signals, despite being strong, can be lost within the fingerprint region of organics and other interfering species. FTIR spectroscopy has not been used to identify the speciation of any silicates in this thesis.

1.3.8: UV-Visible spectrophotometry[62]

UV-visible spectrophotometry for silicon is a colorimetric method in which a light source is passed through a solution containing silicon. Shining a light source through a light-active compound causes an excitation of bonding and non-bonding electrons from the highest occupied molecular orbital (HOMO) to the lowest unoccupied molecular orbital (LUMO). The

energy gap between the two levels is different for different molecules, and the wavelength of excitation varies with the size of this band gap. Larger wavelengths excite smaller band gaps. This means that each molecule has a unique λ_{max}. This is the wavelength of light that is absorbed the most. If this point is in the visible region, the analyte solution exhibits a colour. Similarly to absorption spectroscopy, UV-Visible spectrophotometry uses the Beer-Lambert law **(Equation 1.1)**. However, solutions containing silicon do not exhibit and light-absorbing properties that can be quantitatively tested by UV-Vis spectroscopy.

UV-visible spectrophotometry is a quantitative analytical technique that can be used to test the concentration of transition metal complexes, or extensively conjugated molecules, both of which are light-active or absorbing. It is possible to form a yellow heteropoly acid complex of silicon with molybdenum, which can either emit a faint yellow-green colour,[63,64] or a vivid dark blue colour,[65,66] depending on the oxidation state of the metal. The molybdate colourimetric tests will be discussed in further detail in **Chapter 2**.

1.3.9: X-ray fluorescence[67]

X-ray fluorescence is a quantitative analytical method that can be used to calculate the elemental composition of a powdered sample. The procedure is particularly useful in elucidating the elemental composition of dried soils or organic plant material. X-rays are directed into the powder, causing nuclei in the powder to ionise. The energy from the radiation is sufficiently strong to remove electrons from the inner orbitals of the atoms in the sample. This causes the outermost electron to fall into the vacant inner orbital. Energy from this process is released in the form of radiation, hence the “fluorescence”. This emitted radiation has a unique energy level depending on the source element. As each energy level is

unique to each element, Planck's law can be applied to calculate the wavelength of the fluorescence detected using **Equation 1.2**. Where λ = wavelength (m), h is Planck's constant (6.626×10^{-34} J·s), c is the speed of light (3×10^{8} ms^{-1}), and E is energy (J).

Equation 1.2: $$\lambda = \frac{hc}{E}$$

The count-rate of emitted energy from the sample at each wavelength or energy level is detected by the device, and can be used to obtain the concentration levels of several elements simultaneously. Portable X-ray fluorescence has been successfully trialled on ground plant matter containing low levels of silicon.[68] This is achieved by manually constructing a calibration curve of ground cellulose powder containing known amounts of silicon. Calibrants ranged between 0% Si to 10% Si by weight, with a limit of detection stated by the researchers of 0.014% for Si.[69]

The advantage of this procedure is that no digestion or chemical preparation of the plant material is required,[68–70] which is usually required when preparing samples for analysis in solution. Often, digesting plant material containing silicon requires a potent mixture acids including hydrofluoric or perchloric acids, to break down the network of Si-O bonds and form soluble forms of silicon. "Safer" digestion methods, such as in warm HCl are generally less reliable at breaking down any polymeric biogenic silicon in the foliage. It can also provide an alternative to a dry-ashing procedure in a high temperature furnace, which still requires digestion of the ash in warm acid.

While it is possible to quantify silicon content in powders using portable devices,[69] the traditional benchtop TXRF (total X-ray fluorescence), studies powdered samples suspended in tiles containing silicon. This means it is not possible to test for silicon due to interference from the glassware.

1.4: Environmental and biological systems

1.4.1: Silicon

Silicon is only found in trace levels in animals, with the vast majority of ingested silica passing through the digestive system and excreted by herbivorous mammals.[71] It does however have a number of important roles within biology. Silicon is distributed *via* a global Si cycle, in a similar way to the more commonly known carbon or nitrogen cycles.[72–75] The cycle begins by solubilising the silicon present in naturally occurring silicates in mineral rocks. Chemical and physical weathering of these rocks is responsible for the solubilisation of these silicates.[76–80] Physical weathering of silicates is caused by the friction generated by fast moving water or wind, resulting in the breakdown of large rocks to smaller rocks that are more susceptible to chemical weathering. Chemical weathering of silicates occurs when CO_2 from the atmosphere is dissolved in water to form carbonic acid (H_2CO_3) in a dynamic equilibrium.[78,80] Carbonic acid then begins to dissolve the mineral silicates in the Earth's crust to consume the CO_2 to form metal carbonates such as $CaCO_3$, which remain in our oceans.[81]

Soluble silicon most commonly naturally accumulates in volcanic waters, where hydrothermal activity is at its most common. This mostly originates from molten rocks and quartz. Importantly, approximately 80% of the ocean silicon net inputs,[73] originated from rivers

flowing into the ocean, are utilized by aquatic ecosystems. Silicon is an extremely important element to algae in both freshwater and marine habitats.[82] Soluble silicon is biomineralized by many algal species but perhaps the most studied example is the diatom, a phytoplankton which selectively absorbs soluble silicon in the form of monosilicic acid ($Si(OH)_4$). Diatoms are extremely important in the biogeochemical cycle of silicon, as they prevent the oversaturation of silica within our oceans. They generate approximately 40% of all primary produced organic matter within the oceanic environment,[83] making them a key producer on the aquatic food chain.

The reason that silicic acid has been found to be biologically active is that it is the most likely form of silicon able to pass through natural barriers such as cell walls and membranes, and therefore be susceptible to uptake as a nutrient to serve a purpose to the plant. In the case of diatoms, silicon is taken up actively when there is a need for it, by silicon transporter proteins.[84,85] The silicic acid is dimerised during transport *in-vivo*, which encourages further polymerisation to complex oligomers, and eventually accumulates in deposits called frustules.[86,87] Eventually, this bioactive silicon forms a glassy protective shell around the diatom. There are tens of thousands of these species, which take on different shapes and forms. Their dependence on silicon for structural stability is key to all aquatic lifeforms in the food chain. Uptake, transport and biomineralisation of silicon by diatoms has been documented frequently.[88–90] Many siliceous structures have been investigated under the microscope,[91–93] and digested material has been subjected to studies such as Mass Spectrometry and NMR studies to confirm the silicon content.[50,93–95] Uptake and transport processes have also been studied using $Ge(OH)_4$ radiotracers as a replacement to $Si(OH)_4$, due to similar reactivity.[96]

1.4.2: Agricultural applications

While silicon has not been identified as one of the essential elements for plant growth and development by legislation, there have been several studies highlighting its potential applications as a micronutrient.[38,97–100] A micronutrient is defined as an element that is essential for plant or human development, which has a minimum intake level requirement needed to prevent a nutrient deficit.[101] This is not to be confused with macronutrients, which are required in larger quantities for plant survival. In addition to water, carbon dioxide and oxygen, there are at least 14 elements that are required by plants in some capacity to result in improved growth.[102] Essential elements (see **Table 1.5**) are defined as elements that will cause a significant drop-off in plant health and yield if they are not present in the minimum concentration required for the plant to have sufficient uptake of that nutrient.

Due to the very low concentration requirements and potential risk of toxicity due to overabundance of the nutrient, most micronutrient mixtures are applied to the plants in the form of foliar sprays. The contents of these sprays permeate either through the cuticle layer on the top of the leaf, or more rapidly through the stoma on the bottom of the leaf. Foliar sprays require an adjuvant or wetting agent, which raises the permeability of the solution into the cuticle by allowing it to pass through the hydrophobic waxy protective layer **(Figure 1.3).**

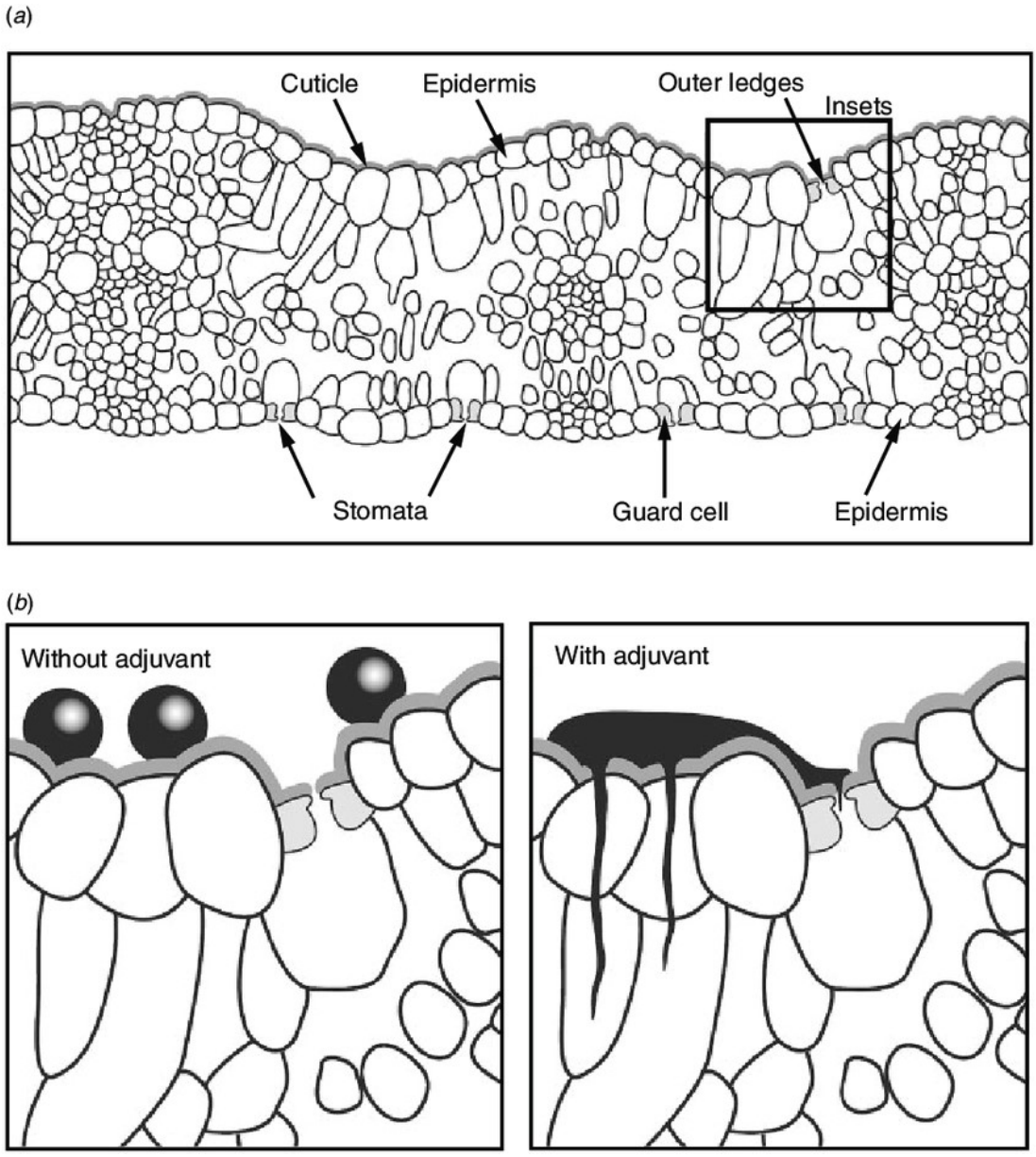

Figure 1.3: Cross section of a leaf on a wheat plant (a), and the uptake of foliar sprays with and without an adjuvant (b).[103]

Unlike micronutrients, macronutrients are usually added directly to the soil in the form of fertilizers. Often some of these elements, such as the heavy metals, could have environmental implications if allowed to build-up to excessive levels in the growth medium, as they could leach into the water table and cause toxicological damage other species.

Table 1.5 The essential elements for plant growth and development.[102,104–109]

Element	Essentiality	Minimum concentration required for healthy leaf (mg g^{-1} DM)	Toxicity limit in leaf (mg g^{-1} DM)
Nitrogen	Essential	15-40	N/A
Potassium	Essential	4-40	> 50
Phosphorous	Essential	2-5	>10
Calcium	Essential	0.5-10	>100
Magnesium	Essential	1.5-35	>15
Sulphur	Essential	1.0-5.0	N/A
Chlorine	Essential	0.1-6.0	4.0-7.0
Boron	Essential	5-100 $x10^{-3}$	0.1-1.0
Iron	Essential	50-150 $x10^{-3}$	>0.5
Manganese	Essential	10-20 $x10^{-3}$	0.2-5.3
Copper	Essential	1-5 $x10^{-3}$	15-30 $x10^{-3}$
Zinc	Essential	15-30 $x10^{-3}$	100-300 $x10^{-3}$
Nickel	Essential	0.1 $x10^{-3}$	20-30 $x10^{-3}$
Molybdenum	Essential	0.01 $x10^{-3}$	1
Sodium	Beneficial	N/A	2.5
Selenium	Beneficial	N/A	10-100 $x10^{-3}$
Cobalt	Beneficial	N/A	10-20 $x10^{-3}$
Silicon	Beneficial	N/A	N/A
Aluminium	Beneficial	N/A	2-5 $x10^{-3}$

From **Table 1.5**, the elements nitrogen, potassium, phosphorous, calcium, magnesium and sulphur are classified as essential macronutrients, while chlorine, boron, iron, manganese,

copper, zinc, nickel and molybdenum are classified as essential micronutrients. The remaining elements have not been classified as essential for plant survival. However, these elements have shown evidence that plant yield is decreased when they are not present at high enough levels. [109] What is particularly interesting in the case of silicon is there is no reported evidence of silicon toxicity as a result of an oversaturation of the element in any of the studies discussed in this thesis, provided the sources of silicon are safe to the plant. It has been found that up to 10% of plant tissue weight can be attributed to silicon in plants that have a higher affinity to silicon.[110]

It has been widely reported that certain plant species have a much higher affinity to silicon than others.[110–112] Particularly, monocot species such as cereal varieties, grains and grasses, as well as arecale species (*e.g.* palms) have a far higher affinity to silicon uptake compared to dicot species, which include tomato, lettuce, cabbage and legumes. It is therefore important to note that the efficacy of silicon-based micronutrients may also vary markedly among different plant species.

While silicon uptake mechanisms from the soil and subsequent transport through the xylem is well-documented,[111,113,114] the mechanism of direct uptake and biomineralisation of silicon through foliage is less clear. A potential clue lies in the synergistic properties between boron and silicic acid. Boron has been found to be strongly responsible for activating cellulose production, and the fibrous monocot grasses and cereals are both richer in cellulose and silicon, it is possible that silicic acid is utilised by the plant in a similar manner. Electron and X-ray microscopy studies on plant material have shown that silica tends to build up in areas where transpiration (nutrient solution flow from roots to shoots) is at its highest, such as the

stoma, vascular systems and in epidermal cells.[69,115,116] This relates strongly to the uptake of silicon through the roots and xylem, where transpiration rates are higher.

1.4.3: The importance of boron

Silicon-based micronutrient sprays tend to work more effectively when partnered with low levels of boron in a water-soluble form such as boric acid or sodium tetraborate (commonly known as borax, $Na_2B_4O_5(OH)_4.8H_2O$).[117–119] It is reported that there is a synergistic effect between silicic acid and boron and that this aids the uptake of silicon into the foliage and results in a markedly better overall yield. It has not been established whether these results are due to the plants being boron-deficient prior to spraying, or whether this synergistic effect is essential to providing the best formulations.

Boron's status as a plant micronutrient was first studied in detail in 1923 by Warington.[120] Notably, unlike many micronutrients, boron is taken up by plants as an uncharged molecule such as boric acid, $B(OH)_3$ rather than as a charged ion. It is known to improve photosynthesis, and is a key activating agent for enzymes responsible for cellulose production. [121,122]

1.5: **Boron**

1.5.1: Elemental boron and its discovery[18]

In comparison to silicon, boron has a low natural abundance. It does not naturally occur in its elemental form on the Earth's crust, but is rarely present in meteorites. While boron-containing materials such as the naturally occurring mineral borax have been used for centuries, it was only first recognized as an element in 1808. Boron can be found in mineral outcroppings, with the majority of the world's supply found in Turkey and California.[18] Naturally occurring boron is often bound to oxygen or silicon, in the form of borates or borosilicates.

It was first isolated by Sir Humphrey Davey, Joseph Louis Gay-Lussac and Louis Jacques Thénard by an electrolysis method.[18] Davey discovered that a brown deposit of boron formed on an electrode when an electric current was passed through a solution containing borates. To confirm the existence of elemental boron, the alternative method of reducing boric acid using potassium metal was explored. Subsequently, Gay-Lussac and Thénard carried out high temperature reductions of boric acid using iron.[18] They also uncovered that boric acid was produced when oxidizing the elemental boron in air, thus completing the cycle. These forms of boron were highly impure, often containing large quantities of carbon. Henri Moissan later successfully isolated elemental boron at >95% purity by reduction of B_2O_3 using magnesium.[18] The first reported synthesis of analytically pure crystalline boron (> 99%) was carried out by reducing boron halides using hydrogen gas in the presence of a hot filament. [123]

Although elemental boron does not spontaneously oxidise into boron oxides at room temperature, it has similar bonding affinity for oxygen as that of silicon. This means that

borates can form large polymeric structures. Boron also shares similarities to carbon in that it prefers to form large covalently bonded structures. The main difference to carbon and silicon is that boron has a formal oxidation state of +3. Therefore, it forms uncharged trigonal planar units. Such bonding is evident in BF_3 (boron trifluouride) and $B(OH)_3$ (boric acid) **(Figure 1.3)**.

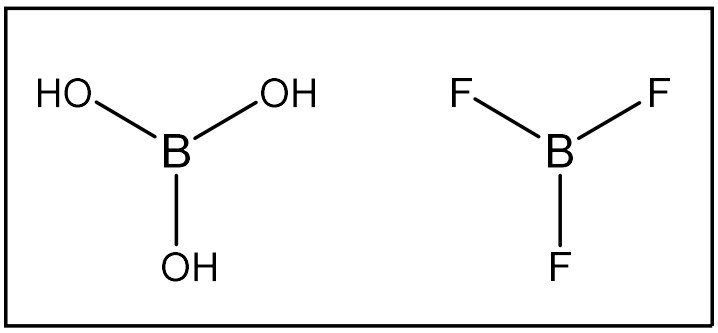

Figure 1.4: Uncharged trigonal 3-coordinate boron

This means that when boron is trigonally bonded, there are only 6 valence electrons in its outer shell - unlike many elements, boron ignores the octet rule. This deficiency of electrons results in boron centres behaving as Lewis acids. Lewis acids have a high affinity to nonbonding electron pair donors, such as oxygen. This character also means that boron bonds strongly and has a higher affinity to the more electronegative elements such as fluorine.

In addition to the uncharged trigonal fragments, boron is capable of forming 4-coordinate tetrahedral anionic units. These are particularly common in boron oxides and in the tetrafluoroborate anion BF_4^-. **(Figure 1.5)**

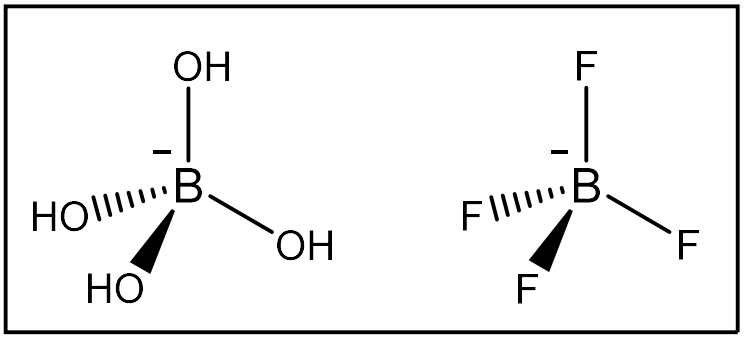

Figure 1.5: Tetrahedral 4-coordinate boron anions

The most common naturally occurring borate mineral, borax **(Figure 1.6)** shows two examples of each bonding environment. In the solid state, these tetraborate(2-) units are held together in a polymeric network by complex hydrogen bonding, and hydroxyl groups donating hydrogen bonds to bridging oxygens on adjacent molecules, and interstitial Na^+ cations filling spaces in the lattice. Borax forms part of a series of polyborates; which can be isolated as solids templated by alkali metal cations, alkaline earth metal cations, transition metal complex cations, organic cations and even rare earth metal cations. There is a vast collection of resolved crystal structures of synthetic polyborates incorporating a range of cations, and a review summarizing these will be presented in **Chapter 4**.

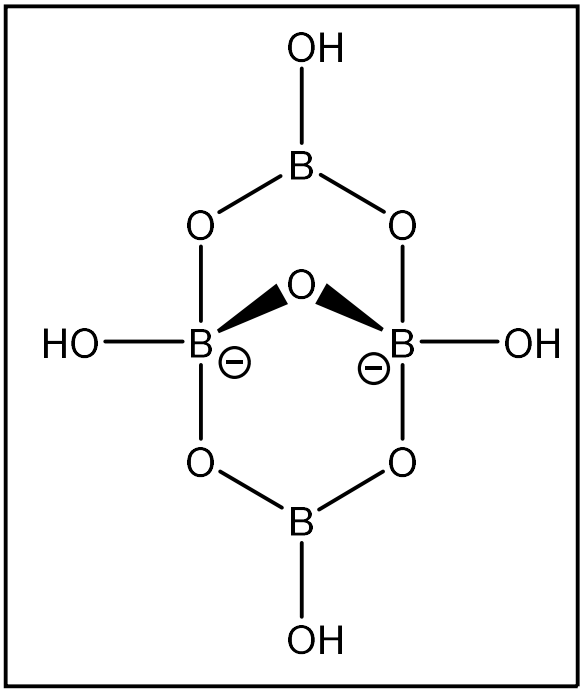

Figure 1.6: The tetraborate(2-) anion as found in borax

Boron is present in nature as two isotopes: ^{10}B and ^{11}B. These NMR active isotopes are 19.6% and 80.4% abundant respectively.[124] ^{10}B has a spin number of I=3, while ^{11}B has a spin number of I=3/2. The large spin number of each isotope would typically result in complicated splitting patterns based on the 2nI+1 rule. However, this splitting is rarely seen in NMR spectroscopy of boron-containing materials. It is almost exclusively present in small molecules such as boron hydrides and fluorides.

The less common naturally occurring isotope ^{10}B has some interesting and unique properties that are not observed in ^{11}B. The isotope has a very high affinity to capturing thermal neutrons and this has been utilised in boron neutron capture therapy (BNCT).[125] The principle behind this process is that ^{10}B absorbs a neutron, forming an excited ^{11}B atom. In this excited state, the excited atom spontaneously undergoes nuclear fission, releasing high energy alpha particles (^{4}He) nuclei and high energy ^{7}Li nuclei.[126] These nuclei spontaneously ionize,

releasing large amounts of energy into the immediate surroundings. The range of this energy release is sufficiently small to occur inside a cell with minimal damage to surrounding tissues.[127] This facilitates the targeted destruction of cells found in tumours. The advantage of this treatment over radiotherapy is that none of the nuclei present in this process are radioactive, which limits damage to surrounding healthy tissues. This forms the basis of (BNCT).

The ^{10}B source for this therapy is typically a boron hydride based icosahedral B_{12} moeity (**Figure 1.7)**.[128] This particular structure is also common among crystalline allotropes of elemental boron, and is the basis for the boron hydride series, known as boranes.

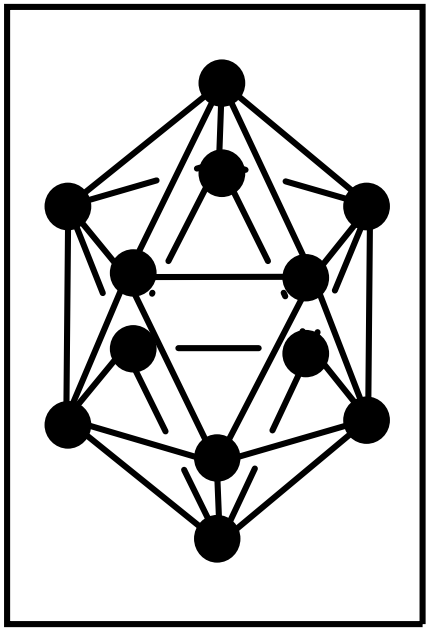

Figure 1.7 The icosahedral B_{12} provides a structural basis for the borane series. Each boron atom • is bonded to an additional hydrogen atom. Derivatives of dodecaborate $(^{10}B_{12}H_{12})^{2-}$ are used in BNCT, and these clusters continue to receive a lot of interest in medical research.[125–130]

1.5.2: Borates in aqueous solution[18]

Upon dissolution to aqueous systems, borates behave as Lewis acids. The primary example is the dissolution of $B(OH)_3$, which readily accepts a hydroxyl ion from the solvent, to form the tetrahedral anion $[B(OH)_4]^-$. This results in a slight reduction in pH of the solution, as H_3O^+ is also formed (**Scheme 1.5**).

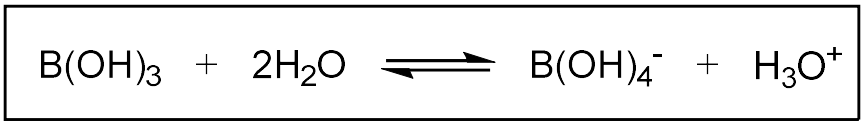

Scheme 1.5: Dissociation of boric acid in equilibrium

At low concentrations there is an equilibrium of $B(OH)_3$ with $[B(OH)_4]^-$. In more concentrated solutions, the monomeric species are susceptible to polymerization. This phenomenon can result in the formation of solid state polyborate anions (known as polyoxidoborates using IUPAC nomenclature),[131] which self-assemble from solution. When dissolved in aqueous solution, boric acid forms a number of polyborate anions in dynamic equilibrium, in addition to the equilibrium in **Scheme 1.5**. The borates present in this equilibrium form a Dynamic Combinatorial Library (DCL) of polyborate anions.[132] The formation of one particular polyborate product in the solid state over other potential products from the DCL is dictated by the pH of the solution, atmospheric temperature and the relative concentration of boron.[133] In order for this to occur, a suitable cation must be present in the solution. A more basic solution encourages the preferential self-assembly of polyborate anions. Therefore, suitable templating organic cations must be sufficiently basic. When solid polyborates are redissolved in water, they dissociate to re-establish the equilibrium. This is considered in more detail in **Chapter 4**.

1.6: Research Aims

In this thesis, the aim was to develop some additives that were capable of stabilising monosilicic acid at low pH, with a long shelf-life (*i.e.* remaining bioactive for at least 2 years). Formulations were subjected to stability trials to test the efficacy of the stabilising agent. A selected formulation was then prepared and used as a prototype. Glasshouse trials were then carried out using several different crops (including monocot and dicot examples) to see if the formulations were capable of improving foliar development and plant yield. Additional nutrients such as fulvic acid, and additional micronutrients including boric acid were also included in studies to explore any possible synergistic effects.

Assays were then carried out on the resulting plant products to see if there were elevated levels of silicon and other elements as a result of the foliar spray relative to appropriate controls. Observations were made regarding the general health of the plants, as well as the quality and size of the produce. These results were then reviewed and compared with previously reported crop trials from other workers with similar products. This will help to determine whether our silicic acid formulations are sufficiently beneficial to plant development to be viable mainstream alternatives to current growing methods.

In addition to foliar silicon formulations, this thesis contains a separate chapter on the synthesis and characterisation of novel solid state polyborates templated by the same organic quaternary ammonium cations and dications. An explanation of the potential applications of polyborates as well as the crystallographic data of the products is presented within this chapter.

Chapter 2: Foliar Silicon Formulations

2.1: Introduction

Silicon-containing formulations for agricultural use have already been extensively studied,[38,97,115,134–136] and thus must be considered when identifying potential silicon-containing species as candidates for formulations. There are several possible delivery methods of providing silicon as a micronutrient to plants and these will be covered in this section.

2.2: Silicon nutrients in the soil

There is a relatively high silicon content already present in most soils, averaging at around 28 % by weight depending on the soil type, ranging from 0.5 % to 48 %.[137] The silicon present in most soils exists in the form of silicate minerals, polymeric silicon dioxide moieties, and/or aluminosilicates.[40] While some of the silicon species may be biogenic (previously absorbed biologically active silicon, which is reintroduced to the soil from decomposing foliage),[75,138] the vast majority of silicon in the soil is not bioavailable.[139] It has been widely established that the only generally accepted form of silicon to be bioactive is monosilicic acid,[38] sometimes known as orthosilicic acid, $Si(OH)_4$.

2.3: Silicon materials in agriculture

Many growers try to improve the silicon availability in the soil by adding additional silicon-rich materials to the medium in an attempt to increase the silicon uptake through plant roots.[140–144] These silicon fertilizers can contain silicate minerals, polymeric and oligomeric silicon dioxide. Biogenic silicon (usually in the form of harvested plant by-products of silicon-rich plants such as rice husks, which contain up to 20 % silica) can also be used.[145] The marine-based diatomaceous earth alternative also contains some biogenic silicon,[146] which accumulates in the glassy protective shells from silicic acid uptake in diatoms.[147,148]

Addition of these silicon-based fertilisers does result in a net improvement in monosilicic acid concentration within the soil, and have been found to result in an improvement in silicon uptake by the plants[149]. This therefore leads to the positive outcomes intended in the research aims of this thesis. However, these silicon based fertilisers also all result in a net increase in soil pH,[150] as well as reducing the relative nutrient content of the more essential elements such as nitrogen, phosphorus and potassium that traditional fertiliser would provide.[151] This leads to a longer-term nutrient deficiency in the soil over multiple growing seasons due to the accumulation of non-bioactive silicon from poor silicon fertilisers. This increase in pH will also make the soil less well-suited to crops that prefer more acidic soils. Additional, pH-buffering nutrients may also need to be added to the growing medium to propagate a more acidic growing environment.

An alternative to applying solid silicon-based fertilizers directly to the soil is to apply silicon in the form of a foliar spray. The logic behind this method of application is that it will either substitute or cooperate with a poor uptake of silicon *via* the roots from the soil. It also provides an alternative nutrient flow rather than requiring the biogenic silicon to travel from the roots to the leaves through the xylem;[97] this simplifies the overall silicon uptake process. This also reduces the need to add nutrient-poor, silicon-rich fertilizers that are not completely bioactive.

2.4: Foliar silicate sprays

The silicon in foliar silicate sprays falls into one of three main water-soluble forms:

1) Soluble silicate minerals,[152–159]
2) Silica nanoparticles,[41,116,160–166]
3) Silicic acid, stabilized by additional compounds.[97,98,118,135,167–169]

2.4.1: Soluble silicate minerals

Many silicate minerals are water soluble and the most popular soluble silicate minerals are sodium silicate ($Na_2SiO_3.xH_2O$), and potassium silicate ($K_2SiO_3.xH_2O$). These can be marketed as solid powders that can be dissolved in water to form alkaline solutions. Adjustments can be made to the overall pH of the solution, but dramatic pH changes to silicate solutions can lead to a reduction in bioactive silicon as a result of increased polycondensation to silica colloids or gels.[170] These sprays tend to show less evidence of improving crop growth and product yield than traditional silicon-based soil fertilizers, but are beneficial to the crop's resistance to pathogens by providing a resistant barrier with some additional fungicidal

properties.[171,172] In rare cases, an increased Si leaf content was observed,[158] but it is not clear whether the silicon was biomineralised within the leaf's cellular structure, or present as deposits on the surface of the leaf. It is most likely the case that the silicon species present in these sprays is not able to pass through a leaf membrane since the silicon does not exist as silicic acid in solution.

2.4.2: Silica nanoparticles

Some silicon-based foliar fertilisers provide silicon to the plant in the form of silica nanoparticles.[173] Silica nanoparticles can be used as part of a pesticide, and also have antifungal properties. They can also be used to protect against the toxicity of heavy metals in the growing medium.[174] We are more interested in its use as a fertilizer, acting as a micronutrient source. Most silica nanoparticles are produced from tetraethylorthosilicate, $Si(OC_2H_5)_4$, or from one of the common inorganic silicates such as sodium silicate, $Na_2SiO_3.xH_2O$.[61] Silica nanoparticles in agricultural sprays tend to exist at between 20-60 nm in diameter,[162,163,174] and are fairly easily adapted to this size range by alteration of the production methods. The concentration of nano-silica in these sprays was generally optimal at below 400 mg/L and varied with the plant species sprayed.[160]

2.4.3: Silicic acid formulations

The agricultural benefits of silicic acid has been widely studied since the discovery of successful developments to produce stable formulations. Stabilized silicic acid is a water-soluble, plant-available source of silicon, in which the natural tendency of the silicon to polymerize into silica gel is inhibited by the introduction of an additive. Orthosilicic acid has not been isolated in a crystalline solid form from aqueous solution, however there have been crystal structures of silicic acid as a monomeric species and as small oligomers when co-crystallised with ammonium halides from non-aqueous amide-containing solvents.[175] Conventional organic solvents have not been effective in isolating crystalline moieties of orthosilicic acid derivatives, as they are not effective in inhibiting the condensation polymerization process. It is therefore possible that these amide-type solvents are capable potential stabilizing agents, but they cannot be used in agriculture due to a number of other important factors such as phytotoxicity, environmental impact, and cost.

As the vast majority of silicon present in a formulation containing stabilized silicic acid is bioactive, the actual silicon content can be quite low (but the silicic acid concentration is high) compared to traditional soil-based silicon fertilizers. Previous workers have explored several different types of additive. Some silicic acid products are stabilized by sterically hindering polymers such as poly(ethylene glycol),[34,98] while some products use agents such as choline,[176] a quaternary ammonium salt. Both formulations are acidified in their storage forms to below pH 1, to prevent polymerization to silica gel or colloids. For a foliar spray, the formulations are significantly diluted by up to 1000 times, causing the pH of the spray to rise to between 4-7. The addition of wetting agents to the formula can guarantee permeation of the spray onto waxy hydrophobic foliage.[38] All stabilized silicic acid sprays contain less than

50 ppm Si after dilution. This particular form of silicon shows a lot more promise in the levels of improvement to foliar growth and yield, compared to the inorganic silicates or silica nanoparticles.[134,168,177] If accompanied with the addition of very low levels of boric acid and other micronutrients such as trace metals,[118] then this growth effect might be further enhanced. The synergistic effect of boric acid-silicic acid sprays is particularly interesting, although caution must also be raised regarding the toxicity of boron towards certain plant types.[122]

Not all water-soluble silicon-containing formulations are suitable as micronutrient fertilizers. Organosilicates seem to have no nutritional benefit to the plant. Indeed, some examples exhibit strong phytotoxic effects upon the foliage even at very low concentrations.[178] This significantly limits the pool of potential candidates for silicon-containing formulations. It is also very important to ensure that the additives for stabilized silicic acid also show no toxicity towards the target crop, and a very limited environmental impact on the field and its surroundings. This is perhaps most possible when the concentration of reagents is very low in the spray, which is why stabilized silicic acid has been highlighted as the best area for expansion in the area of silicon micronutrients.[38,97]

2.5: Results and Discussion

2.5.1: Selecting a stabilizing compound

Potential additives for the stabilisation of silicic acid have been widely reported in the literature,[26,31,36,37,56,179–183] and range from sterically hindering polymers to small non-metal cations. While sterically hindering polymers such as PEG have their advantages; they are non-toxic and require little or no synthetic work or purification, many of them have already been patented at lower molecular weights. We originally considered the use of PEG 10,000 and PEG 20,000 as stabilizing compounds due to the lack of concerns around their toxicity and the huge potential for hydrogen bonding from such a large polymeric molecule. PEG has also already been patented and registered as a suitable candidate.[135]

However, there were concerns relating to limited solubility of both the PEG and the silicic acid. In our studies, we found that after several days there was a loss of homogeneity in the PEG-silicic acid solutions caused by the formation and deposition of a white suspension. This was most likely to be insoluble Si species, which would provide no nutritional benefit to the plants, thereby reducing the efficacy of these formulations. These observations were supported by a previous study,[34] where large PEG molecules were studied for their potential to remove unwanted silicon deposits from water pipes, where the precipitates were studied under the microscope. Despite these reservations, a PEG-containing formulation was included in one of our crop trial studies for comparative purposes.

There have also been some previous studies that suggested that small quaternary ammonium salts such as choline chloride were very good stabilizing agents for silicic acid food supplements,[23,180,184,185] choline-silicic acid has already been patented in agriculture.[167] We were therefore interested in looking at similar species to choline, which might undergo similar stabilising effects.

Choline consists of a quaternary ammonium head, and a primary alcohol tail, thus providing potential hydrogen bonding sites. To enhance this hydrogen bonding potential, we decided to investigate the addition of a secondary alcohol to the β-carbon of the tail end of the molecule. This could be easily accomplished by replacing the synthetic precursor to choline (ethylene oxide) with glycidol, which contains an additional hydroxymethyl group branching away from the epoxide. This could easily lead to the production of a series of tetraalkylammonium cations with 1,2-diol tails. Not only would these qualify as alternatives to choline from an intellectual property standpoint, but they would also provide potential chelating effects from the diol. Some effects have been observed in relation to an interaction with boric acid by previous researchers.[186,187] We confirmed this effect by addition of excess $B(OH)_3$ to these choline derivatives in an attempt to broaden our library of polyborates. Upon recrystallisation, excess $B(OH)_3$ crystallised out of solution, but the remaining oil was found by ^{11}B NMR to contain a mixture of mono- and bis- chelated borate, in which both alcohols in the substituted choline were contributors. This chelate effect could potentially give rise to formulations containing both $B(OH)_3$ and $Si(OH)_4$, which are said to have synergistic properties with each other with regards to plant micronutrients.[117,119]

2.5.2: Synthesis of TAA[OH] Salts

Based on the literature analysis in **Section 2.5.1**, a series of new tetraalkylammonium hydroxide **TAA(1)-TAA(7)** salts were targeted by the addition of different tertiary amines to a cold solution of glycidol **(Scheme 2.1)**. They can be simply defined as substituted β-hydroxymethyl choline derivatives with varying functionality on the quaternary ammonium "head" of the molecule.

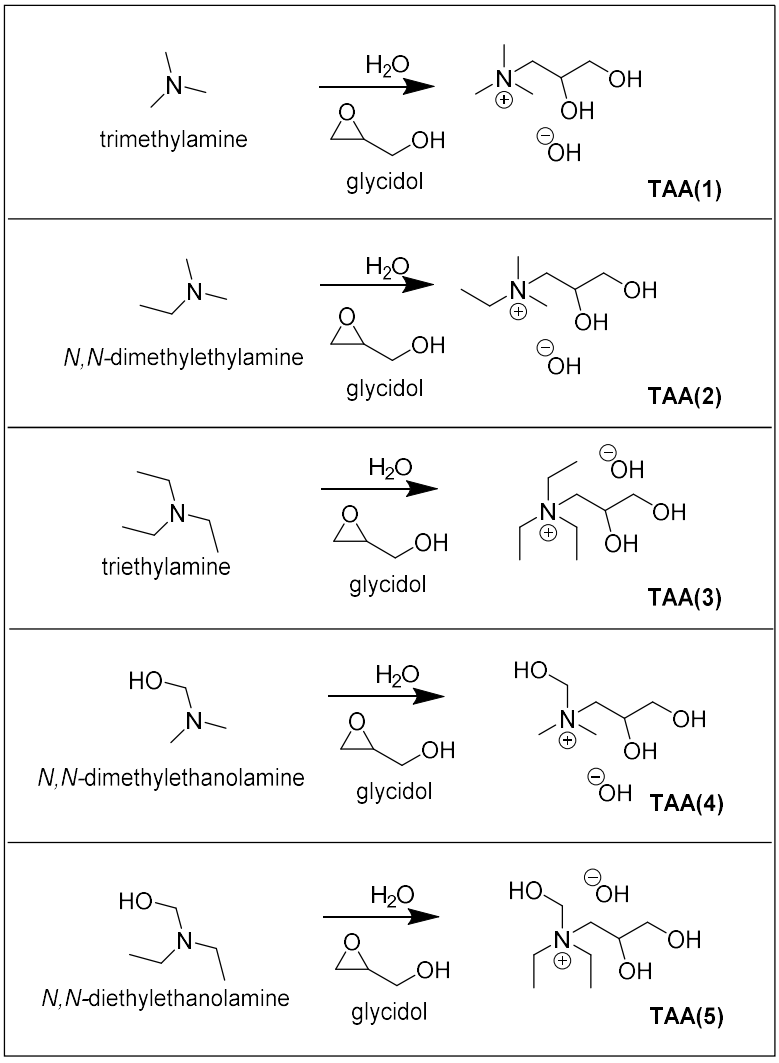

Scheme 2.1 Synthesis of **TAA(1)-TAA(5)** compounds using a tertiary amine, glycidol and water.

TAA(1) and **TAA(2)** were produced and purified reliably in high yields (> 90 %). The yields were calculated by finding the concentration of $(OH)^-$ via an acid-base titration against 1M HCl using universal indicator. It was found to be possible to concentrate the product in solution by removal of water solvent and any volatile unreacted reagents such as tertiary amines by rotary evaporation, allowing for the possibility of more concentrated formulations to be produced. Any unreacted glycidol could then be removed by multiple extractions with chloroform prior to removal of any volatiles. After concentrating the solutions, a drop of each solution was added to 0.5 mL D_2O and subjected to NMR studies (^1H, ^{13}C). These NMR studies were consistent with literature data.[186] The formation of the products generally featured a steady rise in temperature from 10 ^oC to approximately 30 ^oC after dropwise addition of glycidol. The reaction vessel was then cooled again to 10 ^oC in an ice bath, before a further exothermic reaction occurred upon initial quenching with water. Here the temperatures sometimes exceeded 50 ^oC before being cooled back down to the temperature of the ice bath.

TAA(3) was obtained in considerably lower yield (~35 %). It is not immediately clear why this should be the case, but it may be linked to steric effects. Triethylamine was the most sterically hindered of the substituted amines investigated, and there were no additional hydroxide groups present on the amine to raise any potential hydrogen bonding activity.

The synthesis of **TAA(4),** however, was considerably more exothermic than the other derivatives. It is not immediately clear what is responsible for the sudden sharp rise in exothermicity relative to the other amines studied, although this derivative represented the least sterically hindered trialkylamine featuring a primary alcohol side chain. The first attempt to synthesise **TAA(4)** resulted in a sudden change of colouration to dark brown, coinciding

with a rapid rise in temperature from 15 °C to in excess of 100 °C. NMR studies of the resulting 'sludge-like' product were inconclusive, containing a considerably different pattern to the other products, and most likely indicates a series of unwanted side-products as a result of thermal degradation arising from the sharp rise in temperature. The reaction to form **TAA(4)** was repeated with addition of cold water at the time when discolouration of the glycidol-amine mixture and a rise in temperature was initially recorded. This seemed to quench the reaction sufficiently, preventing the discolouration, and improving the purity of the final product markedly. However, this resulted in a lower yield (~75%), possibly due to the need to prematurely quench the reaction between glycidol and the *N,N*-dimethylethanolamine.

The synthesis of **TAA(5)** did not show unexpected problems, suggesting that the increased reactivity provided by the additional hydroxyl group, similar to that found in **TAA(4)**, had been off-set by the more sterically hindering ethyl groups present in the less reactive **TAA(3)**, however the yield of the product was lower at approximately 60%.

2.5.3: Investigating PEG-choline hybrids

Pre-existing patents have disclosed PEG-500 formulations that are very efficient inhibitors of the polymerisation of silicic acid.[135] Whilst there are several products on the market that make use of this property, there have been very few investigations into functionalised PEG-500 species. As the use of tetraalkylammonium hydroxide salts has also been efficient in producing formulations that maintain bioactivity of silicon, we decided to try and formulate a compound that incorporates a "PEG-500" chain with tetraalkylammonium hydroxide groups on each end of the polymer. In order to do this, we obtained a PEG-500 diglycidyl ether; which theoretically allows the addition of a tertiary amine through the same mechanism as the ring-

opening reactions that glycidol performs in water. The synthesis was carried out according to **Scheme 2.2**.

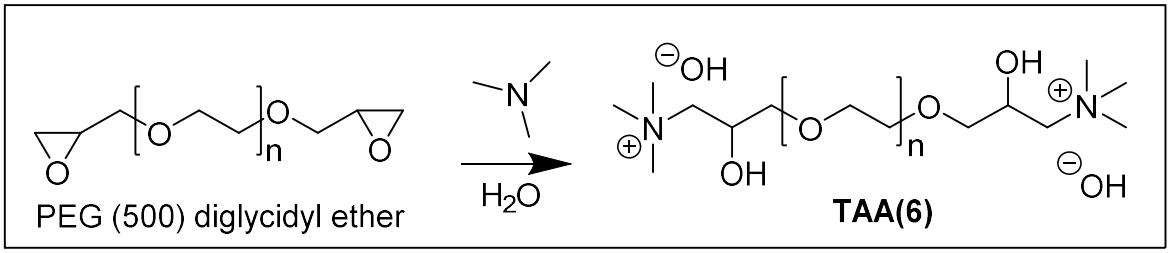

Scheme 2.2 Synthesis of a **TAA(6)**, using a glycidyl functionalised PEG-500, trimethylamine and water.

Reactions followed a similar pattern to our previous studies with glycidol; upon addition of the amine and then water, an exothermic reaction occurred to form a yellow oil, and the excess water was evaporated under reduced pressure to concentrate the product.The concentration of the product was determined by an acid-base titration with 2M HCl. However, it was found to be considerably lower than the previous derivatives, with the concentration being approximately 1M. This is most likely due to the higher molecular weight of the product, whilst there are two $[OH]^-$ counterions present on each PEG-500 diammonium molecule, the mass ratio of $[OH]^-$ to the large diammonium salt is considerably lower than those of **TAA(1) – TAA(5)**.

The oily product was characterised by ^1H and ^{13}C NMR spectroscopy; ^1H NMR analysis of PEG should result in one large peak at around 3.6 ppm representing the repeating CH_2 unit. ^1H NMR of the yellow oil confirmed this was present, but with four additional peaks. One of these, a large singlet at 3.11 ppm integrated to approximately half the integration of the CH_2 repeat unit. In a PEG-500 diglycidyl ether starting material, the number-average molecular

weight is 500 $gmol^{-1}$. By subtracting the combined weights of the two glycidyl ether functional groups, we can approximate that there are 10-11 repeat units of ethylene glycol present. This fragment should contribute roughly 40 protons as CH_2 groups. The successful addition of trimethylamine to each end of the molecule would add six CH_3 groups to the final product, contributing 18 protons in total. This CH_3 peak was assigned an integration of 18, which resulted in an integration of 40 for the large peak at 3.6 ppm relating to the ethylene glycol CH_2 repeat unit. In addition to the peak at 3.11 ppm, the three further peaks, at 4.25 ppm, 3.45 ppm, and 3.35 ppm, integrated to 2, 4 and 4 protons respectively. These signals are likely to be associated with a CHOH group formed by the ring opening of the glycidyl ether, the terminal CH_2 of the PEG chain, and the CH_2 group attached to the NMe_3 group, respectively.

^{13}C DEPTQ (Distortionless Enhancement by Polarisation Transfer, including Quaternary nuclei detection) NMR spectroscopy was utilised to identify the carbon environments and multiplicities.[188] The results of this study further supports this analysis, with three major 'upwards' peaks between 69 ppm and 70 ppm relating to the three CH_2 environments. A 'downwards' peak at 54 ppm identifies the three CH_3 groups on the substituted ammonium group, and a smaller 'downwards' peak at 65 ppm representing the CHOH caused by the glycidyl ether opening. (^{1}H,^{13}C)-HSQC (Heteronuclear Single Quantum Coherence) analysis was used to confirm the which protons were bonded to each carbon atom in the minor peaks, as these were difficult to resolve due to their broadness in the original ^{1}H experiment.

These NMR observations are consistent with similar observations made in the **TAA(1)-TAA(5)** series of compounds. It should be noted that the **TAA(1)-TAA(5)** compounds do not have the strong signals relating to the polymer. There are no previous literature reports of a synthesis

of a PEG-500 capped on each end by substituted diammonium salts, and it is possible that this reaction could be repeated with different tertiary amines with success. However, upon long term exposure to light, the yellow oil product darkened to become dark orange in colour indicating potential decomposition; despite this, there were no notable differences in the NMR spectra of the oil after 30 days of shelf-life.

The resulting solution obtained after a few hours standing after the addition of the acidified product to sodium silicate (Si:N ratio of 1:2), was subjected to ^{29}Si NMR spectroscopy. Major signals were present at -71.44 ppm (Q^0), -79.12 ppm (Q^1), and -81.40 ppm (Q^1).[15,58,59] Minor signals were found at -87.24 ppm (Q^2) and -89.38 ppm (Q^2).[15,58,59] Any potential signals further upfield were lost within the noise signals caused by the glassware. After several days, however, a gel began to form in the flask containing the mixture – a sign that the additive has failed to stabilise the silicic acid. Upon further standing, water-insoluble crystals were formed. NMR spectroscopy by dissolution of the crystals using a aqueous solvent was not possible due to the insolubility. Substituting the water solvent with aqueous sodium hydroxide solution caused dissolution of the crystals to form a solution of sodium silicate; confirmed by ^{29}Si NMR spectroscopy. It is likely that the original crystals were of a polymeric silica network.

Attempts to coordinate the synthesised PEG-500 diammonium hydroxide oil with $B(OH)_3$ to form a polyborate in an acid-base reaction were also unsuccessful, as a solid product was not isolatable from the resulting oily solution. The most likely explanation is that the long polymeric PEG chain was too bulky and flexible to template a rigid polyborate network required to obtain a crystalline product.

2.5.4: Preparation of formulations

Attempts to produce formulations featuring **TAA(1)-TAA(5)** as stabilising agents gave rise to a mixture of outcomes. Acidified solutions originally containing **TAA(1)**, **TAA(2)** and **TAA(4)** were successful in stabilising silicic acid. However, the bulkier reagents **TAA(3)** and **TAA(5)** formed insoluble white precipitates upon acidification and addition of silicate after acidification. These precipitates only redissolved upon addition of NaOH to adjust the pH to alkaline. In both of these cases, silica gels formed within a few hours. When prepared without acidification, **TAA(3)** and **TAA(5)** remained in solution.

In addition to **TAA(1)-TAA(5)**, further potential stabilizing agents were explored, including the functionalised PEG **TAA(6)**. Additionally, one of the non-metal dications explored in **Chapter 4** of this thesis was also identified as a potential candidate *i.e*: *N*,*N*,*N'*,*N'*-tetramethylethylenediamine to form **TAA(7)**, **(Scheme 2,3).**

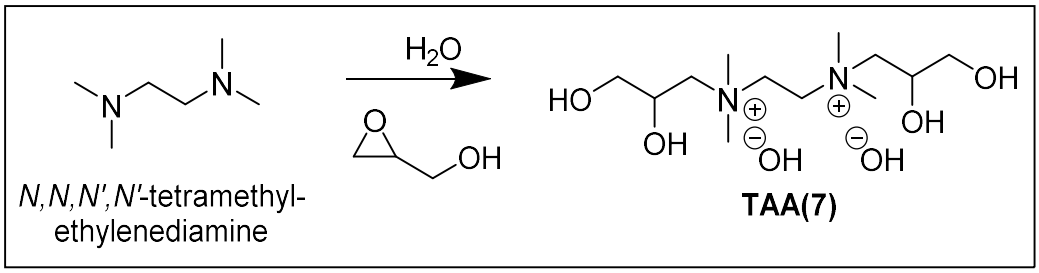

Scheme 2.3 Synthesis of **TAA(7)** using *N*,*N*,*N'*,*N'*-tetramethylethylenediamine, glycidol and water.

TAA(7) is able to undergo a similar reaction with glycidol to the trialkylamine cations present in **TAA(1)-TAA(5)**, but there are two tertiary amines on the molecule, so this is likely to react at both ends of the molecule. A reaction with a slight excess of two equivalents of glycidol resulted in very similar NMR spectra to those of the successful **TAA(1)-TAA(5)** additives. This

product was also acidified and added to sodium silicate, and a similar colour change and foaming effect occurred to the successful **TAA(1)**, **TAA(2)** and **TAA(4)** formulations. The silicate remains in solution, so there is strong evidence that a stabilising effect on silicic acid was possible with this diammonium salt.

2.6: Stability tests on formulations

2.6.1: The silicomolybdate method

Stabilized silicic acid is defined as a water soluble biologically active silicate species that cannot undergo condensation polymerization to colloidal solution or silica gel due to the presence of a polycondensation-inhibiting species. In order to test the stabilising effect of these inhibiting species, an analytical method is required that selectively measures the concentration of silicic acid, but does not respond to polymeric silicon. It is therefore important to identify a reliable water testing method that only provides a positive reading for monosilicic acid species. Literature searching indicated that the silicomolybdate test was such a method.[34,63,64,189] Here a colour change is exhibited when monomeric (Q^0) and dimeric (Q^1) silicate species react with ammonium molybdate forming silicomolybdic acid. This is indicated by a yellow-green colour, which can be quantified by a spectrophotometer at *ca.* λ = 400 nm. This method was chosen as a much more economical and time-efficient method to other alternatives.

An alternative NMR study involving investigating relative integrals between Q^0-Q^4 silicon would require ^{29}Si-enriched formulations, which are highly expensive. Other analyses of aqueous solutions such as AAS can be unreliable, while ICP-OES was not readily available on

our research premises and was discounted as a possible alternative since it would not able to distinguish the bioactive silicic acid from any other silica species present such as colloids or gels.

2.6.2: Shelf-life determination of the storage TAA(1) formulation

The first objective of the stability trials was to identify the shelf-life of the **TAA(1)-**stabilised silicic acid, using the molybdate method. It is important that these storage formulations remain stable over a period of at least 2 years at room temperature (ranging from 12^{o}C to 25^{o}C, depending on seasonal variation) in a dark cupboard. This would fall in line with competitors and allow growers and farmers to use the same containers for several growing seasons, reducing the need to unnecessarily dispose of waste chemcials.

A shelf-life trial was carried out on acidified formulations. Three separate **TAA(1)** formulations were produced over the course of 2 years at one year intervals. Therefore, there was one 24 month old formulation, one 12 month old formulation, and one freshly prepared formulation. These formulations were intended to contain the highest concentration of silicate possible without experiencing problems either with solubility of the initial metal silicate salt, or by not having enough stabilizing compound to completely suppress gel formation. It was found that the strongest silicate concentration that did not undergo any of these circumstances was approximately 13,000 ppm "SiO_2". The three identical formulations were produced at 12 month intervals according to the procedures described in section **5.2** and eventually subjected to the silicomolybdate test, resulting in the results shown in **Table 2.1**

Table 2.1 Stability data of **TAA(1)** 13,000 ppm formulation over 2 years.

Batch	**Absorbance at λ= 400nm**	**Relative concentration**	**"Concentration SiO2" /ppm**
TAA(1) Fresh	0.229	100 %	500
TAA(1) 12 Months	0.224	98 %	490
TAA(1) 24 Months	0.200	87 %	435

Other attempts to use the silicomolybdate test identified a lack of repeatability when using the absorbance to calculate the concentration of molybdate-active silicon. Therefore, the fresh-batch absorbance has been expressed to contain 500 ppm "SiO_2", with the assumption made that there little to no loss of molybdate active monosilicic acid between the production of the formulation and its molybdate analysis. Subsequent readings are then expressed as "ppm SiO_2" relative to the fresh batch based on the change in absorbance readings over time.

Using the acidic pH stability results, it is clear that **TAA(1)**-stabilised silicic acid remains stable for at least two years. A 13% reduction in molybdate-active silicon content after 2 years in storage would still render the formulations a strong source of silicic acid, with the original 13,000 ppm stock containing *ca.* 11,300 ppm molybdate-active silicon when considering the dilution factors for the molybdate test.

2.6.3: Stability tests of the TAA(1) storage formulations diluted to pH 7

One of the key questions posed to the research group by the company partner was regarding the stability of potential formulations after they had been significantly diluted and added to a farmer's tank mix. Many stabilised silicic acid formulations stated on the bottle label that the diluted sprays could not be stored in a foliar spray tank mix for more than 72 hours with guaranteed efficacy, whereas the original formulations could be stored for several years without loss of activity. To test the efficacy of the formulations, **TAA(1)** was chosen as an ideal candidate to carry out stability trials.

A stability trial using the silicomolybdate test was set up in which a sample of an acidic storage formulation containing **(TAA 1)** would be diluted to a theoretical concentration of 500 ppm with regards to the "SiO_2" concentration, as well as neutralised to pH = 7 before being left to stand in a cool, dry location to test its stability. This quoted concentration is not to be confused with the concentration of the silicon-containing reagent added to the formulation.

A storage formulation was developed that contained 5.5 mL of 5.93 M **TAA(1)** hydroxide, diluted to 25 cm^3 in distilled water and acidified to pH <1 using HCl. To this solution was added 0.35 g $Na_2SiO_3.5H_2O$, to result in a solution containing 3962 ppm "SiO_2". It is important to note that the order of addition of each reagent in making the formulation is key to ensuring good stability and a long shelf-life. **TAA(1)** hydroxide is first acidified with 8M HCl, with the pH level digitally monitored using a pH meter. The acidification process is exothermic, resulting in an acidified solution at approximately 35 ^oC . Once the pH reading is less than pH = 1, the required level of $Na_2SiO_3.5H_2O$ is added and stirred vigorously. Slight foaming occurs during this process and the solution gains a slightly yellow colouration. If the reagents are added in the

incorrect order, a gel will rapidly form at this stage and render the formulation spoiled. In future formulations used in crop trials, the silicate concentration was increased make the formulations stronger, and it was found that the strongest formulation to remain stable contained *ca.* 13,000 ppm "SiO_2".

2.6.4: Identifying a suitable formulation pH

At the beginning of the project, the initial molybdate stability tests were carried out at pH = 7, based on a previously reported trial.[34] This original trial was not related to agricultural studies, and focussed on preventing silica gel build-up in water supply pipes by using poly(ethylene glycol). Some existing patents suggest that choline was an effective inhibitor of silicic acid polymerisation at acidic pH, but does not achieve the same results in neutral solution. It is therefore possible that **TAA**-stabilised formulations had no real long-term effect on silicic acid stabilisation at neutral pH.

A further argument to support the use of HCl (or other pharmaceutically acceptable acid) to acidify any formulations is that this facilitates the release of the bioactive H_4SiO_4 from the Na_2SiO_3. This is observed in the human body when dilute silicates are exposed to stomach acid.[23] It is likely that the molybdate-active silicon observed in this trial is not bioactive silicic acid, but simply a dilute solution of sodium silicate.

TAA(1) – **TAA(5)** samples diluted to 500 ppm SiO_2 at pH = 7 (considerably stronger than the SiO_2 levels found in the diluted foliar sprays), were kept in the same storage conditions for 18 months. Upon retrieval of these solutions, there was evidence of gel formation at the bottom of the bottles. There was also evidence that some of the silicon had formed colloidal solutions,

in which small particles were found suspended in the solutions. Both the gels and colloidal solutions would be unable to pass through a cellular membrane barrier in order to be bioactive in plants. It became apparent that silicic acid could not be stabilized in solution using these compounds over the required period of time at neutral pH.

To gain some idea of how other formulations overcame long-term storage issues, a sample of "Siliforce" was obtained (a patented competitor product using poly(ethylene glycol) as the stabiliser). This formulation was found to be pH=1 using litmus paper. With this and the previous results in mind, it was then decided that the pH of the **TAA**-stabilised storage formulations should be adjusted to < 1 for long term storage and subsequent stability trials to best model the potential shelf-life.

2.6.5: Limitations and modifications to the procedure

One of the key problems that needed to be addressed during the development of the stability trials concerned the repeatability of the experiments. Some of the shorter 72 hour experiments were repeated over the course of the project with significant differences in the absorbance readings. Calculating "ppm SiO_2" from the absorbance readings and applying a dilution factor, using a literature value for the extinction coefficient also provided inconsistent results. In addition to this, even the fresh storage batches of **TAA(1)**-stabilised silicic acid provided absorbance readings that converted to considerably lower "ppm SiO_2" levels than expected.

In all stability tests of storage solutions at acidic pH, the fresh silicic acid batch absorbance readings would be expressed as "100% concentration". Dilutions were still applied to the

formulations tested to aim for absorbances in the region of the previous tests, as this range provided sensible absorbance readings. The solutions were then left over time, and the absorbance readings recorded in yearly intervals, and calculated as a percentage loss of molybdate active silicon relative to the original fresh samples. Unfortunately, this means that the exact concentration of molybdate-active silicon could no longer be modelled, but this offered the alternative that we could now conclude that the formulations remained stable from the day of production until the end of the 2 year storage period.

2.7: Concluding Remarks

The objective of this work was to prepare a series of formulations containing bioactive soluble silicic acid, capable of remaining stable and homogenous for a shelf-life of at least 2 years. In order to test this capability, the silicomolybdate test was utilised and developed to test the levels of stabilised silicic acid over the shelf-life period. A series of 7 tetraalkylammonium cations were successfully synthesised. **TAA(1)**, **TAA(2)**, **TAA(4)** and **TAA(7)** were found to be effective stabilisers at the desired pH (pH 7) in which the silicic acid is at its most active. Molybdate tests and visual observations showed no dramatic change in the composition of the formulations over this period. **TAA(3)**, **TAA(5)** and **TAA(6)** failed to remain in solution upon acidification, and couldn't be included in stability studies.

TAA(1) has been incorporated into a series of formulations and then diluted and used as foliar sprays for a series of crop trials, with the intention of investigating whether these diluted formulations containing silicon (with and without boron) as a micronutrient would result in improvements to crop yields and plant development. The process and outcomes of these trials are presented in **Chapter 3**.

Chapter 3: Field trials of foliar silicon formulations

3.1: Introduction

The purpose of this chapter was to study the impacts of a series of foliar stabilised silicic acid sprays on the growth and development of various crop species in controlled environments. Furthermore, the potential synergistic effects of adding additional nutrients or micronutrients to the formulations was studied. This chapter describes several crop trial designs, before explaining the experimental procedures used in the silicic trials and the outcomes.

3.2: Designing Field Trials

Existing silicic formulations, stabilised by poly(ethylene glycol), have been successfully trialled on a number of different plant varieties.[38,97] A few examples of field trial designs will now be presented as well as some of their reported yields.

3.2.1: Randomised Complete Block Design (RCBD) [168,190,191]

The RCBD model is a crop trial design carried out by research institutions in outdoor field trials. This method involves splitting the available field space into equally sized blocks. Each block contains at least one plant representing each spray application. These plants are not moved for the entire trial. This type of trial minimises variations in temperature or light quality within the growing area by evenly distributing each application type across the blocks within the testing facility. This method is typical of trials carried out in large soil beds or fields containing multiple plants. An example trial is shown in **Figure 3.1:**

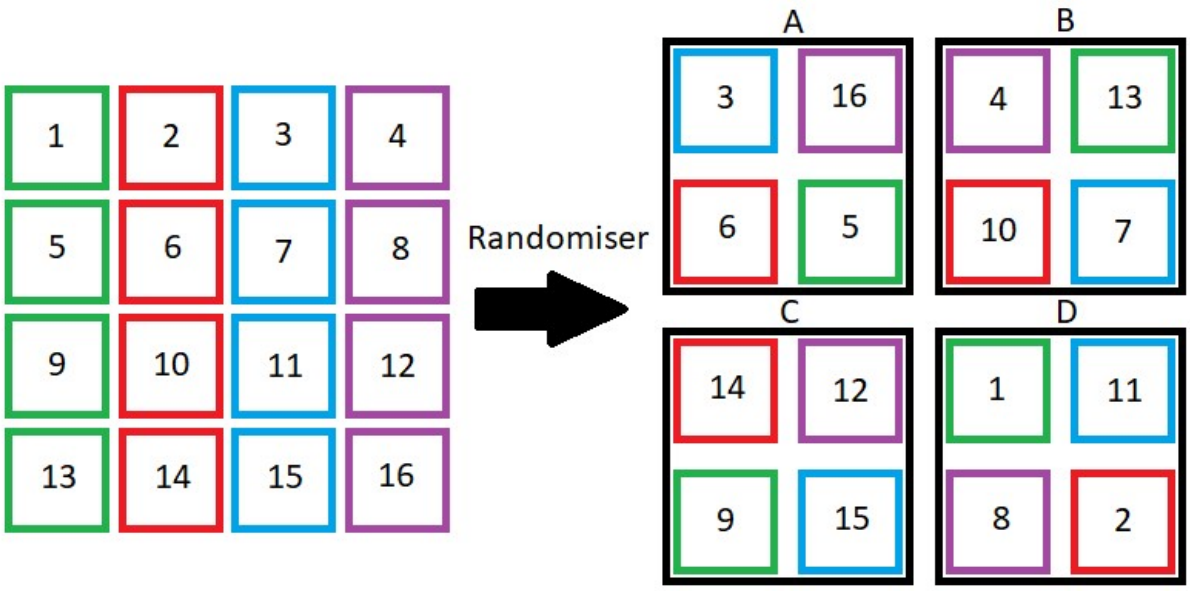

Figure 3.1: Typical example of a randomised complete block design (RCBD)

Using the above model and before any sprays are applied, plants 1-16 are each assigned with a treatment (represented by the colours in the figure). They are then 'randomly' assigned to blocks A-D, taking care to ensure that each block contains at least one of each treatment, with the location within each block randomised. Each plant is tagged with a colour and individually sprayed within its block.

The trials,[98,100,106,192–195] using the RCBD method (and reported effects of stabilised silicic acid + boric acid micronutrient sprays) are shown in **Table 3.1**

Table 3.1 Analysis of RCBD trials using foliar silicic acid and boric acid formulations

Country of Trial	Formulation	Crop Tested	Reported yield change %	Ref.
India	A	Rice	+ 13.2 %	[98]
India	A	Grapes	+ 15 – 45 %	[192]
India	A	Sugarcane	+ 39 %	[106]
Columbia	A	Papayas	+ 36 %	[193]
India	B	Chili Peppers	+ 39 %	[100]
India	B	Tomato	+ 31 %	[194]
India	B	Finger Millet	+ 39 %	[195]

In all of the above cases, a significant improvement to the yield was reported. Formulation A contains PEG-400 stabilised silicic acid, boric acid and potassium chloride, diluted in deionised water. Formulation B contains PEG-stabilised silicic acid, boric acid, molybdenum and zinc in deionised water. One set of controls contained only deionised water, a second set was a control containing only PEG-400 in deionised water, and the third set was a formulation containing PEG-400 and boric acid. The purpose of those sets of controls is to exclusively test the efficacy of the stabilised silicic acid and eliminate potential nutrient responses from the other variables.

3.2.2: Completely Randomized Design (CRD)[154,158,196]

A simplified alternative to the RCBD trial is the completely randomized design. In this trial design, each plant in the trial has an equal random chance of being applied by any type of spray. If any of these individual plants are significantly more or less successful than average, then this is justified as an experimental error. It is therefore better to use a CRD in a controlled environment such as a glasshouse where the external conditions (*i.e.* temperature, light, moisture) are evenly distributed between the replicates. CRD is rarely utilised in outdoor field trials, as the potential for experimental errors would be higher due to the variable environmental factors.

When carrying out pot-based trials, it is possible to re-randomise the location of the replicates at regular spraying intervals over the course of the trial within the growing environment to limit the effects of external conditions further. **Figure 3.2** shows an example CRD setup for the first two treatment weeks of a pot-based trial.

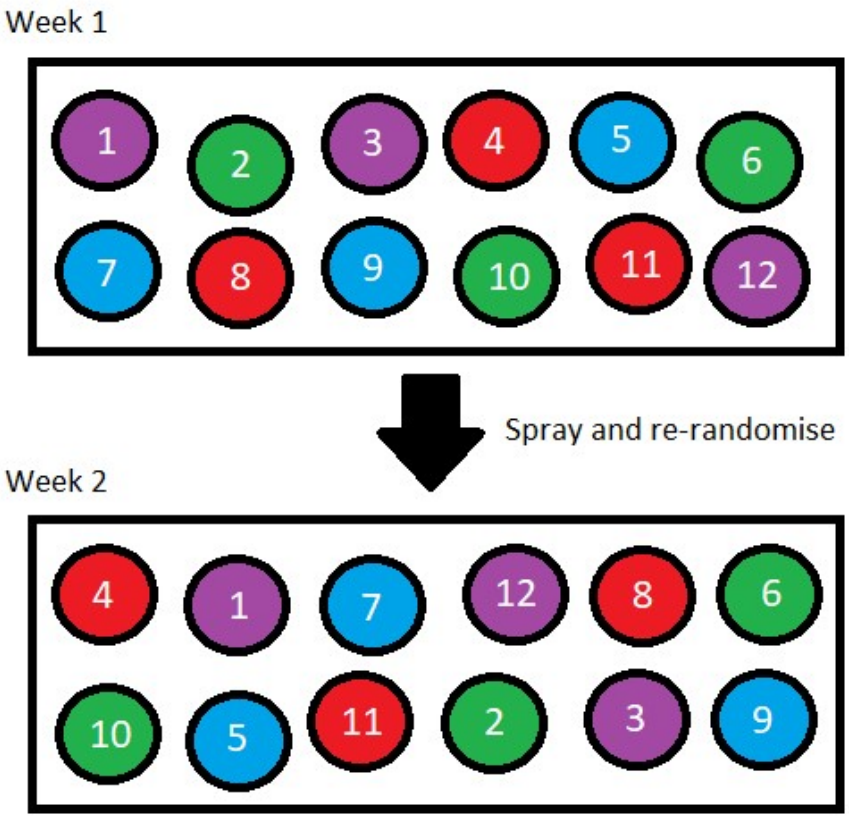

Figure 3.2: An example of a CRD trial on 12 plants with 4 different types of foliar spray (denoted by colour) carried out in triplicate. Pots are randomly rotated around the work space with each treatment.

3.2.3: Extension Trials and Farmer's Trials[38,197]

Extension trials are usually carried out on a farmer's field or a greenhouse.[197] The difference between an extension trial and a farmer's trial is that in an extension trial an academic expert in agriculture and additional extension agents oversee the trial. Extension trials may be carried out using similar designs to trials carried out in research institutions, with pre-planned layouts and growing conditions. The farmer often contributes to the general maintenance and feeding or application of treatments to the crop under the advice of the academic extension agent or staff.

A farmer's trial is an agricultural experiment carried solely by farmers who are interested in attempting new growing methods to improve upon existing yields and hence result in a better profitability for the crop. They are often carried out in parallel to older methods to compare yields. Treated crops are often simply grown in a separate area of the field to untreated crops, so there is limited randomisation of crop location to eliminate external growing conditions. A variety of different crops were grown using the same PEG-stabilised silicic formulations as the RCBD trials by Laane.[38,97] **(Table 3.2)**

Table 3.2: Extension and Farmer's trials reported by Laane between 2003 and 2017.[38,97]

Country of Trial	Formulation	Crop Tested	Reported yield compared to control %	Type of Trial
Netherlands	A	Potato	+ 6.5 %	Extension Trial
Netherlands	A	Onion	+ 10.8 %	Extension Trial
Netherlands	A	Apple	+ 17 %	Farmer's Trial
India	B	Eggplant	+ 44 %	Extension Trial
India	B	Sweetcorn	+ 34 %	Extension and Farmer's Trials
India	B	Watermelon	+ 38 %	Extension and Farmer's Trials
India	B	Cardamom	+ 26 %	Farmer's Trial
Romania	B	Wheat	+ 340 %*	Farmer's Trial
Algeria	B	Wheat	+ 37 %	Farmer's Trial
Ukraine	B	Wheat	+ 19 %	Farmer's Trial
Netherlands	B	Wheat	+ 5 %	Farmer's Trial
India	B	Rice	+ 46 %	Farmer's Trial

*Trial carried out in extremely saline soil

3.2.4: Additional requirements of formulations

While it is of primary importance to farmers to improve crop yields, there are additional reported benefits to the use of silicic acid sprays. The global demand for reliable and healthy food supplies continues to increase, which places pressure on growers and strain on the land used for farming.[198] There is a growing threat of drought conditions as a result of increasing global temperatures, in addition to an increasing number of inclement weather events such as drought.[199–202]

In addition to these increasing abiotic stresses, there is the biotic threat of pests and plant diseases. These cause considerable damage to the crop.[203] Poor management of existing chemical treatments can cause irreversible damage to surrounding ecosystems; chemical treatments designed to eliminate pests can run off the fields into nearby water supplies, adversely affecting the chemical balance in rivers and streams.[204] Over-use of typical fertilisers (nitrogen/phosphorus/potassium) can cause algal blooms in local water supplies, which deplete the oxygen levels in the water and cause localised extinction of aquatic species in stagnant waters.[203] There are escalating calls to outlaw certain chemicals that have been used in agriculture for decades due to their effect on the environment.[205–207]

One of the key benefits of silicic acid formulations as viable alternatives are that dissolved silicon is already naturally present in streams and rivers as a result of mineral erosion in low levels.[208] If stabilised silicic acid formulations provide direct benefits to a multitude of crops, they could substitute or reduce the need to overspray crops with other, potentially damaging chemicals.

Based on these arguments, a number of additional parameters were studied in previous trials. Many of the farm trials were carried out in sub-optimal conditions. For example, the abiotic stress tests included soils that were of abnormal pH for optimal growth,[209] salt-stressed soils,[160,210,211] polluted soils containing elevated levels of heavy metals, [174,176,212] drought conditions,[177,213–216] areas of high wind,[217,218] periods of cold weather.[136] Additional studies looked at biotic stresses such as powdery mildew infections,[115,155,156,171,178,219–222] brown spots,[139,223] bacterial blight, [224] rice blast, [77,141,154,158] and resistance to a variety of pests.[225]

3.3: Field trials using TAA(1)-stabilised silicic acid formulations

A series of field trials were carried out on different crops over the course of the project, to test the efficacy of the formulations prepared in **Chapter 2**. Foliar sprays were applied directly to the leaves of several different crops, and some additional biostimulants and micronutrients were studied.

3.3.1: Field Trial 1: Glasshouse Potato Pot Trial

3.3.1.1: Trial Protocols

Growth effects of the **TAA(1)**-stabilised silicic acid formulations were carried out in glasshouse pot trials on the *cultivar swift* **potato** variety, chosen due to its fast growing cycle. An additional biostimulant, fulvic acid, was utilised in this trial.

The name fulvic acid does not refer to a specific molecule, but a family of polymeric organic acids (**Figure 3.3** outlines two example structures). The primary source of fulvic acids is from the biodegradation of lignin, which is found in plant material. Fulvic acids are derived from humic acids but are considerably smaller in molecular weight and have a greater proportion

of oxygen in their structures (present largely as phenols, carboxylic acids and ketones). They are shown to be excellent biostimulants due to their high affinity to chelating to metals as a result of the high oxygen content,[226] providing an uptake pathway into the leaf. They are highly hydrophilic molecules, attracting moisture from the surroundings.[227] As a result, improved yields have been reported for several crops as a result of foliar fulvic acid sprays.[228]

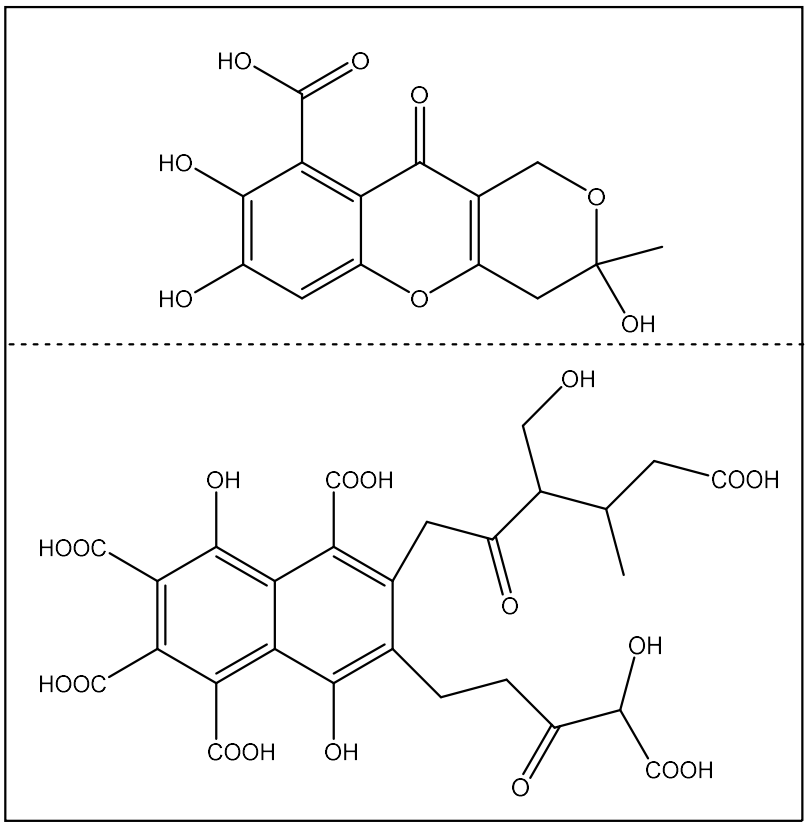

Figure 3.3: Two examples of fulvic acids, used as potential biostimulants.

For the entirety of the trial, the glasshouse growing environment was maintained at a minimum of 20°C daytime temperature, and 14°C at night. *Cultivar swift* tubers were planted one per pot in early January and left to develop for 16 days. The potato plants were watered regularly (at least once every 2-3 days, and given a standard tomato fertiliser feed weekly).

On the 16th day, the 40 potato plants were randomly assigned using the CRD model **(Section 3.2.2)** into 5 sets of 8 replicates.

One blank set was given a foliar application of tap water, whilst another set was applied with the **TAA(1)**-silicic acid formula. A third set was sprayed with a foliar application of fulvic acid, and a fourth set was sprayed with a formulation containing both fulvic and **TAA(1)**-silicic acid. The final set was sprayed on alternate weeks with the **TAA(1)**-silicic acid spray.

Figure 3.4: *Cultivar Swift* **potato** plants approaching maturity in glasshouse trials at Henfaes Research Station, Bangor University.

3.3.1.2: Results and discussion

The overall tuber yield results **(Graph 3.1)** appears to show no significant difference between treated and untreated plants. A contributing factor to the lower average overall yield within the 'red' silicic set was that one of the plants was damaged early in the trial, causing one of the stems to fail. This resulted in a significantly reduced yield of tubers from that replicate. The cause of the damage was unknown.

Graph 3.1: Box Plot analysis of marketable tuber yield (>25 mm diameter) of *cultivar swift* **potato** treated with a range of foliar sprays.

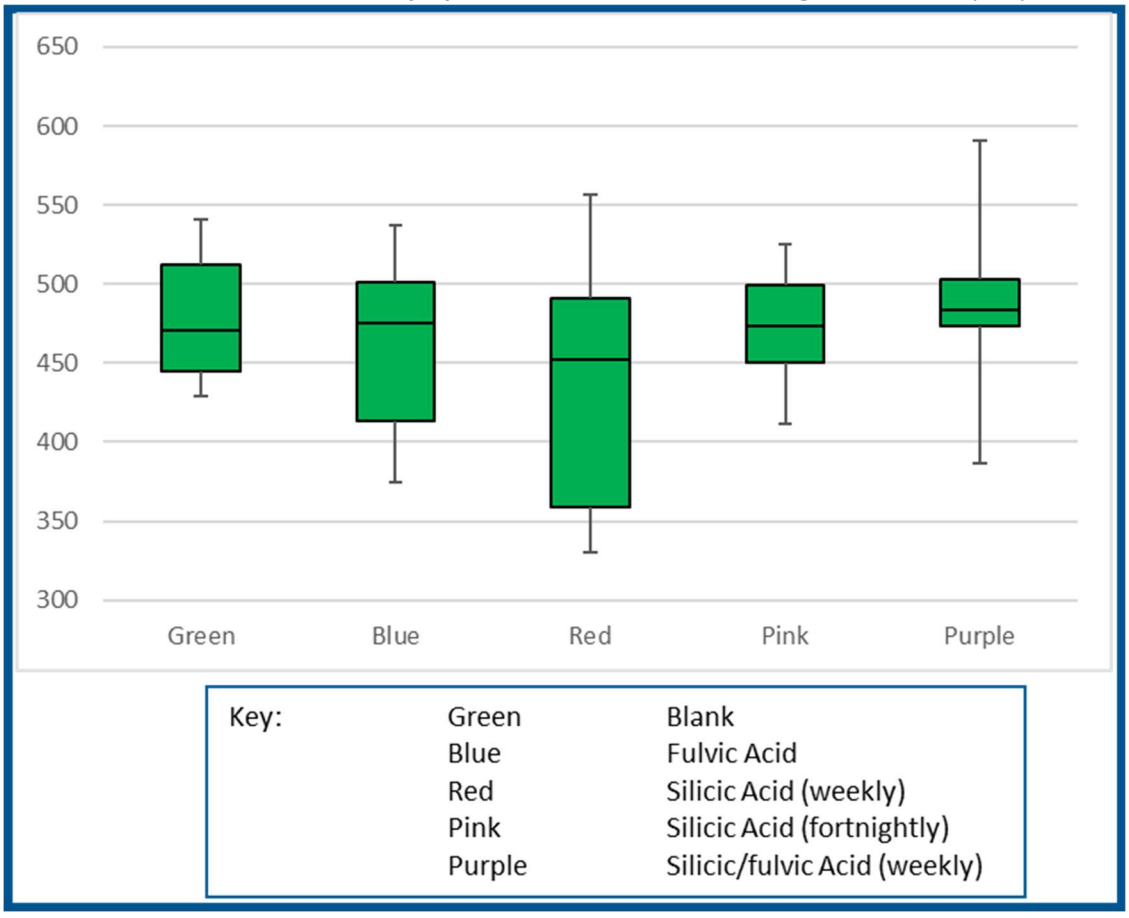

Tubers were also studied qualitatively for defects such as bruising on the skin or signs of damage from parasites. The frequency of damage to the potato skin or flesh was recorded for each size category of tubers. Skin quality tests were carried out by individually counting the scabs and areas of skin damage on each tuber, however a very small minority of tubers

contained significant areas of damage covering over 20% of the skin surface area. Overall, there was significantly more scabbing present on the skin of the control tubers relative to the four treated test samples **(Graph 3.2)**.

Graph 3.2: Tubers from each **potato** plant were collected together and the number of skin scabs were counted. The figures based on the average number per plant across the 8 replicates per treatment.

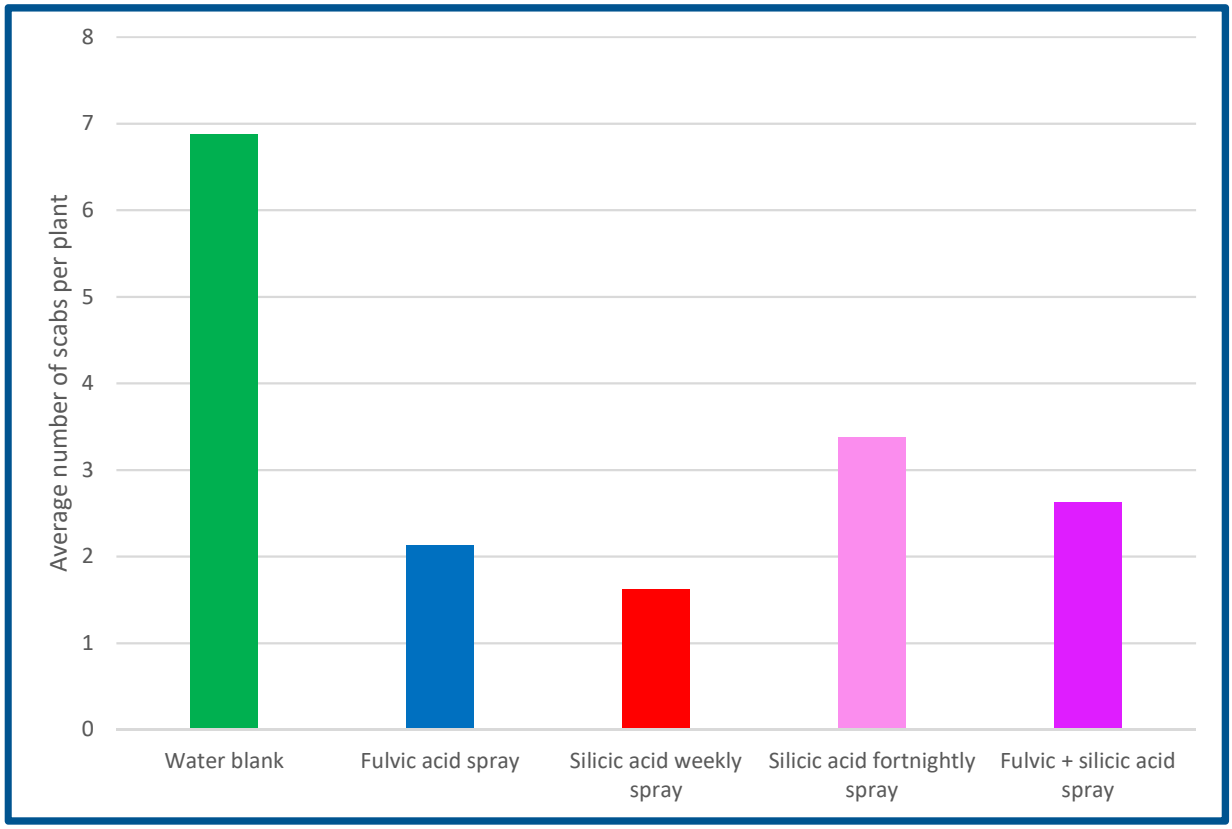

In addition to skin damage, the damage to tubers caused by pests needed to be recorded. While no insect-damaged tubers were identified in the untreated controls, a small number of insect damaged tubers were observed when they were treated with silicic or fulvic acid **(Graph 3.3)**.

Graph 3.3: The average number of tubers per **potato** plant damaged by insect bites across each set of 8 replicates.

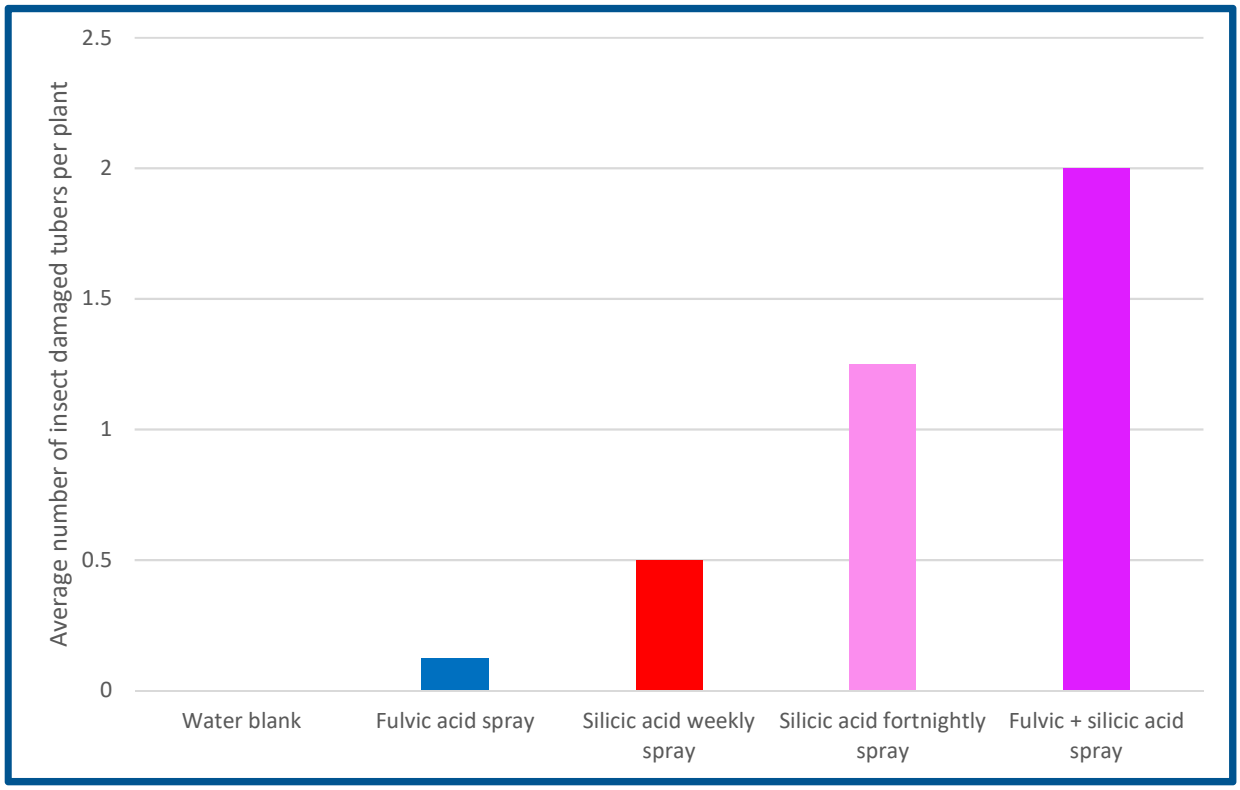

Tiny white slug-like insects were photographed on one of the damaged tubers and they were also seen on and inside other damaged tubers **(Figure 3.5)**. It is likely that they were originally present in the soil. It is difficult to predict if the foliar sprays were responsible for their emergence, or whether this was coincidental as a result of nutrient changes in the tubers.

Figure 3.5: In some cases, insect bites were found, with small insects (*Ca.* 3-5 mm in length) present on some of the affected tubers.

Based on the findings of the potato trial did not provide any evidence that **TAA(1)**-stabilised silicic acid, or fulvic acid provided any beneficial improvements to tuber yield. The nature of the trial provided some limitations that could have affected the outcome. For example, using potted potato replicates limited the amount of soil and growing space available for the tubers to develop. Tubers were growing throughout the available volume of the pot, with some exposed to natural light as they broke through the topmost layer of soil. Carrying out a future trial in large beds or in an open field may eliminate the possibility that tuber development was hampered by limited access to nutrients or by a lack of growing space.

Another potential factor to the lack of efficacy of the formulation regards the strength of the sprays. The formulations contained 11500 ppm "SiO_2", and were diluted 1:1000, providing *Ca.* 11.5 ppm SiO_2 in a spray. On average, each potato plant would have received approximately between 6 mL and 35 mL of foliar spray, depending on the week of spraying and the maturity of the plant. Therefore, the levels of silicic acid entering the plant would be extremely low. However, this should not be a problem for biostimulants or micronutrients. No assays for silicon or mineral content were planned for this trial, and therefore would be planned for in future experiments to test for uptake of silicon in the leaves.

3.3.2: Field Trial Two: Paragon Spring Wheat and Winter Cabbage glasshouse pot trial

3.3.2.1: Trial protocols

Based on the outcomes of the previous glasshouse potato pot trial **(Section 3.3.1)**, some modifications were made to the procedure to carry out similar pot trials on different crops. Some plant families have a greater need for silicon than others. Fibrous plants like grasses and monocotyledonous plants have a considerably higher uptake of silicon than the broader leaf dicotyledons. The previously studied *cultivar swift* potato is an example of a dicotyledonous plant.

In addition, a stronger spray of silicic acid was prepared. Boric acid was also incorporated into the formulation to study the possible synergy with silicic acid. An additional formulation was prepared containing PEG-20,000 stabilised silicic acid, due to the simpler nature of the formulation (*i.e.* the lack of need to carry out any synthetic procedures in making the compound). To increase the strength of the silicic sprays, the dilution factor was reduced; 2 mL of formulation would be diluted by 1 L of tap water. Boric acid formulations contained an

approximate ratio of 1:4:8 of B:Si:N, as boron can have phytotoxic effects at higher levels on some plant species and this needed to be prevented.

The chosen crops for this trial were the monocotyledon paragon spring wheat, and the dicotyledon winter cabbage. Both were chosen as the trial ran over the winter period over 4 months. Paragon spring wheat and winter cabbage seeds were pre-germinated prior to sowing. They were placed in flasks containing deionised water, and air was bubbled through them for 24 hours. They were then placed in dampened trays and left in a warm place for a further 3 days to germinate.

On the day of sowing, winter cabbage seeds that had begun to sprout were placed in individual 10 L pots, 2 inches deep in a growing medium of coconut coir as opposed to silicon-rich diatomaceous soils. Paragon spring wheat seeds were sowed three per pot in 1 L pots using the same medium. Some of the wheat seeds failed to develop into plants after sowing, so there was some variation in the number of successful shoots per pot. All plants were well-watered every 2 days and given a tomato feed weekly. Plants were grown in a heated glasshouse with a minimum temperature of 14^{o}C at night and a daytime minimum of 18^{o}C. Approximately halfway into the 4-month cycle, the temperature was raised to 22^{o}C to benefit other trials sharing the space.

Approximately 2 weeks after planting, when early leaves were presenting, the pots were randomly allocated a spray using a similar CRD model to the potato trial. Where possible, the paragon spring wheat pots were randomly assigned to treatments with an equal spread of

pots containing 1, 2 or 3 successfully emerged seeds in each treatment category, as the sharing of pot space and nutrients may influence on the foliar yield of individual plants.

There were 4 different treatment sets applied: these were a water blank, PEG-stabilised silicic acid, **TAA(1)**-stabilised silicic acid, and the **TAA(1)**-stabilised silicic acid with added boric acid. Leaves were sprayed to run-off three times per week after watering. It was found during the first spray application that the waxy leaves on the winter cabbage were hydrophobic and therefore repelled droplets from the sprays. This was resolved by adding a drop of detergent into the formulation, as this allowed the sprays to bypass the waxy layer. In future trials, specialist wetting agents should be added to formulations to avoid a repeat of this issue.

The plants were maintained in this manner for approximately 4 months, from late December to April. They were then allowed to dry out for 10 days, to aid for an easier root harvest. Fresh weights and dry weights were obtained by segregating roots and shoots of individual plants. The taproot of the cabbage plants was separated from the leaves and roots as it represented a large proportion of the mass.

All harvested cabbage plants were healthy and uniform in shape, with no signs of damage. Expired leaves, such as the early flag leaves, which were shed within the first few weeks, were retained in the soil and included in fresh/dry foliar weights where possible. Harvesting took place at the point where the cabbage heads had just started to develop, as at this point in plant development the flow of nutrients changes significantly and becomes more complicated to predict.

There was a significant aphid problem that presented in the wheat approximately 2 months into the 4-month trial. Aphid-killing sprays containing ~30% v/v isopropyl alcohol, ~70% v/v water, and few drops of household detergent were applied every few days. This was successful in extermination of the aphids without disruption to the foliar silicon sprays. However, the damage caused by the infestation had a significant influence on the success of this crop, and many of the stems were damaged, limiting the overall development of the plants. Of the total sample of wheat crops, only one plant fully matured to produce a healthy ear, although most had a healthy flag leaf after the final treatment.

Roots from each treatment category were collected by vigorous sifting from the dried soil. They were collected into treatment groups and an average weight was calculated from the total. After removal of soil, the roots were washed of any residues and left to dry in open air for 3 days to obtain a fresh weight. Upon 5 days of drying in a 60^{o}C oven, the dry weights were obtained.

3.3.2.2: Results and Discussion

Fresh and dry weights of the **cabbage** plants were obtained by segregating the leaves from the single stem and taproot. Each plant component was separately weighed. Cabbage plants generally lost between 50 and 65% of their total weight in water upon drying in an oven. **(Graph 3.4)** shows a set of box plots presenting the distribution of yields for each set of replicates.

Graph 3.4: The distribution of the total dried foliar weights (leaf, stem and taproot) for **winter cabbages** treated with four different foliar sprays.

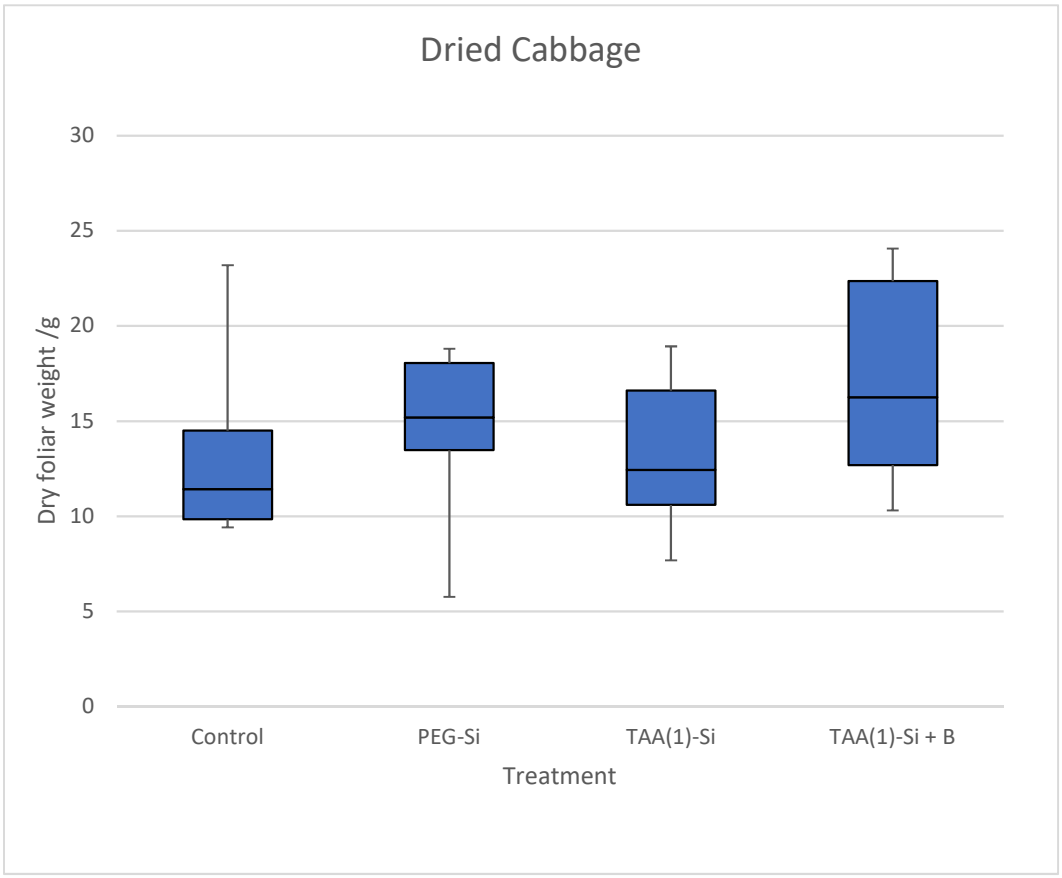

Notably, the top 50% of yields the **PEG-Si** treated cabbages, and the top 75% of the **TAA(1)-Si-B** formulations were higher than the top 25% of control plants. **TAA(1)-Si** and **PEG-Si** – treated plants did not show a statistically significant improvement in overall dry foliar yield, with T > 0.1. **TAA(1)-Si-B** treated plants resulted in a statistically significant improvement in yield (t = 0.027 for dry leaf yield, and t=0.035 for overall foliar yield). This suggests that the silicic formulations generally resulted in an improvement in foliar development, with average yields of dried plant matter increasing across the board **(Table 3.3)**.

Table 3.3: Average dried foliar yields of **winter cabbage** after spraying with several different treatments.

Treatment	Average Leaf dry weight /g	Average Stem dry weight /g	Total average dry foliar weight /g	% Change
Control	11.1	2.2	13.2	N/A
PEG + Si	11.7	2.8	14.5	+ 9.3%
TAA + Si	10.8	2.6	13.3	+ 0.8%
TAA + Si + B	14.2	3.0	17.2	+ 30.21%

This was somewhat surprising, as it is often stated that broadleaf dicotyledon species tend to have a low response rate to silicon micronutrients.[229] Adding boron to the formulations also appeared to raise the number of higher yields, but without a positive control spray containing boron and no silicon, it is difficult to tell if this was due to a nutrient response of boron or a result of the synergy with the silicic micronutrient spray.

The **wheat** foliage was separated from the roots and weighed dry and fresh as separate replicates. Wheat roots were also collected but were weighed together in batches per treatment and an average was calculated for each treatment. Only 10-25% of the fresh weight was lost upon drying, with the less healthy replicates losing less water than the healthier plants. There was an increase in yield in plants treated with **TAA(1)-Si** and **TAA(1)-Si-B** sprays, but a slightly decreased yield in the **PEG-Si** set when comparing the yield distributions to the water blank **(Graph 3.5)**.

Graph 3.5: The distribution of the dried yield of **wheat** (stem, leaf and ear) when treated with four different foliar sprays.

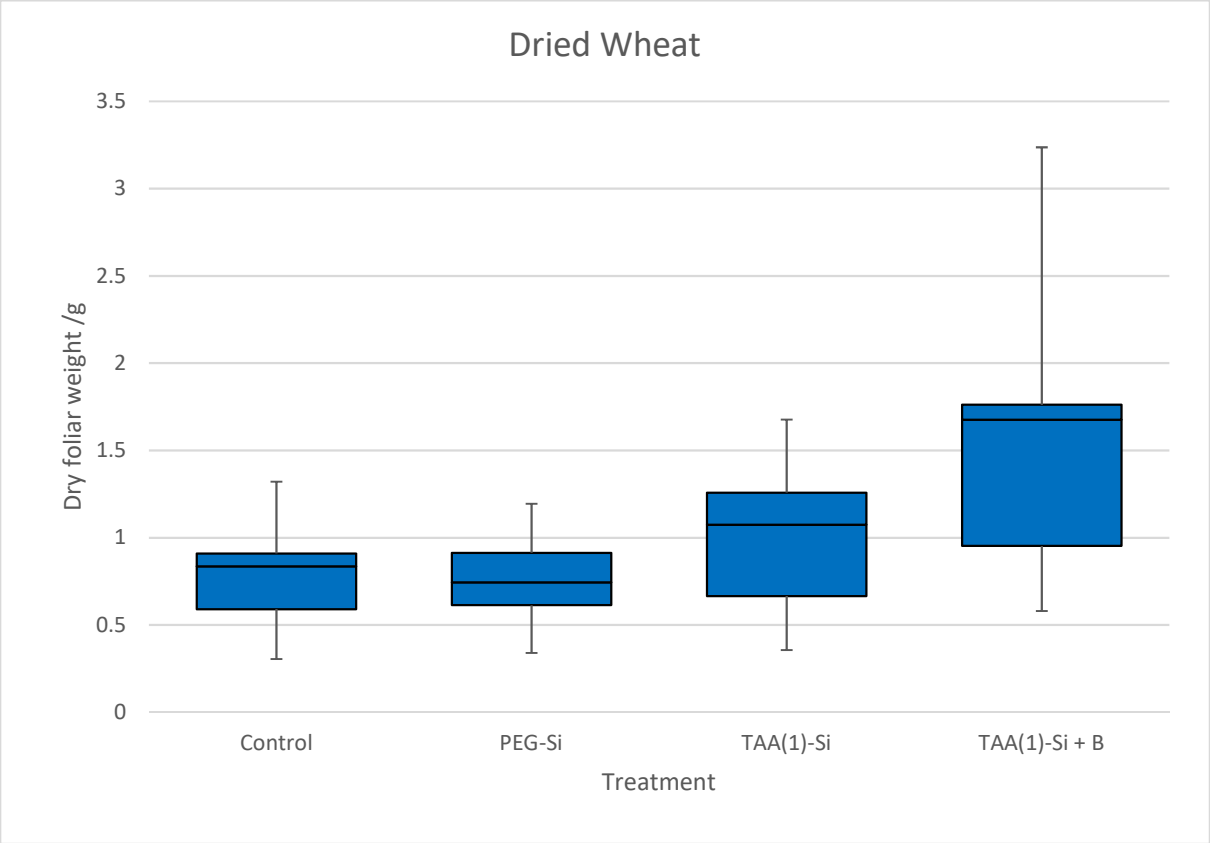

By far the most significant improvement (t= 0.35) was found in the **TAA(1)-Si-B** treatments, where approximately half of the replicates were of a higher dry weight than the maximum yield of any other plants in the study. It is likely that there may have been a boron deficit in the other plants, but no positive controls for plants treated with boron-only sprays were included to test this null hypothesis. A similar improvement in the root yield was seen for both **TAA(1)** foliar sprays. **(Table 3.4)**

Table 3.4: Average dried shoot and root yields per **wheat** plant.

Treatment	Average Dry shoot Weight /g	% Difference	Average dry root weight /g	% Difference
Water blank	0.82	N/A	0.19	N/A
Si + PEG	0.79	-3.8 %	0.18	-5.5 %
Si + TAA(1)	0.98	+19.5 %	0.25	+31.6 %
Si + B + TAA(1)	1.56	+90.2 %	0.28	+47.4 %

The yield data of roots and shoots for paragon spring wheat suggests a significant improvement in both **TAA(1)** formulations over the control replicates, but a slight decrease in the **PEG-Si** formulations. It is however difficult to conclude that the silicic sprays would have been as effective in a healthy crop. The damage to the crop caused by the aphids was too severe to render these results reliable enough to conclude the efficacy of the sprays based on yield alone. Samples of the dried wheat shoots will be tested for their mineral content and to see if the Si levels increase as a result of the foliar sprays to attempt to form a better conclusion.

3.5.3: Nutrient determination of plant material

Prior to analytical experiments on the mineral contents of the foliage, the dried stems and leaves were broken down into fine strips using a food blender. Several techniques and digestion methods were attempted to obtain some information on the nutrient content of the harvest. Attempts to digest wheat samples in concentrated nitric acid without further treatment proved unsuccessful; digest samples were subjected to the molybdenum blue method to attempt to measure trace silicon levels and there were no useful colour changes observed using this method. It is generally agreed that using HNO_3 digestions alone will not break down Si-O networks to solublise the silicon for analysis, and most postulated alternatives use HF or perchloric acid mixtures. These methods would not be permitted to use within our department.

An alternative method of dry ashing was carried out. Foliar samples were placed in an automatic grinder, to obtain fine powders. The powders were dried, and 0.2 g of powder was weighed into 20 mL furnace resistant glass vial (in triplicate). The vials were placed into a

muffle furnace and ashed at 500^{o}C overnight. The resulting ash was dissolved in 1 mL of warm 20% (w/w) HCl and vortexed. To this extract was added 9 mL of deionized water, with the dilution factor noted for future calculations.

The analyses performed included attempted colourimetric tests for Si, which provided no conclusive results for Si content. Silicon content was then explored by AAS analysis of the plant digests. There were some positive signs of an increased uptake of Si in both the treated cabbage and wheat samples relative to controls, however these results were unreliable, as precipitates settled in the plant extract solutions that may have contained undissolved silicon. TXRF analysis was carried out on powdered plant material, but the results of this were unreliable due to large variations within the triplicate sample sets. Results will be included in the experimental procedures (see **5.2.3.1(c)**), but will not be discussed further here.

3.3.3 Field Trial 3: Tomatoes grown in nutrient flow at IBERS (Aberystwyth)

3.3.3.1: Trial Protocols

Another area of interest was to see if foliar silicon sprays had any positive influence in hydroponics. In hydroponic growing environments, all of the nutrients are provided by a continuous liquid feed, with no solid growing medium (*i.e.* soil). Hydroponic crops tend to be more expensive and labour intensive, with a higher income per hectare than a crop grown in an open field. This leads to a higher demand for specialist fertilisers or nutrient feeds to improve the efficiency of the crop. Another advantage of carrying out a crop trial in a nutrient flow system is that any silicon that would have been present in the soil is eliminated from the trial, and can also be eliminated from the nutrient flow system. The hydroponic system contained all of the necessary dissolved nutrients for healthy plant development.

An early-stage crop trial was planned in which the *moneymaker* **tomato** variety would be grown in a nutrient flow system for 50 days to test if silicic sprays had a positive influence on the growth rate of early stage stem and leaf. Tomato seeds were sown in a 50/50 peat/sand medium and kept at 20^{o}C with light watering. After 9 days, the seeds were removed from the medium and placed into nutrient flow containers at one seed per pot. Plants were allowed to develop to their second true leaf stage, before the earliest germinators were removed from the study to establish a uniform crop. The remaining replicates were left to adapt to the nutrient solution for a further 20 days.

The 108 replicates were then randomly assigned a foliar spray, with an equal spread of foliar applications across the tanks similar to an RCBD experiment. There were 6 different treatment types in this trial: One control set were sprayed with just water. The positive controls sets included one with a diluted solution of **TAA(1)** with no micronutrients, one with a diluted solution of **TAA(1)** with boron, and one set were sprayed with a PEG-stabilised competitor product. The remaining replicates were either sprayed with **TAA(1) + Si**, or **TAA(1) + Si + B**. The strength of the sprays was increased to 1:300 formulation:water dilution, however this resulted in an acidic spray. KOH (1M) was added to these sprays to bring the pH to 6. 0.1% v/v Triton X-100 was added as a wetting agent to improve permeability into the leaf. Spray treatments were applied up to 6 times to run off over a 2 week window. 4 replicates from each treatment were removed from the tank on the day of the first spraying (without spraying), and after the first week. 5 replicates of each treatment were removed from the tanks in the following two weeks to obtain an incremental yield over 4 weeks. Every harvested

plant was initially weighed fresh as a full plant, before being separated into leaf, stem and root. Each fraction was dried and weighed separately to obtain dried yields.

3.3.3.2: Results and Discussion

The fresh leaf yield over 4 weeks (**Graph 3.6**) shows that none of the silicic sprays had a significant effect on the growth rate of the early foliage of the **tomato** plants. There was one exceptionally large plant among the water blank control set, but this can only be attributed to random error and was not discounted from the average yield. It was interesting to note that the competitor product also did not outperform the blank, despite the presence of additional micronutrients in their formulation.

Graph 3.6: Dry leaf yields for **tomato** plants harvested at weekly intervals in a hydroponic growing environment and applied with different foliar sprays.

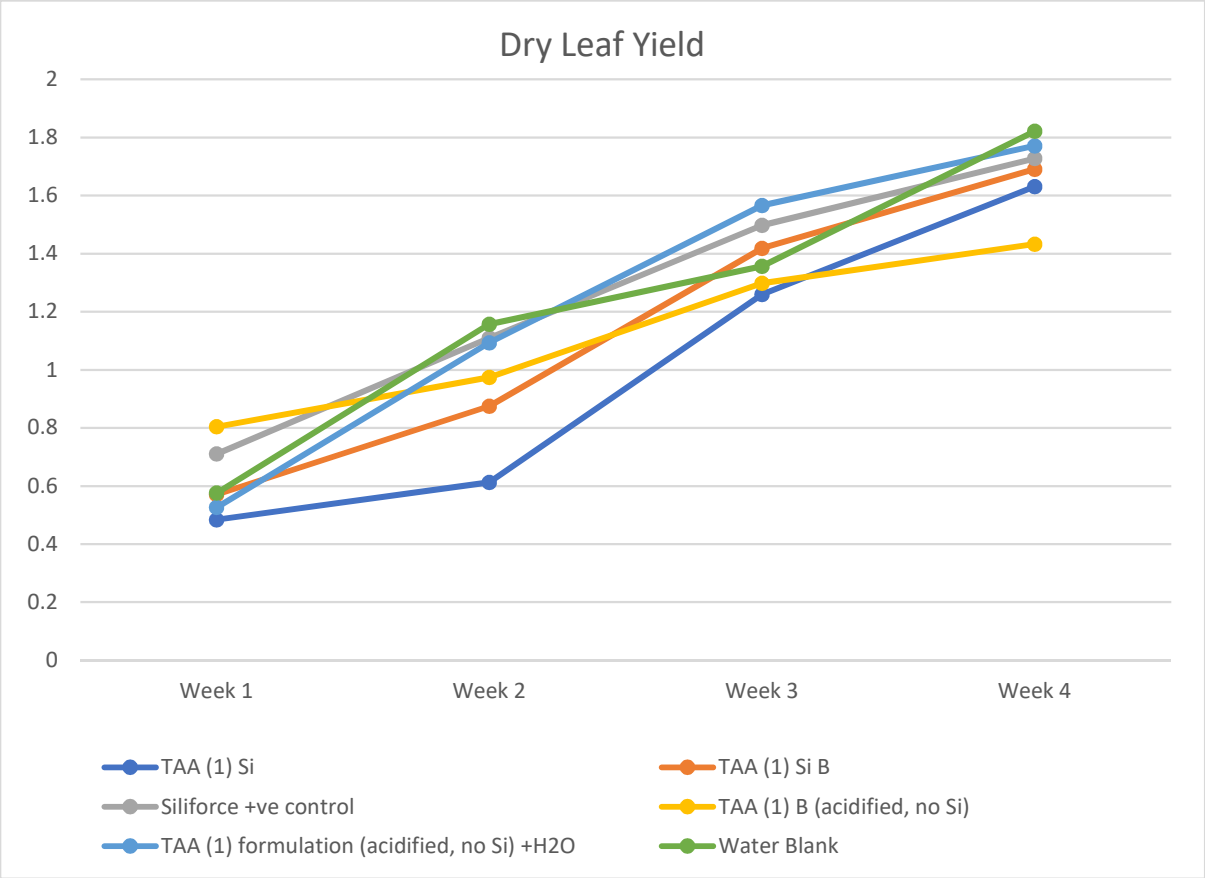

3.4: Concluding Remarks

Three separate crop trials have been carried out on a set of silicic sprays on 4 different types of crop; **potato**, **tomato**, **wheat** and **cabbage**. No significant improvement in growth rates or yields were reported in the **potato** trial, possibly due to the very low levels of silicon delivered to the plant as well as limited growing space in the potato pots. A similar conclusion was drawn from the **tomato** hydroponic trial, where no significant improvements were seen by any of the sprays, including a patented competitor. Results from the **wheat** and **cabbage** trials were more encouraging, with significant increases in foliar yield recorded for silicic sprays and further improvement when boron was added. Yield results from the **wheat** trial were positive, but lacked reliability due to the influence of pests on the health of the crop. The **cabbage** trial showed both an increase in foliar yield and an increase in silicon uptake which improved further when boron was added to the sprays.

In summary, from these initial experiments it is not possible to categorically state whether these stabilised silicic sprays have an overarching benefit to crop growth. More studies to be done with more formulation and crop varieties to make any broader conclusions regarding the efficacy of these sources of micronutrients for growth and marketability as fertilisers.

Chapter 4: Non-metal polyborates with substituted ammonium cations

Some of the work presented within this chapter has been published in the following journal articles:

M. A. Beckett, B. I. Meena, T. A. Rixon, S. J. Coles and P. N. Horton, *Molecules*, 2019, **25**, 53.[230]

M. A. Beckett, S. J. Coles, P. N. Horton and T. A. Rixon, *Phosphorus. Sulfur. Silicon Relat. Elem.*, 2019, **194**, 952–955.[231]

4.1: Introduction

4.1.1: Uses of polyborates

Polyborates (described as polyoxidoborates by IUPAC nomenclature) can exist as minerals in the Earth's crust, and a large number of synthetic derivatives of them have been prepared.[131,232] Polyborates have uses in the glass industry,[232] and are used as flame retardants, which can be applied to polymeric materials to improve thermal stability.[233] Zinc borates provide zinc and boron as micronutrients to crops while sodium borates are also commonly used to improve agricultural yields.[232] Additional properties have also been observed in some polyborates, including luminescence,[234–237] non-linear optical properties,[238] and they can also be semiconductors.[239] One of the most industrially important naturally occurring borates,[232] borax, $Na_2[B_4O_5(OH)_4]\cdot 8H_2O$, is used in cleaning products, pH buffers, and can form a slime-like viscous substance when mixed with products containing polyvinyl acetate, used in educational toys.

4.1.2: Structural features of polyborate systems

In **Chapter 1** it was stated that polyborates are comprised of two types of boron centre; the $B(OR)_3$ uncharged trigonal centre, where R is either a hydrogen or an additional boron atom; or the $B(OR)_4^-$ negatively charged tetrahedral centre. The most common fragment present within a polyborate lattice is the boroxole ring (B_3O_3),[131] which is particularly prevalent in the well-known pentaborate anion, $[B_5O_6(OH)_4]^-$ in which two boroxole rings are fused together through a central spiro $[BO_4]^-$ unit **(Figure 4.1)**. Similar cases are observed throughout polyborate chemistry, and will be discussed in more detail in the following sections.

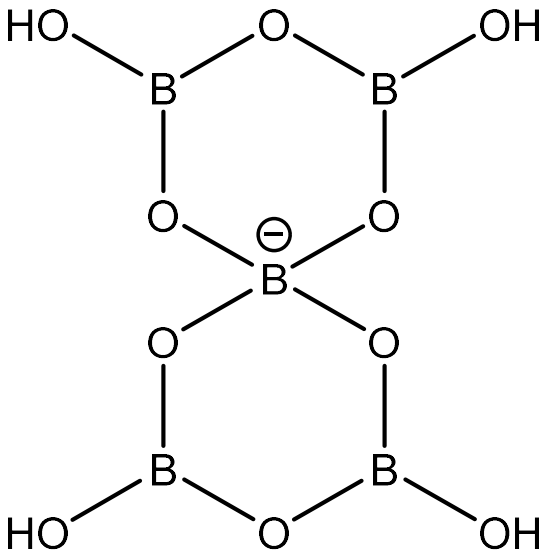

Figure 4.1: The isolated pentaborate(1-) anion.

To counterbalance the negatively charged borate anions, a cation must be present. The cation exhibits a structure-directing effect onto the borate network, giving rise to a variety of self-assembled crystalline networks upon crystallisation from aqueous solution. Many naturally occurring borate minerals such as zinc borate, $Zn[B_3O_4(OH)_3]$, require only a metal cation.[240] Polyborates have been reported with transition metal complex cations including Ni, Fe, Co, Cu and Zn.[131,241–245] These examples incorporate metal complexes into vacant spaces in the lattice, with ligands sometimes forming templating hydrogen-bonding interactions with the borate lattice. In a few cases, the polyborate can coordinate directly to the metal complex as a ligand.[244] This can happen when labile transition metal complexes undergo rapid ligand exchange with the borate species in solution.[246]

Borate units are able to form a polymeric lattice due to hydrogen bonding interactions between donating hydroxyl groups and accepting oxygen atoms on adjacent borate units. Numerous motifs are possible, including large ring systems, cages or simple chains.[131] The repeating 2D patterns can condense further into more complex 3D units through loss of H_2O

and additional hydrogen-bonding between layers. Additionally, hydrogen-bonding "spacer" solvent or boric acid molecules can further complicate the borate lattice.[247] These examples often have unique crystal structures that are more difficult to classify using established labelling schemes.[248]

In solution, borate species exist in a dynamic equilibrium of a number of fragments.[249] In order for polyborates to self-assemble through crystallisation, a slightly alkaline environment needs to be established.[249] Boric acid is more likely to crystallize if the solution is neutral or acidic. Therefore, in order to template the formation of polyborate anions, a cation must be introduced that is a base, which is able to raise the pH. For example, an organic amine can be methylated, decreasing its pK_b value, raising its basicity, and raising the likelihood of forming a polyborate when introduced to a solution of boric acid. Exhaustive methylation of an amine would form a salt, which would then require a metathesis procedure to obtain the basic hydroxide salt.[131]

Hydrated polyborate compounds were originally classified based on a series of rules developed by Christ and Clark.[250] Each boron centre is defined as a Fundamental Building Block (FBB), and each block is termed either as a trigonal centre Δ, bonded to three oxygen atoms, or a tetrahedron, T, bonded to four oxygen atoms. Taking the pentaborate $Na[B_5O_6(OH)_4]\cdot H_2O$ **(Figure 4.1)** as an example, there are four trigonal boron centres and one tetrahedral boron centres per borate unit, with the total number of FBB = 5. This example can be classified as 5:(4Δ + T) using shorthand notation.

While the original shorthand system described the number of trigonal and tetrahedral sites in a borate anion, it did not explain the shapes or topographies of the borate anions, with some isomeric compounds providing identical notations. Burns *et al.*[251,252] expanded upon the labelling system by labelling individual boroxole (B_3O_3) rings separately, and adding descriptors to show how they are bound to adjacent boroxole units. Using the previous $Na[B_5O_6(OH)_4]\cdot H_2O$ example, the Burns' descriptor would be 4Δ1□:<2Δ□>-<2Δ□>. This notation states that a pentaborate(1-) anion consists 4 trigonal boron centres, and one tetrahedral boron centre, featuring two boroxole rings, featuring two trigonal boron sites and one tetrahedral boron site each, and the two boroxole rings are linked together *via* one boron centre.

4.1.3: Synthetic and naturally occurring borate anions

Borate anions vary in the number of boron atoms per unit, as well as the charge provided per unit. They can occur as "isolated" systems, where the borate does not directly bond or coordinate to a cation, or they can coordinate directly to a cation.[131] In addition, "polymeric" species are possible, where a borate FBB is bonded directly to an adjacent FBB *via* oxygen bridges. "Polymeric" borate anions are categorised and described using separate notation to "isolated" systems, and will not be discussed further in this thesis. When oxygen bridges are not present, 'isolated' polyborates are often interconnected by hydrogen bonds to form a giant lattice.

(a) The monoborate anion

Monoborates differ from other borate systems due to the manner in which they are formed. Boric acid behaves as a Lewis acid when mixed with a suitable cation in aqueous solution. However in very rare cases, boric acid can behave as a Bronsted acid, capable of forming monoborate salts. The conjugate base anion of boric acid, $[BO(OH)_2]^-$ **(Figure 4.2)** has been observed by mixing boric acid and tetramethylammonium hydroxide with 2 molecular equivalents of urea to form a urea inclusion compound $[(CH_3)_4N][BO(OH)_2]\cdot 2(NH_2)_2CO\cdot H_2O$.[253]

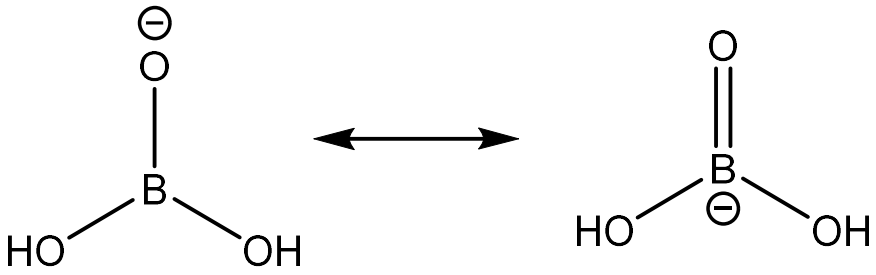

Figure 4.2: The monoborate anion $[BO(OH)_2]^-$

The lattice water plays a key part in the self-assembly of the crystalline network, which consists of ribbons of urea molecules hydrogen-bonded to ribbons of $[BO(OH)_2]^-$ anions. The tetramethylammonium cations fill the channels formed by the borate lattice.

(b) Triborates

The triborate(1-) anion **(Figure 4.3)** is uncommon , but has been reported with the organic cations $[H_3N(CH_2CH_2)NH_3]^{2+}$,[254] $[HOCH_2CMe_2NH_3]^{+}$,[255] and bis(triphenylphosphine)iminium.[247] Zinc borate, $Zn[B_3O_4(OH)_3]$ also occurs as a triborate. [232,240]

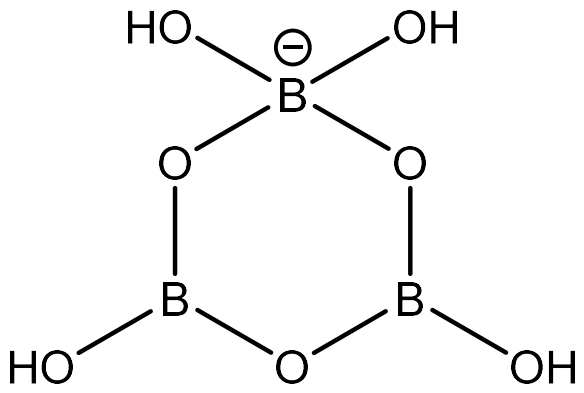

Figure 4.3: The isolated triborate(1-) anion, described as 3:(Δ+2T) or <Δ2□>

(c) Tetraborates

The tetraborate(2-) anion **(Figure 4.4)** is well known from its presence in sodium tetraborate, $Na_2[B_4O_5(OH)_4]\cdot 8H_2O$. It is one of the less common anions found partnered with a non-metal cation and this is possibly due to its small size but higher charge. It has been reported as part of a unique mixed-anion 1,2-ethylenediammonium salt $[H_2en]_2[B_4O_5(OH)_4][B_7O_9(OH)_5]\cdot 3H_2O$,[256] which also contains a rare example of a heptaborate anion. It has also been successfully coupled with the cyclohexane-1,4-diammonium cation in the salt $[C_6H_{10}(NH_3)_2][B_4O_5(OH)_4]\cdot 2.5H_2O$.[257] In both cases, the tetraborate(2-) anion's charge must be compensated for by protonation of both nitrogen atoms in the diammonium cations, since a tetraborate lattice typically provides only small vacancies to accommodate these cations.

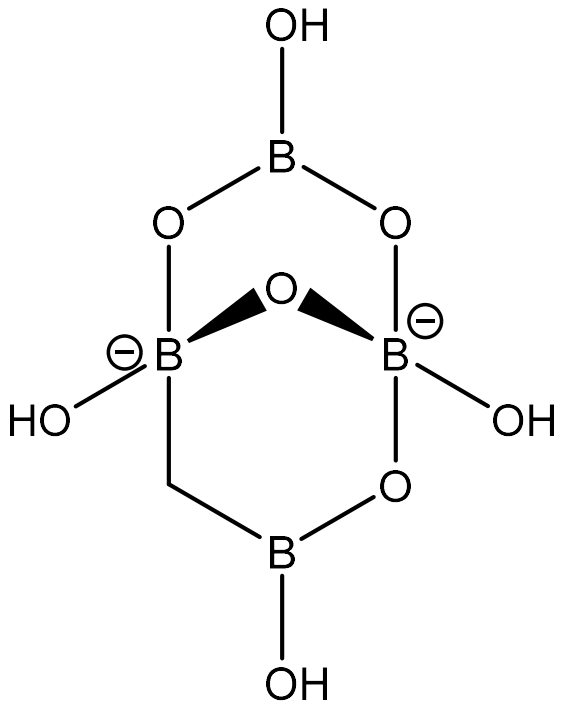

Figure 4.4: The tetraborate(2-) anion above is described as 4:(2Δ+2T) or 2Δ2□:<Δ2□>=<Δ2□>.

(d) Pentaborates

Pentaborates represent the most easily formed borate species and are easily prepared in standard laboratory conditions in the presence of a suitable cation.[248,258,267–271,259–266] The pentaborate anion **(Figure 4.1)** forms favourably in aqueous solution at moderate pH, which is commonly attained when a non-metal cation such as an alkyl amine or a hydroxide salt is stirred with 5 equivalents of boric acid in aqueous solution. This is the most favoured (1-) anion in the borate series due the conveniently located hydrogen bonding sites providing scope for lattice growth relative to the alternative triborate anion.

Each pentaborate anion is responsible for 4 H-bond donors, *via* the four $^{-}$OH groups on each of the corners of its spiro bicyclic structure. One of the more easily recognisable pentaborate hydrogen bonding systems was first described by Schubert as the "α,α,α,β" pentaborate motif.[248] Such notation is based upon the positions of the oxygen H-bond acceptor on the adjacent molecules **(Figure 4.5)**.

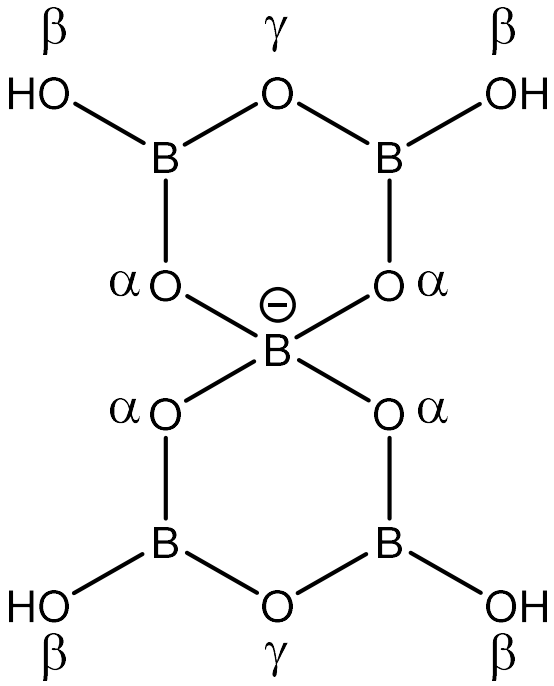

Figure 4.5: The pentaborate anion has shorthand descriptors of 5:(4Δ+T) or 4Δ1□:<2Δ□>-<2Δ□>. Each oxygen atom represents a potential H-bond acceptor site on the pentaborate(1-) anion, and are classified by Schubert as either α, β or γ.[248]

Some examples of these types of structures were obtained during the project and will be explained further in the results and discussion section **(Section 4.2)**. There is often a symmetry in the manner that α H-bonding interactions occur, which allows adjacent pentaborate anions to donate H-bonds to each other in a reciprocated fashion with the formation of an 8-membered-ring system between anions. The nature of the three reciprocated α,α,α

interactions allows each borate unit to form a “T-shaped junction”. This leads to an ordered lattice that appears as a 2-dimensional plane when viewed along the correct crystallographic axis. These planes are connected to adjoining layers in the third dimension by β or γ H-bonds. Cations are formed in the vacant channels to counterbalance the charge of the borate anions.

(e) Hexaborates

The hexaborate(2-) anion is unusual in that it contains a positively charged trivalent oxygen bridge in the centre of the molecule, linking three anionic tetrahedral boron atoms **(Figure 4.6)**.[131] There are no reported examples of synthesised hexaborates with non-metal cations, and has never been obtained in an “isolated” form (*i.e.* not coordinating to a cation). However, it has been successfully coordinated directly to a Co(2+) ion in the [1-cyanopiperazinium][Co{$B_6O_7(OH)_6$}$_2$] salt.[272]

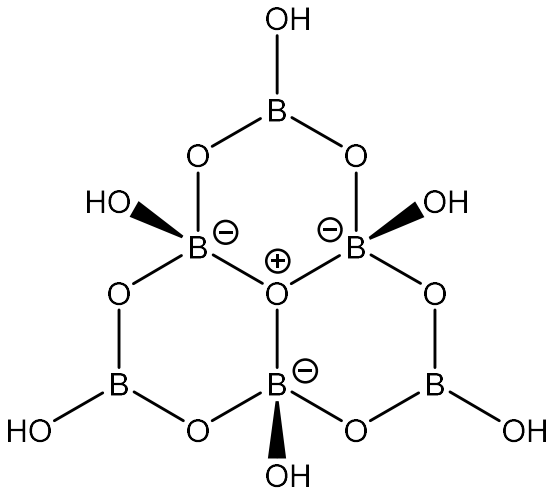

Figure 4.6: The hexaborate(2-) “O^+” anion, described as 6:(3Δ+3T) or 3Δ3□:[ϕ]<Δ2□>|<Δ2□>|<Δ2□>| using shorthand notation.

(f) Heptaborates

Although uncommonly reported in the literature, there are three different topologies of heptaborate anion. There are two different isomeric examples of heptaborate(2-) anions **(Figure 4.7)**, and are distinguishable using descriptor notation. One isomer resembles an 'extended' pentaborate anion, forming a "chain"-like structure of three boroxole rings.[273] The other example, known as the "O^{+}" isomer,[274] is similar to the hexaborate(2-) anion, with three tetrahedral boron anions bridged to a formally positively charged three-coordinate oxygen. The remaining 4 boron atoms are trigonal.

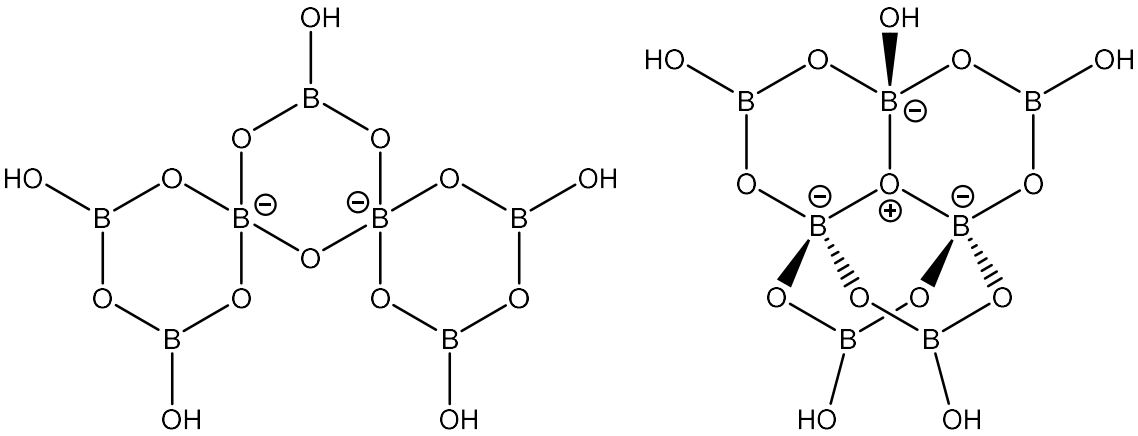

Figure 4.7: The heptaborate "chain" isomer and the "O^{+}" isomer, classified as 7:(5Δ+2T) or 5Δ2□:<2Δ□>-<Δ2□>-<2Δ□>, and 6:(3Δ+3T)+Δ or 4Δ3□:[ϕ]<Δ2□>|<Δ2□>|<Δ2□>|=<Δ2□>, respectively

There is also one example of a heptaborate(3-) anion,[243] which has been isolated with a cobalt complex cation. This example is almost identical to the chain-like example, with the exception of an additional 4-coordinate boron centre on the outer edge of one of the boroxole rings. This example is classified as 7:(4Δ+3T) or 4Δ3□:<2Δ□>-<Δ2□>-<Δ2□> using shorthand notation.

(g) Octaborates

Isolated octaborate(2-) anions are also uncommon, and an example of one is found with a non-metal cation in $[H_3N(CH_2)_7NH_3][B_8O_{10}(OH)_6]\cdot 2B(OH)_3$ **(Figure 4.8)**. [248] This example could be described as a pentaborate(-1) anion linked to a triborate(1-) anion *via* condensation of the two polyborates, liberating a water molecule to form a bridging oxygen.

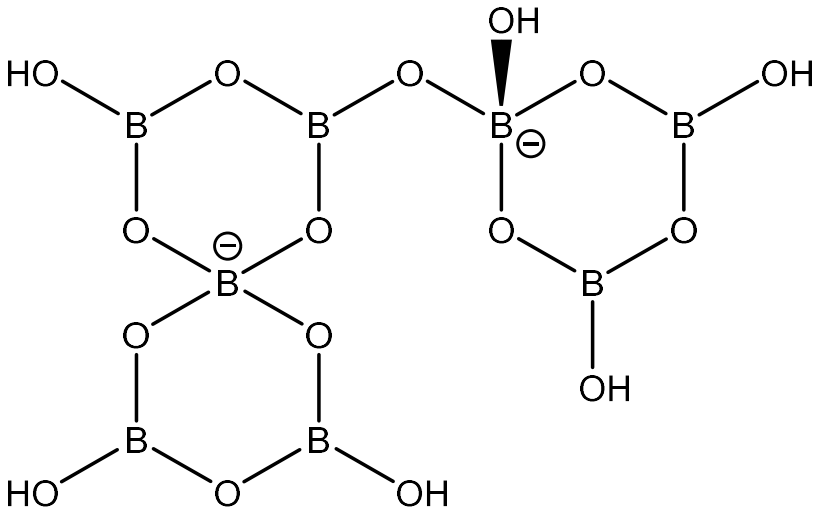

Figure 4.8: The octaborate(2-) anion, classified as a pentaborate anion bonded to a triborate anion, 5:(4Δ+T)+3:(2Δ+T) or 6Δ2□:<2Δ□>-<2Δ□><2Δ□>

(h) Nonaborates

The isolated nonaborate(3-) ion **(Figure 4.9)** is uncommon due to its high charge-size ratio, providing limited vacancies for low charged cations to sit. Therefore only small, strongly basic cations such as guanidinium or imidazolium have been successfully partnered with them.[275,276] In both examples, three protonated cations were required per nonaborate(3-) anion, demonstrating how tightly-knit this lattice would be for the templating cation.

The nonaborate extends further from the chain-like heptaborate example to feature four boroxole rings fused together by three tetrahedral anionic boron centres.

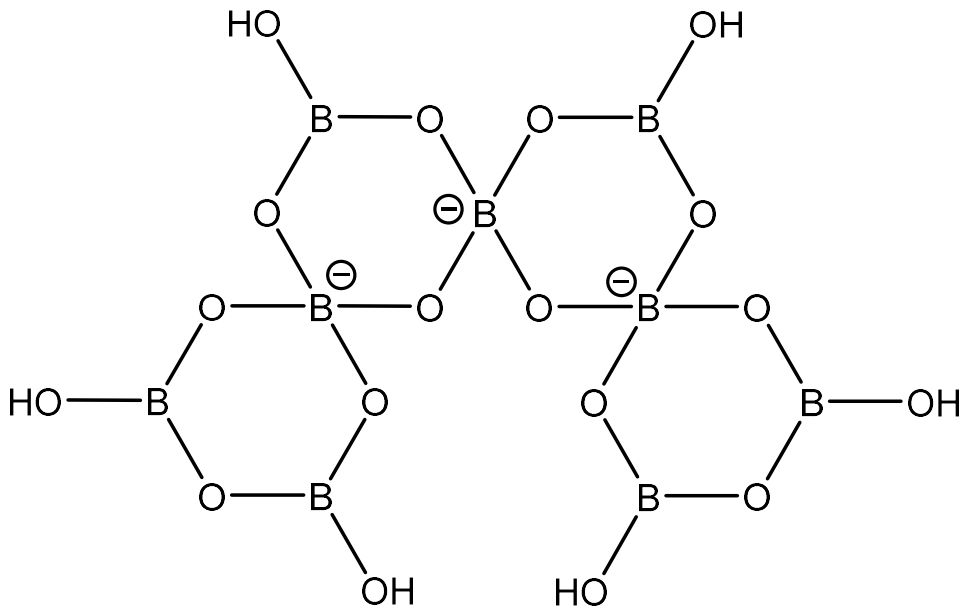

Figure 4.9: The nonaborate(3-) anion classified as an extended chain of 4 boroxole rings, or 9:(6Δ+3T) or 6Δ3□:<2Δ□>-<Δ2□>-<Δ2□>-<2Δ□>

(i) Large polyborate systems

There are a few examples of extended isolated borate systems with larger overall charges **(Figure 4.10)**. There are a few examples of dodecaborate(4-) or dodecaborate(6-) anions with metal cations.[277] The tetradecaborate(4-) anion has been prepared in a series of non-metal cation salts including $[H_3N(CH_2)_nNH_3]_2[B_{14}O_{20}(OH)_6]$ (where n = 2, 3, 4 or 6).[239,273] The tetradecaborate(4-) anion has also been prepared with a non-metal cation to form $[H_2dien]_2[B_{14}O_{20}(OH)_6]$.[271] These examples resemble two chain-like heptaborate(2-) anions, linked together by 2 oxygen bridges to form a larger ring structure.

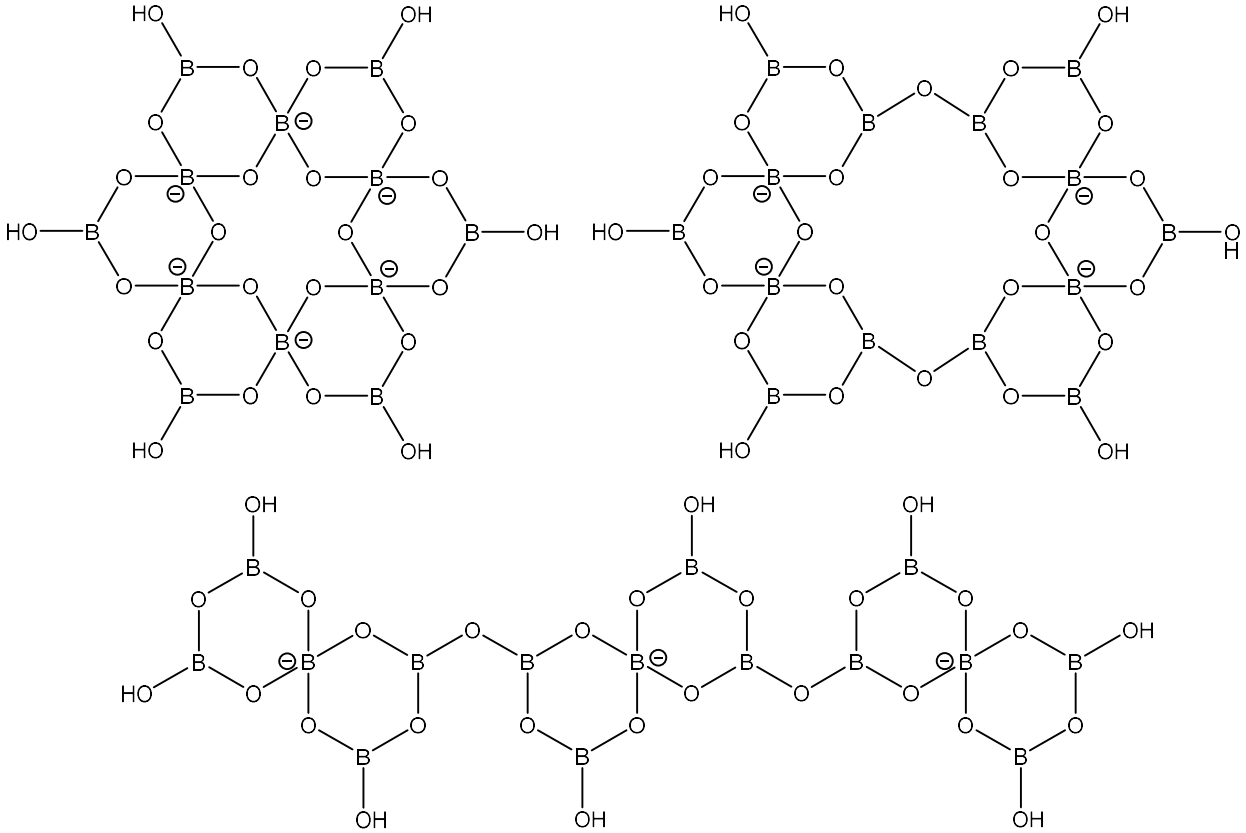

Figure 4.10: Isolated dodecaborate(6-) anion {3:(Δ+2T)}$_6$, {Δ2□:(Δ2□)-}$_6$; the isolated tetradecaborate(4-) anion {7:(5Δ+T)}$_2$, (5Δ2□)$_2$:(<2Δ□>-<Δ2□>-<2Δ□>)$_2$; and the isolated pentadecaborate(3-) anion 5:(4Δ+T)+5:(4Δ+T)+5:(4Δ+T), 12Δ3□:<2Δ□>-<2Δ□><2Δ□>-<2Δ□><2Δ□>-<2Δ□> consisting of three pentaborate(1-) anions bridged in a chain by oxygen atoms.

The pentadecaborate(3-) anion resembles three pentaborate(1-) anions condensed together in a chain *via* oxygen bridges. This example is a naturally occurring mineral, ammonioborite,[278,279] $[NH_4]_3[B_{15}O_{20}(OH)_8]\cdot 4H_2O$. It is formed when three pentaborate(1-) anions undergo a condensation reaction, releasing two water molecules and forming the oxo-bridges.

(j) Preparative methods for borate salts

The most common pentaborate(1-) anions are generally expected products at room temperature, in a pH ~ 8 solution of boric acid with a suitable cation.[131] This anion is most well-suited to forming rigid hydrogen-bonding lattices, as it can easily form ordered channels to accommodate the occupying cations.[131] In order to obtain more uncommon borate species, the reaction conditions need to be adjusted.

Using a small cation with higher charge, *i.e.* a transition metal complex, can force polyborate products to form with lower boron-to-charge ratios, such as the tetraborate $[Co(en)_3][B_4O_5(OH)_4]Cl.3H_2O$.[280] This example utilizes a Co^{3+} complex cation to form a tetraborate(2-) anion with an additional Cl^- anion balancing the overall charge. Similarly, small organic strong bases such as guanidinium can template borates with a lower boron-to-charge-ratio as seen in the nonaborate(3-) anion.[275] Such rarer borate fragments become more favoured in equilibrium in more alkaline solutions.[249] Some procedures incorporate non-participating miscible solvents to raise the pH of the solution, for example pyridine.[271,281,282]

The temperature of the crystallising solution can also impact on the type of polyborate formed.[133] Higher crystallisation temperatures can be achieved using a solvothermal procedure.[242,268,275,283,284] In such a procedure, the boron source and a suitable cation are mixed in a very small volume of solvent, often in the presence of pyridine, in a sealed tube.[271] At room temperature, these reagents are insoluble in the low volume of water, but at temperatures above 100^oC these reagents are soluble and the equilibria of borate fragments can be established. The sealed vessel containing the reagents is then allowed to cool after several days at a controlled rate. The polyborate crystallises slowly from solution at the higher

temperature. These higher temperature solvothermal procedures often give interesting and unusual products, although their synthesis is less often by design.

4.2: Results and Discussion

4.2.1: Synthesis and characterisation of new polyborate salts

A total of 27 new polyborate salts were prepared during this project using non-metal cations. Seventeen of these salts were characterised crystallographically, by Dr P. N. Horton at the UK National Crystallography Service, Southampton. Crystallisations were carried out at room temperature under standard pressure. Several solvothermal syntheses were attempted in parallel to these studies, but pure crystalline products could not be achieved.

4.2.1: Attempted preparation of polyborates using the monocations TAA(1) - TAA(3)

As substituted choline derivatives were the main focus in the TAA series of silicate formulations in **Chapter 2**, the initial aim here was to see if these cations were capable of forming polyborate salts. The initial formation of the choline derivatives from glycidol provided them in their hydroxide salt form. This is beneficial as no ion-exchange is required to prepare the compounds for an acid-base reaction with boric acid. Five molecular equivalents of boric acid (calculated using the previous acid-base titrations of **TAA(1)** -**TAA(3)**) were dissolved in warm deionised water and added to the alkaline cationic solution. After several hours of stirring, the solvent was removed under reduced pressure to form crude white powders.

Analysis of the crude powders by ^{1}H and ^{13}C NMR spectroscopy showed consistency with the spectra of the original cations. The ^{11}B spectra however showed unexpected mixtures of boron-containing species. For example, ^{11}B NMR spectrum of the TAA(1) pentaborate powder identified 5 separate signals.

Three signals, at 19.0 ppm (75% abundance), 13.1 ppm (14.3% abundance), and 1.2 ppm (3.1% abundance) indicate fragments of the commonly published pentaborate anion, as was the dominant product.[249,258–260,285] Further evidence of pentaborate speciation was present within the FT-IR spectrum of a sample of the powder. Signals at 1103 cm^{-1}, 1028 cm^{-1}, 923 cm^{-1}, 783 cm^{-1}, 696 cm^{-1} are widely attributed to B-O asymmetric stretching and B-O ring stretching, with a signal at 923 cm^{-1} being particularly diagnostic of pentaborate anions.[254]

The remaining signals at 10.4 ppm (2% relative abundance), and 6.1 ppm (6% relative abundance) were consistent to literature reports of mono-chelate and a bis-chelate of boron by the diols respectively **(Figure 4.11)**.[286]

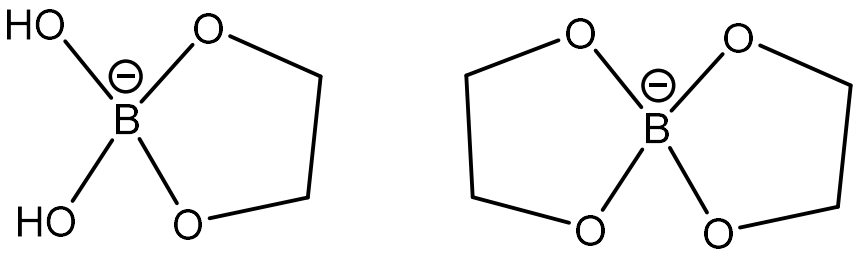

Figure 4.11: Examples of the mono- and bis-diol boron chelates found when **TAA(1)**-**TAA(3)** were added to a solution of boric acid.

Attempts to recrystallize these amorphous powders to form their crystalline polymorphs were unsuccessful. After several days of slow evaporation at room temperature, crystals formed around the rim of the sample vials containing only boric acid. ^{1}H and ^{13}C NMR spectroscopy showed that no organic cation was present in the crystals. Several crops of crystals of boric acid formed from the evaporating solutions, until the solvents were completely removed to leave viscous liquids. It is likely that the chelate species are favoured in solution equilibria, and any excess boric acid is crystallised out as the saturation limit is approached. The remaining viscous oils remained as such indefinitely and contained mixtures of the mono- and bis-chelates.[286] At this point, repeat experiments with further TAA cations were discontinued.

4.2.3: Preparation of polyborates using C_2- or C_3-linked bis(alkylammonium) dications

It was still of interest to attempt to synthesise some novel borates using the alkylated ammonium cations as key components. It was highly likely that the presence of two adjacent hydroxyl groups on the cations was limiting the ability of the TAA cation to crystallise a borate structure. The hydroxyl groups were structure-directing monoborate chelates *via* hydrogen bonding as opposed to promoting the formation of isolated polyborates. Potential alkylated amines have been identified that do not include such additional functionality.

The candidates of interest **(Scheme 4.1)** are similar cations to some existing published structures,[248,287] as well as some unpublished work in the research group, but have not been explored in their methylated forms. Methylation of tertiary amines is relatively easy *via* nucleophilic addition at each amine using iodomethane,[288] with the fully methylated iodide salts crystallising as a synthetically pure form readily from refluxing acetonitrile. These iodide

salts can then be converted into the necessary hydroxide form for an acid-base reaction with boric acid by making use of an ion exchange resin in the $(OH)^-$ form.[258] The resulting hydroxide forms can be reacted with variable amounts of boric acid to potentially obtain a range of polyborate products.

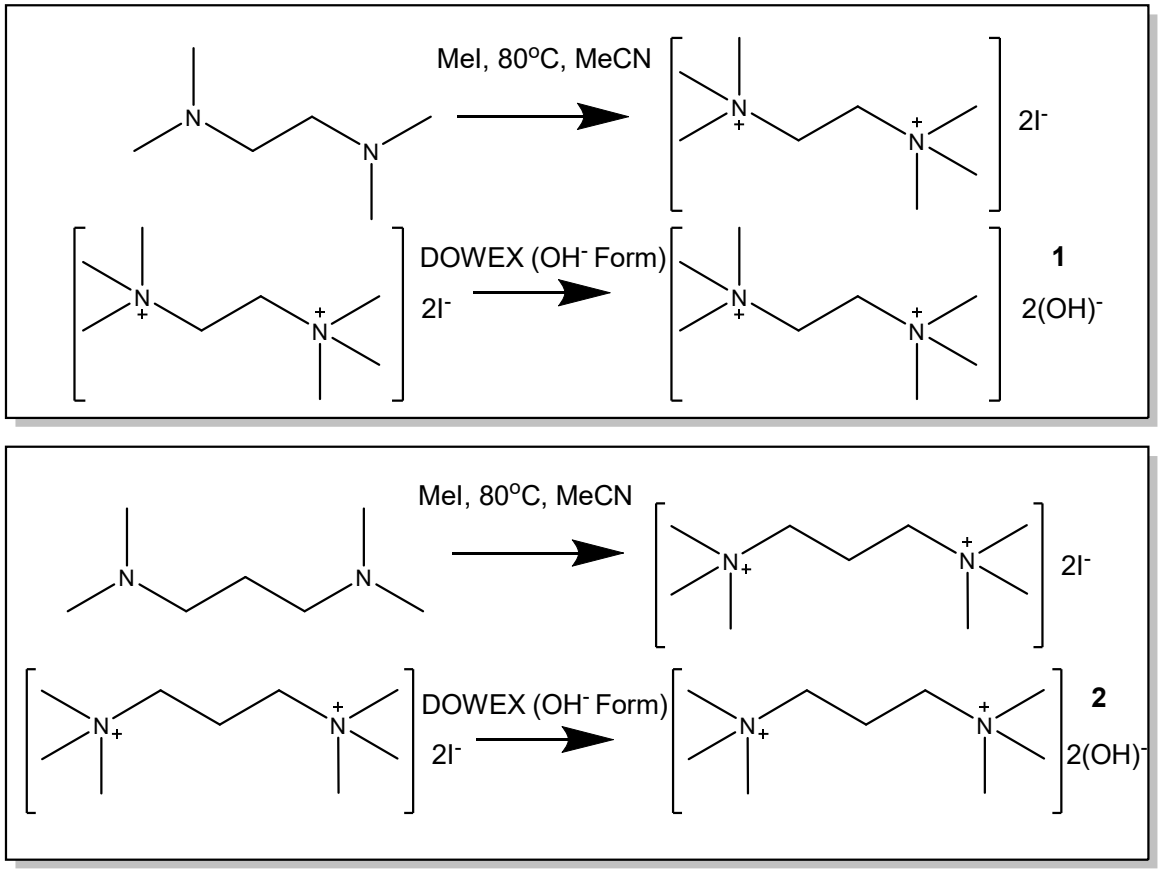

Scheme 4.1: Preparation of bis-(quaternary) ammonium hydroxide salts from their bis-(tertiary) amine analogues.

N,N,N',N'-tetramethylethylenediamine and *N,N,N',N'*-tetramethyl-1,3-diaminopropane were identified as suitable starting materials. Both candidates were methylated using excess iodomethane to form *N,N,N,N',N',N'*-hexamethylethylenediammonium diiodide salt, and the *N,N,N,N',N',N'*-hexamethyl-1,3-propanediammonium diiodide salt in quantitative yields by precipitation of the salts from acetonitrile upon cooling the reaction solution in an ice bath. These salts are dissolved in water and added to an ion exchange resin $(OH)^-$ form, with a

minimum of two “equivalents” of activated resin required to exchange both iodide anions on the diamine to form the hydroxide salts **1** and **2**.

After ion exchange, **1** was added to 3 equivalents of boric acid in water. The solution was concentrated to approximately 7 mL by rotary evaporation of the solvent, and then transferred to a sample vial and left to slowly evaporate at room temperature. X-ray quality crystals formed after 7 days of standing. ^{11}B NMR provided broad signals ranging from 11.7 ppm to 7.4 ppm (96%), and a small signal at 1.3 ppm (4%). These represent a strong correlation to previous work carried out by Salentine on aqueous solutions of potassium tetraborate.[249] The structure was confirmed by single-crystal XRD as the tetraborate(2-) salt $[(CH_3)_3N(CH_2CH_2)N(CH_3)_3]$ $[B_4O_5(OH)_4]\cdot 2H_2O\cdot 2B(OH)_3$, **(1a) (Figure. 4.12)**.

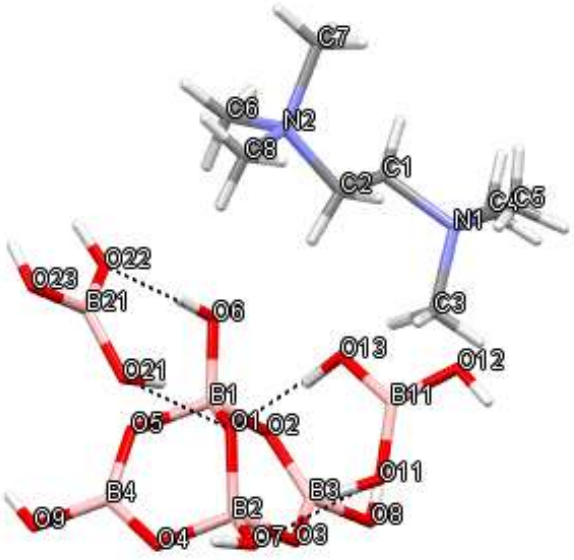

Figure 4.12: The hydrogen bonding interactions of the tetraborate **1a** with adjacent boric acid molecules, with atomic labelling.

The B-O bond distances in **1a** fall in line with expectations for a tetraborate, with B-O lengths for trigonal centres ranging from 1.362(3)-1.374(3) Å and B-O distances ranging from 1.445(3)-1.498(2) Å for tetrahedral centres. The B-O distances found in the $B(OH)_3$ spacer

molecules are typical for a trigonal centre, ranging from 1.357(3)-1.378(11) Å. The bond angles for B1 and B2 (**Figure 4.12**) range from 106.70(15)° – 113.13(15)°, consistent with sp^3 hybridization. Bond angles at B3 and B4 range from 116.19(18)°-122.99(17)°, consistent with sp^2 hybridization. The bonding angles for B11 and B21 in the $B(OH)_3$ molecules also fit within this range.

The tetraborate(2-) anions provide four H-bond donor sites and up to nine potential H-bond molecules, which provide three further H-bond donor and acceptor sites. Further hydrogen bonding potential is provided by the two co-crystallized $B(OH)_3$, which act as "spacer" molecules to bridge the tetraborate anions to form an extended network. For each tetraborate anion, there are also two waters of crystallisation (omitted from the diagram). The hydrogen bonding data is shown in **Table 4.1:**

Table 4.1: Hydrogen bonding interactions in **1a**

Donor	H	Acceptor	Donor-H length/Å	H-Acceptor length/Å	Donor-Acceptor length/Å	D-H-A angle/deg
O6	H6	O22	0.82	1.94	2.752(14)	169.7
O6	H6	O22A	0.82	2.02	2.82(5)	165.4
O7	H7	O32[1]	0.82	1.92	2.738(2)	177.1
O8	H8	O12[2]	0.82	2.05	2.815(2)	155.2
O9	H9	O11[3]	0.82	1.87	2.691(2)	174.8
O11	H11	O7	0.82	1.80	2.6027(18)	165.8
O12	H12	O5[4]	0.82	1.98	2.7972(19)	173.2
O13	H13	O1	0.82	1.83	2.6428(19)	170.9
O21	H21	O1	0.82	1.88	2.662(4)	159.6
O22	H22	O2[5]	0.82	1.80	2.612(14)	167.9
O23	H23	O6[5]	0.82	1.84	2.630(3)	162.3
O32	H32A	O3[6]	0.85	1.95	2.791(2)	170.4
O32	H32B	O21[7]	0.85	2.18	2.899(4)	142.0
O32	H32B	O21A[7]	0.85	2.07	2.830(12)	149.3
O31	H31A	O7[8]	0.85	1.96	2.780(2)	161.5
O31	H31B	O23[9]	0.85	1.94	2.783(7)	168.8
O31	H31B	O23A[9]	0.85	1.72	2.49(2)	149.3
O21A	H21A	O1	0.82	2.00	2.802(18)	167.1
O22A	H22A	O2[5]	0.82	1.93	2.72(4)	162.1
O23A	H23A	O6[5]	0.82	1.92	2.728(16)	167.1

[1]+x,+y,-1+z; [2]-x,-1/2+y,1-z; [3]1+x,+y,+z; [4]-1+x,+y,+z; [5]1-x,1/2+y,1-z; [6]-x,1/2+y,1-z; [7]+x,+y,1+z; [8]1+x,+y,1+z; [9]1-x,-1/2+y,1-z

In a separate experiment, **1** was stirred with 10 equivalents of boric acid in water. The solvent was removed by rotary evaporation, and a sample of the crude white powder was recrystallized in water to form X-ray quality crystals of excellent analytical purity. ^{11}B NMR provided strong signals at 17.1 ppm (85%) and 13.2 ppm (15%), signals assigned by Salentine to a pentaborate.[249] The FTIR spectrum of the product showed a very strong band at 926 cm^{-1}, which was not present in the tetraborate, and is typically diagnostic of a pentaborate anion.[259] Similar bands at 1103 cm^{-1}, 1026 cm^{-1}, 782 cm^{-1}, 697 cm^{-1} were also observed and these signals were consistent with the bands generated by the crude pentaborates discussed earlier. The single crystal XRD analysis confirmed that the product was the pentaborate $[Me_3NCH_2CH_2NMe_3][B_5O_6(OH)_4]_2$ **(1b) (Figure 4.13).**

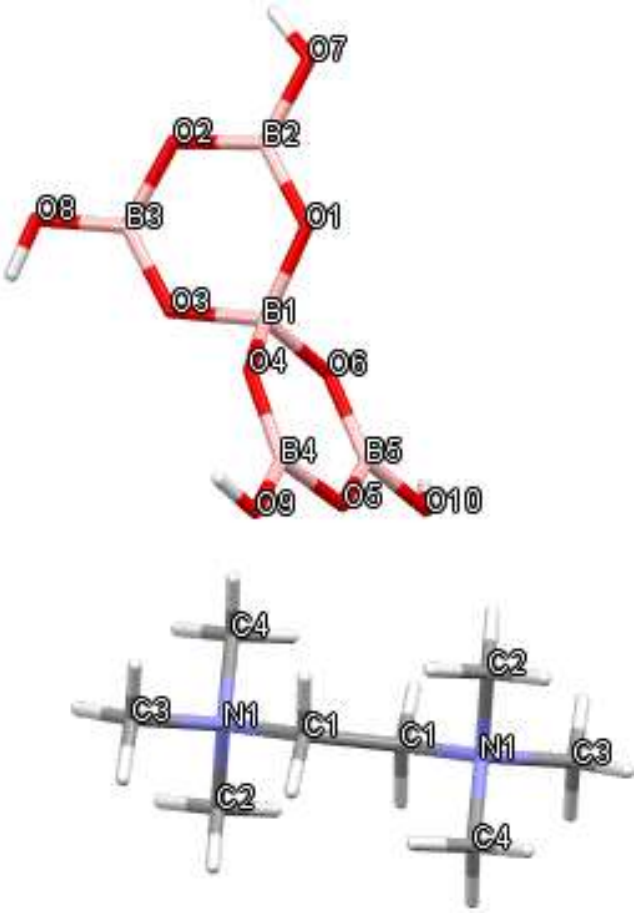

Figure 4.13: Pentaborate **1b** (with atomic labelling)

The B-O bond distances in **1b** are typical of a pentaborate, with B-O lengths for trigonal centres ranging from 1.350(2)-1.385(2) Å and B-O distances in tetrahedral centres being slightly longer, ranging from 1.464(2)-1.479(2) Å. The B-O distances found in both crystallographically independent pentaborate units were similar, indicating no evidence of increased strain for one of the units. The bond angles for B1 (and B11) (**Figure 4.13**) range from 107.03(12)° – 111.40(12)°, consistent with sp^3 hybridization. Bond angles at the trigonal centres B2-B5 (and B12-B15) range from 115.85(14)°-123.00(15)°, consistent with sp^2 hybridization. The two crystallographically independent pentaborate units have slightly different hydrogen bonding environments. A diagram of the H-bonded anionic network is shown in **Figure 4.14**.

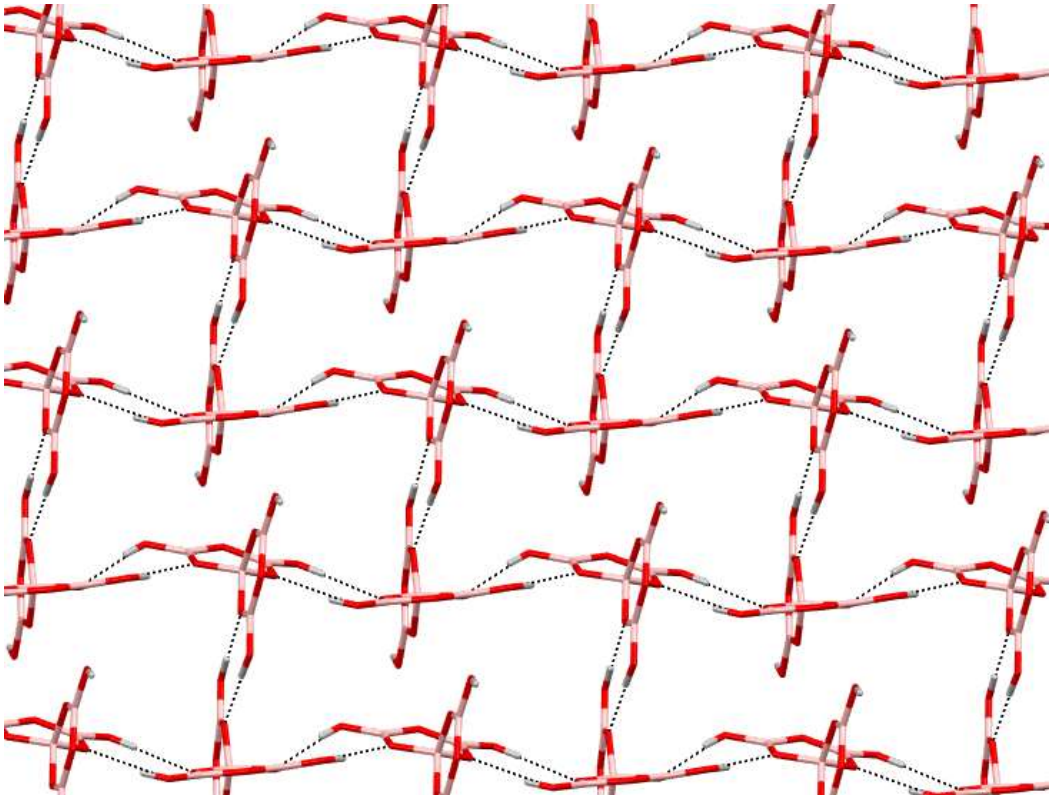

Figure 4.14: "Brickwall"-type arrangement of the pentaborate(1-) anionic lattice in **1b**, the cations fit within the vacant spaces.

As is common with pentaborates, each unit donates four hydrogen bonds to neighbouring partners. Each pentaborate unit donates three hydrogen bonds via ($R_2^2(8)$ reciprocal-α) interactions **(Figure 4.15)**, using Etter nomenclature[289] utilised for describing H-bonding interactions.

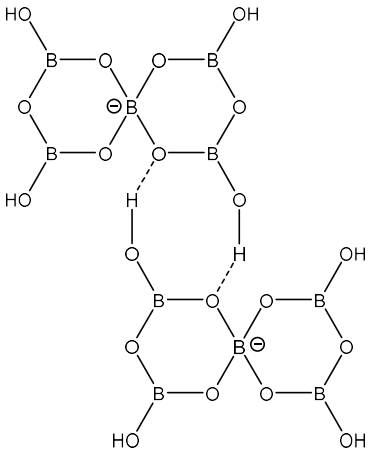

Figure 4.15: The $R_2^2(8)$ reciprocal-α hydrogen-bonding environment, named after the 8-membered ring formed between the two H-bonded pentaborate units.

The fourth hydrogen bonding donation is where the variation between the two independent pentaborates occurs: half of the crystallographically independent pentaborate units in the crystal structure donate a C(8) β-chain to an adjacent pentaborate unit, and half donate an $R_2^2(12)$ reciprocal-β interaction. The hydrogen bonding interactions in **1b** are summarised in **Table 4.2**.

Table 4.2: Hydrogen bonding interactions in **1b**

Donor	H	Acceptor	Donor-H length/Å	H-Acceptor length/Å	Donor-Acceptor length/Å	D-H-A angle/deg
O7	H7	O8[1]	0.84	2.04	2.8745(16)	176.2
O8	H8	O14[2]	0.84	1.81	2.6492(16)	175.6
O9	H9	O13[3]	0.84	1.83	2.6536(15)	167.9
O10	H10	O11[4]	0.84	1.88	2.6955(15)	164.4
O17	H17	O6[5]	0.84	1.96	2.7926(16)	170.2
O18	H18	O4[6]	0.84	1.95	2.7811(16)	167.6
O19	H19	O3[7]	0.84	1.91	2.7471(15)	177.6
O20	H20	O9[8]	0.84	1.92	2.7264(15)	159.7

[1]-1-x,-1-y,1-z; [2]-1+x,-1+y,+z; [3]+x,-1+y,+z; [4]-1+x,+y,+z; [5]1+x,+y,+z; [6]+x,1+y,+z; [7]1+x,1+y,+z; [8]1-x,-y,-z

By the notation devised by Schubert,[248] this pentaborate would be known as the "α,α,α,β" configuration. However, this mixture of β-chain and $R_2^2(12)$ reciprocal-β interactions makes this a "unique" pentaborate network. In this example, half of the pentaborate units accept three hydrogen bonds (all reciprocated α interactions), and the other half accept five hydrogen bonds (3 reciprocated α, one β-chain and one reciprocated β interaction) **(Figure 4.16)**.

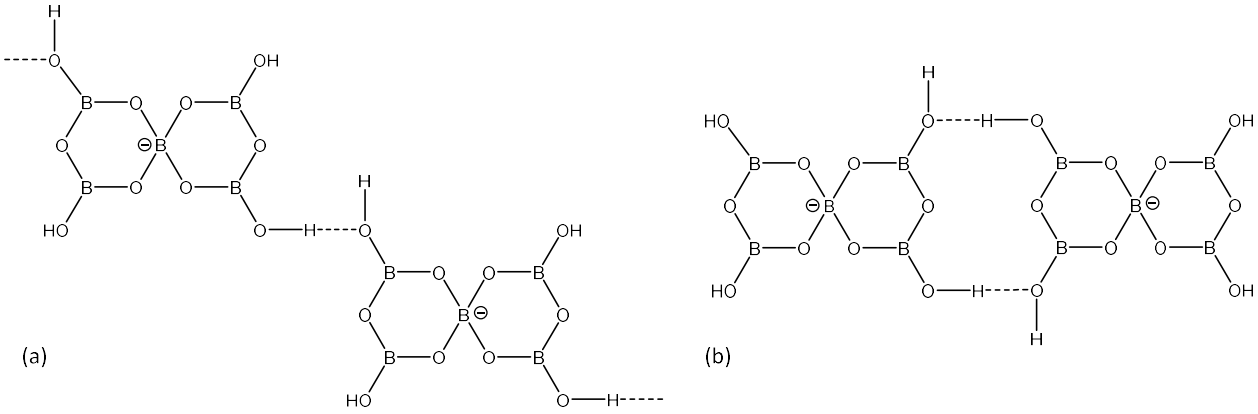

Figure 4.16: **(a)** An example of the linear C(8) β-chain, and **(b)** an example of the $R_2^2(12)$ reciprocal-β interactions, present within the **1b** pentaborate lattice.

Compound **2** was added in three separate ratios (1:3, 1:6 and 1:10) to solutions of boric acid. Each solution was evaporated after several days to dryness in a rotary evaporator and the resulting crude solids were subjected to ^{1}H, ^{11}B and ^{13}C NMR spectroscopy.

A significant difference was observed in the ^{1}H and ^{13}C NMR spectra in comparison to the unreacted cation. The original diagnostic peaks for the cation, namely a quintet at 2.31 ppm, 2H (CH_2), a large singlet at 3.13 ppm, 18H ($6CH_3$-N), and a triplet at 3.37 ppm, 4H ($2CH_2$-N) were present but at a weak intensity, and new higher intensity signals were present at 3.01 ppm, 3.83 ppm, 5.63 ppm and 5.99 ppm. The peak at 3.01 ppm is most likely the (CH_3-N), the

signal at 3.83 ppm has changed from a triplet to a doublet, most likely representing the (CH_2N) from the linking chain. The unexpected low intensity of the signal at 2.31 ppm suggested that a significant proportion of the β(CH_2) group in the middle of the linker chain had been lost from the product. The downfield shift (and subsequent reduction of intensity) of the peak at 3.37 ppm to a second peak at 3.83 ppm, combined with the addition of two new peaks at 5.63 ppm and 5.99 ppm suggested that an alkene has formed within the chain. In at least half of the mixture, one of the quaternary amines has likely been converted in a Hofmann-like elimination,[290,291] as a result of high temperatures during the evaporation process, to form a terminal alkene on the cationic centre as a pentaborate salt **(2a)** according to **Scheme 4.2**.

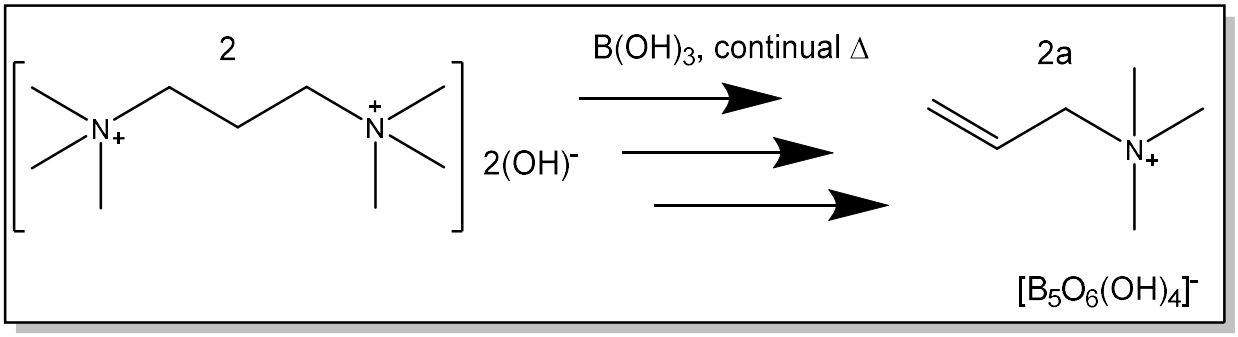

Scheme 4.2: **2a** was unexpectedly formed from **2** in the presence of boric acid at high temperature

By re-dissolving and heating the crude product back to dryness in an oven at 80°C, the original cation peaks are completely removed from the spectrum, leaving only the new "degraded" peaks. The evidence is further supported by the ^{13}C spectrum, where a signal indicating the β(CH_2) group in the propyl linker chain at 17.41 ppm has been completely replaced by two new signals at 124 ppm (CH) and 129 ppm (CH_2), which can be attributed to the presence of an alkene. The ^{11}B spectrum for this product showed signals at 17.1 ppm, 13.4 ppm and 1.5 ppm, strongly indicating that the fragments of a pentaborate are present within solution.[249]

The experiment was repeated using fresh cation with the aim of preventing the degradation of the cation to the final product. The solution is concentrated without initial forced evaporation to dryness, by slow evaporation of the solvent at room temperature to grow crystals from the initial solution. A sample of residue from the walls of the vessel confirmed by ^{1}H and ^{13}C NMR the retention of the original cation, and ^{11}B signals were found at 16.8 ppm and 13.2 ppm, likely to be related to a pentaborate.[249] This further confirmed the theory that subjecting this product to high temperatures in aqueous solution causes a gradual elimination of one of the quaternary amines to form an alkene.[290,291] Crystals suitable for X-ray diffraction were obtained *via* recrystallization of the heat-treated solution **(2a)** and analysed by NMR spectroscopy to contain 100% converted alkene, were subjected to single crystal XRD analysis. After several weeks, the "room temperature" synthetic route resulted in X-ray quality single crystals without degradation of the cation **(2b),** and these were also submitted for single crystal XRD studies.

X-ray crystal studies of the expected **2b** pentaborate and the serendipitously formed **2a** pentaborate provided confirmation of the degradation theory. The unexpected pentaborate $[Me_3NCH_2CH{=}CH_2][B_5O_6(OH)_4]$ **(2a)** structure is shown in **Figure 4.17**, with atomic numbering.

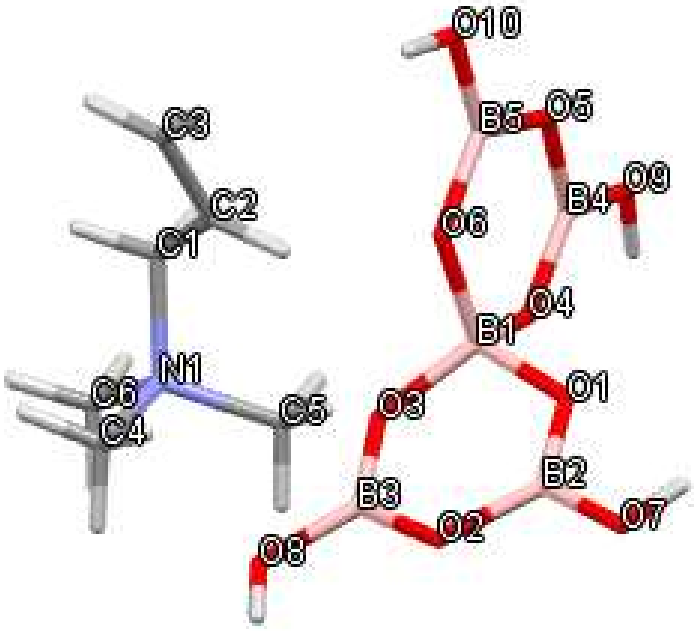

Figure 4.17: Crystal structure of pentaborate **2a** with atomic numbering

The B-O bond distances in **2a** are consistent with previous examples, with shorter B-O lengths for trigonal centres ranging from 1.357(15)-1.388(15) Å and B-O distances ranging from 1.448(14)-1.480(14) Å for tetrahedral centres. The bond angles for the tetrahedral B1 in **Figure 4.17** range from 107.97(8)^{o} – 111.14(9)^{o}, consistent with sp^3 hybridization. Bond angles at the trigonal planar centres B2-B5 range from 116.42(10)^{o}-122.31(11)^{o}, consistent with sp^2 hybridization.

Compound **2a** is classified as the commonly reported α,α,α,β "herringbone" arrangement. When viewed along the crystallographic "a" axis, the pentaborate structure is packed in a recognisable pattern of rectangles **(Figure 4.18)**. Each rectangle is bordered by 6 separate pentaborate units, which are interconnected with three reciprocal-α H-bonds. Each pentaborate in the lattice is shared between three rectangles in this plane. Along the third

dimension, the “herringbone” plane of pentaborates are connected *via* C(8) β-chain hydrogen bonding interactions. The connecting chains project infinite channels inside the rectangles, which provide the necessary space to occupy the cations.

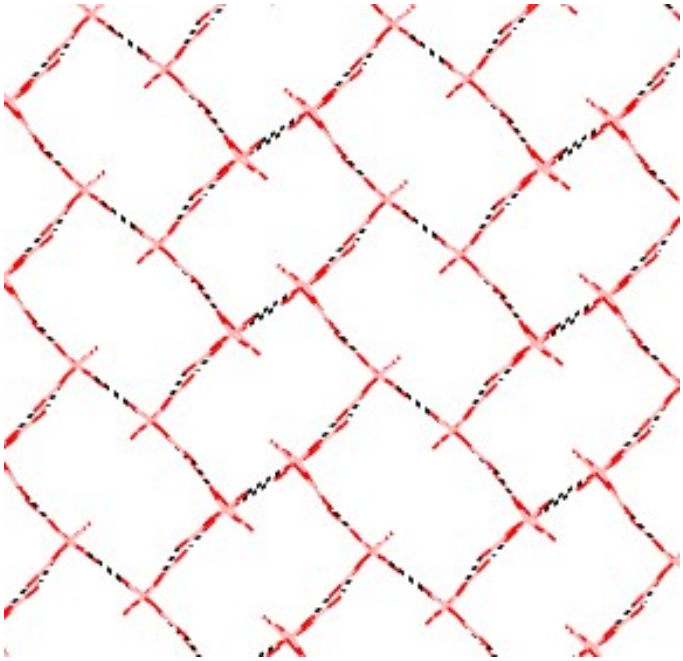

Figure 4.18: Crystal structure of the “herringbone” **2a** pentaborate, viewed along the crystallographic “a” axis.

Compound **2a** only forms 4 unique hydrogen bonding interactions, highlighting the simplicity of the crystal structure. These are presented in **Table 4.3**.

Table 4.3: Hydrogen bonding interactions in **2a**

Donor	H	Acceptor	Donor-H length/Å	H-Acceptor length/Å	Donor-Acceptor length/Å	D-H-A angle/deg
O7	H7	O6[1]	0.84	1.91	2.7454(11)	178.2
O8	H8	O9[2]	0.84	1.97	2.7778(11)	162.5
O9	H9	O4[3]	0.84	1.84	2.6693(11)	171.3
O10	H10	O1[4]	0.84	1.83	2.6639(11)	174.0

[1]+x,3/2-y,1/2+z; [2]-1+x,+y,+z; [3]1-x,1-y,1-z; [4]+x,3/2-y,-1/2+z

The crystal structure of the originally expected product **2b** is that of the pentaborate, $[Me_3N(CH_2)_3NMe_3][B_5O_6(OH)_4]_2$. Atomic labelling is shown in **Figure 4.19**. This structure featured two crystallographically independent pentaborate units (pictured), with some interstitial waters of crystallisation at partial occupancy (omitted from the diagram).

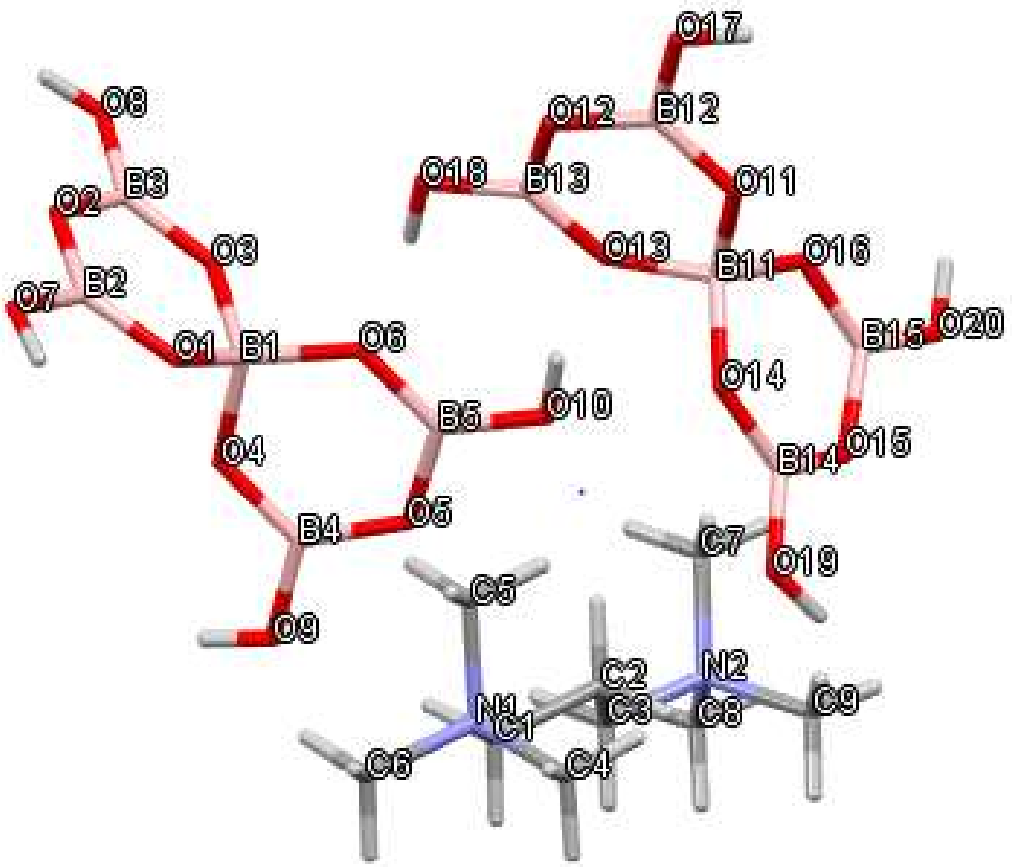

Figure 4.19: Pentaborate **2b** crystallised with two crystallographically independent pentaborate(1-) units with different H-bond accepting environments.

The B-O bond distances in **2b** follow the same pattern as pentaborates **1b** and **2a**, with B-O lengths for trigonal centres ranging from 1.356(14)-1.389(14) Å and B-O distances ranging from 1.456(15)-1.485(15) Å for tetrahedral centres. The bond angles for B1 and B11 (**Figure 4.19**) range from 107.37(9)° – 111.51(9)°, consistent with sp^3 hybridization. The bond angles

at trigonal centres B2-B5 and B12-B15 range from 116.23(10)°-124.17(9)°, are consistent with sp^2 hybridization.

Each of the two independent water of crystallisation has a partial occupancy of 0.25, which means that these molecules are only present in 25% of the sites shown in the crystal structure. These water molecules are hydrogen-bonded to one of the borate units in the lattice, however these h-bonds, originating from O21 and O22 in the structure, are considerably longer than those seen in the borate lattice **(Table 4.4)**

Table 4.4: Hydrogen bonding interactions in **2b**

Donor	H	Acceptor	Donor-H length/Å	H-Acceptor length/Å	Donor-Acceptor length/Å	D-H-A angle/deg
O17	H17	O4[1]	0.84	1.87	2.6942(11)	168.9
O18	H18	O6	0.84	1.85	2.6849(11)	170.3
O19	H19	O18[2]	0.84	1.99	2.7895(11)	158.5
O20	H20	O16[3]	0.84	2.02	2.8343(11)	163.9
O7	H7	O1[4]	0.84	1.90	2.7367(12)	175.0
O8	H8	O9[5]	0.84	1.95	2.7746(11)	165.7
O9	H9	O11[6]	0.84	1.84	2.6764(11)	174.3
O10	H10	O13	0.84	1.82	2.6400(11)	166.6
O21	H21A	O18[4]	0.87	2.63	3.374(5)	144.3
O22	H22A	O8[7]	0.87	2.24	2.831(9)	125.0
O22	H22A	O9	0.87	2.53	3.205(7)	135.0
O22	H22B	O13[8]	0.87	2.16	2.956(7)	151.9
O22	H22B	O16[8]	0.87	2.42	2.981(6)	122.6

[1]+x,1+y,+z; [2]+x,1-y,1/2+z; [3]3/2-x,3/2-y,1-z; [4]1-x,+y,1/2-z; [5]+x,-y,-1/2+z; [6]+x,-1+y,+z; [7]+x,-y,1/2+z; [8]3/2-x,1/2-y,1-z

When viewed along the crystallographic 'c' axis, this structure is similar to the commonly reported "brickwall" arrangement, with an α,α,α,β H-bonding network between borate units **(Figure 4.20)**. Three reciprocal-α H-bonds per pentaborate form this pattern, with a fourth C(8) β-chain interaction linking the plane. It is however not a typical brick wall, as there is

distortion caused by the partial-occupancy waters of crystallisation (not shown in this diagram). The cations sit within the cavities in the lattice.

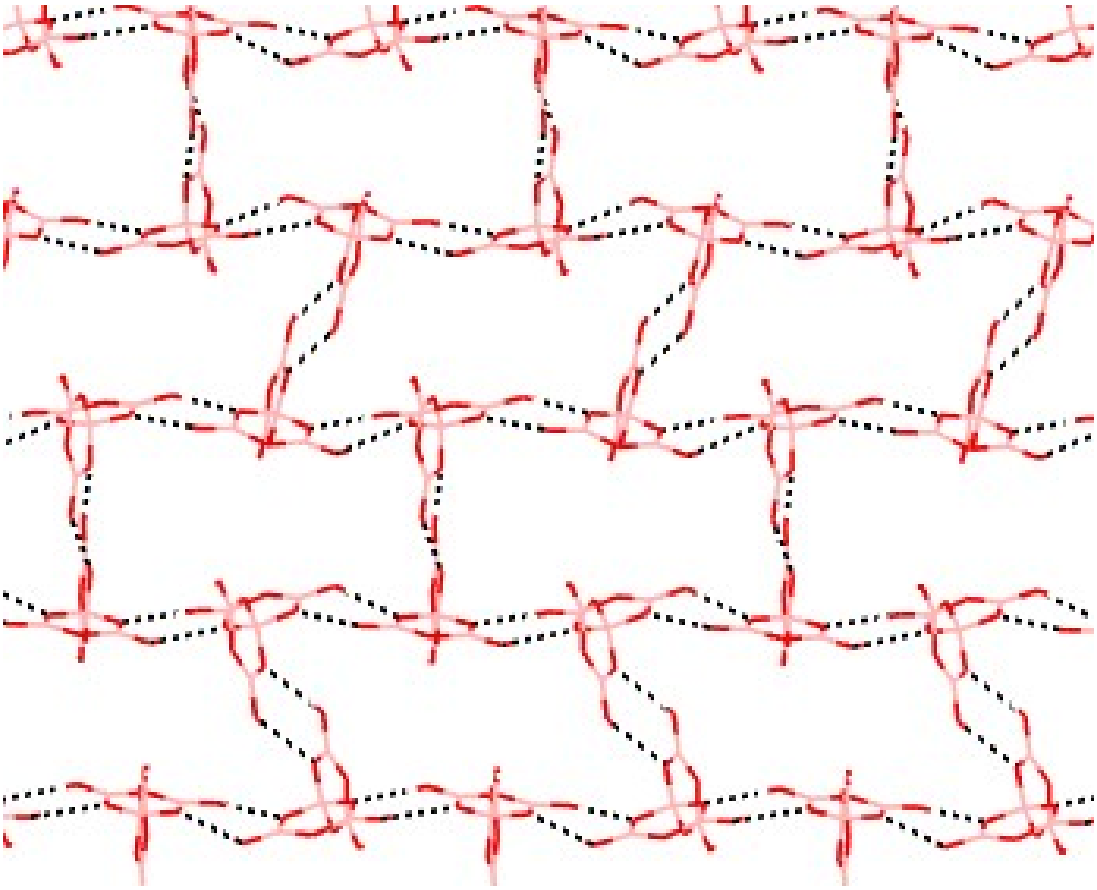

Figure 4.20: Pentaborate(1-) anionic lattice of the **2b** pentaborate structure; similar in shape to the "brickwall" structure. The cations sit in the channels within the lattice.

The tetraborate **1a**, and pentaborates **2a** and **2b** were published as part of a family of C_2- and C_3–linked polyborates.[230] Pentaborate **1b** has been separately published in a short paper proceeding a conference event.[231]

4.2.4: Preparation of other C_n-linked bis(alkylammonium) polyborate salts

In addition to the series of C_2- or C_3-linked bis(alkylammonium) dications, we were interested in a number of other potential candidates as templating cations for polyborates. Schubert successfully reported a series of alkanediammonium polyborates that featured longer linker chains ($C_{5\text{-}12}$) between the amines.[248] It was therefore of interest to test a series of larger, bulkier cations to see if they would be capable of forming polyborates. A series of C_n-linked substituted imidazolium **(3-5)** and pyrrolidinium **(6-9)** halide salts **(Table 4.1)** were kindly provided by Dr. Ahmad Al-Dulayymi within our department, who were also interested in obtaining crystal structures containing the cations, but were unable to obtain suitable single crystals from their halide salts. The compounds studied have been previously used as ionic liquids,[292] phase transfer catalysts,[293] or have been studied for anti-malarial properties.[294]

Table 4.5: C_n-linked imidazolium and pyrrolidinium cations used to template crystalline polyborate salts.

Structure of the halide salt of the cation	Notes on crystal structure of the related pentaborate salt
(3) 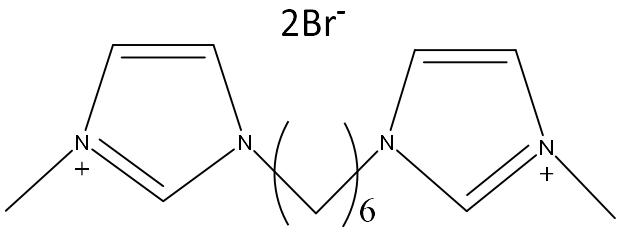	**(3a)** $[CH_3(C_3H_3N_2)(CH_2)_6(C_3H_3N_2)CH_3]$ $[B_5O_6(OH)_4]_2$ Space group $P2_1/c$.
(4) 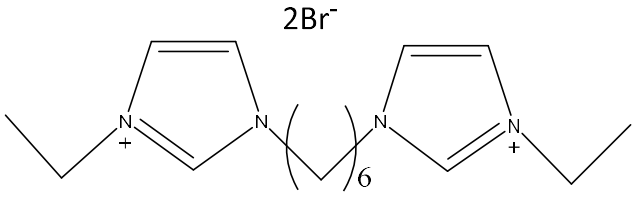	**(4a)** $[C_2H_5(C_3H_3N_2)(CH_2)_6(C_3H_3N_2)C_2H_5]$ $[B_5O_6(OH)_4]_2 \cdot 2H_2O$ Space group *P*-1
(5) 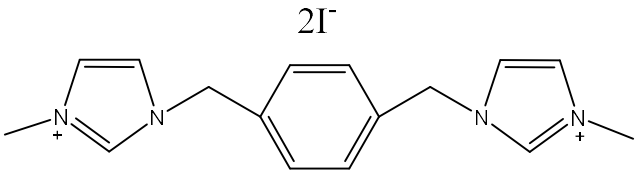	**(5a)** $[CH_3(C_3H_3N_2)CH_2(C_6H_4)CH_2(C_3H_3N_2)CH_3]$ $[B_5O_6(OH)_4]_2$ Space group *P*-1.
(6) 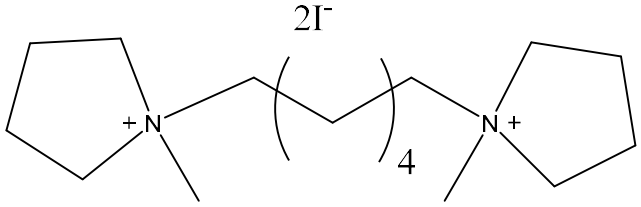	**(6a)** $[CH_3(C_4H_8N)(CH_2)_6(C_4H_8N)CH_3]$ $[B_5O_6(OH)_4]_2$ Space group *P*-1. "Block-like" crystals

Table 4.5 (continued): C_n-linked imidazolium and pyrrolidinium cations used to template crystalline polyborate salts.

Structure of the halide salt of the cation	Notes on crystal structure of the related pentaborate salt
(6) 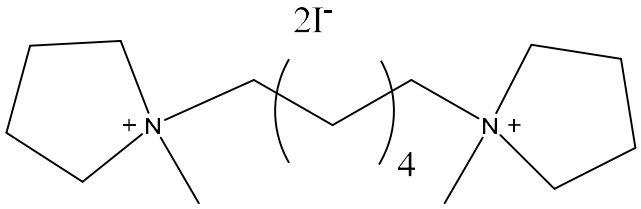	**(6b)** $[CH_3(C_4H_8N)(CH_2)_6(C_4H_8N)CH_3]$ $[B_5O_6(OH)_4]_2$ Space group *P*-1. "Plate-like" crystals
(7) 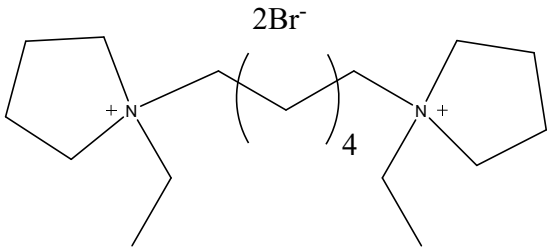	**(7a)** $[C_2H_5(C_4H_8N)(CH_2)_6(C_4H_8N)C_2H_5]$ $[B_5O_6(OH)_4]_2$ Space group $P2_1/c$.
(8) 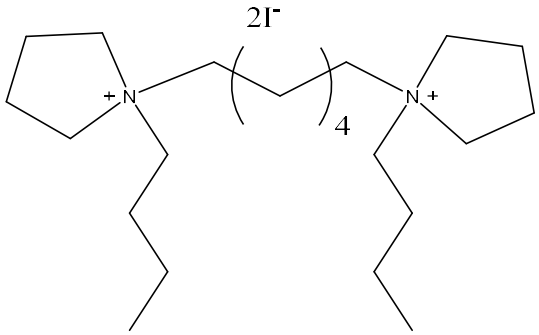	**(8a)** $[C_4H_9(C_4H_8N)(CH_2)_6(C_4H_8N)C_4H_9]$ $[B_5O_6(OH)_4]_2$ Space group *Cc*
(9) 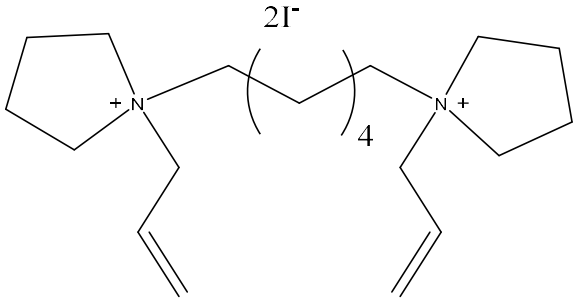	**(9a)** $[C_3H_5(C_4H_8N)(CH_2)_6(C_4H_8N)C_3H_5]$ $[B_5O_6(OH)_4]_2$ Space group $P2_1/c$

All of the above cations were received in their pure halide form and were used without further purification. Each salt was subjected to ^{1}H and ^{13}C NMR spectroscopy before and after the borate synthetic procedure and spectra were found to be consistent with starting material and the crystalline product. The cations were dissolved in water and a minimum of two equivalents of ion exchange resin ($[OH]^-$ form) was added to the solutions and stirred for 18 hours to allow for complete exchange of the halide. In all cases, the exchange resin was removed from the solution by filtration and the filtrates were added to 10 equivalents of boric acid in all cases. Solutions were stirred for 4 hours to ensure complete dissolution of the boric acid and then evaporated to dryness using a rotary evaporator. The crude powders ranged from white to yellow in colour, and were subjected to FTIR and NMR spectroscopy (^{1}H, ^{11}B, ^{13}C). These analytical procedures confirmed the presence of a pentaborate(1-) salts. Samples (0.5 g) of all crude products were then re-dissolved in 20 mL of warm distilled water and then allowed to crystallise at room temperature over several weeks.

The substituted imidazolium dication in **3** formed the typical pentaborate salt **(3a)** with a "herringbone" structure with all pentaborate units in a α,α,α,β arrangement. The rectangular-shaped channels formed by the pentaborate were distorted into diamond-shapes by the occupancy of the cations, which were S-shaped within the channels. The substituted imidazolium dication in **4** formed a pentaborate **(4a)** with a "brickwall" structure with all pentaborate units forming α,α,α,β hydrogen bonding interactions. Two cations sit in parallel to each other and to the direction of the channels projected by the β-chains formed in the brick-wall vacancies. Cation **5** also formed a pentaborate salt **(5a)** with a "brickwall" α,α,α,β configuration, with cations folded into continuous "zig-zag" shapes in the channels, with the central phenyl ring perpendicular to the imidazolium rings.

The pyrrolidinium dication in **6** forms two pentaborate salt polymorphs **(6a)** and **(6b)** and both were "brickwall" α,α,α,β arrangements. In **6a**, the cations occupied the channels as diagonal strips across the channel (as also seen in **5a**), whereas in **6b** two cations sat in parallel to each other and to the channels, as also seen in **4a**. The cations in **7** and **9** formed pentaborate salts **(7a)** and **(9a)**, respectively, with identical α,α,α,γ arrangements; all four hydrogen bond donations on each pentaborate unit were reciprocated. A quick inspection indicates that these salts appear to form 2-dimensional brick-wall structures. However, as the fourth H-bond is a $R_2^2(8)$ reciprocal-γ interaction, the diamond-shaped channels actually project diagonally to this plane, with the cations sitting parallel to the direction of the channel, and thus this cannot be categorised as a typical brick-wall structure. Similar structures have also been reported previously.[285,295]

The pyrrolidinium dication in **8** formed a highly unusual crystalline pentaborate salt **(8a)** in which each pentaborate unit forms two α,α H-bonding interactions with two adjacent boric acid molecules, both of which are incorporated in $R_2^2(8)$ reciprocal-α interactions. In addition to these, there are two further C(8) β-chain H-bonds donated to adjacent pentaborate units. As well as the two H-bonds accepted *via* $R_2^2(8)$ reciprocal-α interactions, two additional H-bonds are received *via* C(8) β-chain H-bonds from adjacent pentaborates, and **two** sets of two additional H-bonds are accepted at α and β positions from double-donor boric acid molecules. This unique example can best be described as an α,α,β,β arrangement, with 4 donor sites and 8 acceptor sites per pentaborate unit. All structural data including hydrogen-bond data for **3a**-**9a** is presented in the supplementary information, pg 52-143.

Imidazolium pentaborate salts **3a**-**5a** appeared to show weak fluorescence under UV light both in solution and as powders. Preliminary UV-visible studies of these solutions were carried out and strong UV activity was observed at *ca.* 220 nm, however this effect was not quantified.

A number of additional halide salts **(10-17) (Table 4.2)** formed pentaborate salts as crude powders **(10a-17a)**, but did not form suitable X-ray quality crystals upon recrystallization. These compounds were prepared in the same way as the crystalline products, and had similar NMR and FTIR spectra, evidencing that the crude powders obtained contained crude pentaborate salts.

Table 4.6: C_n-linked imidazolium and pyrrolidinium cations which formed pentaborate crude products, but did not grow as single crystals.

Structure of the halide salt of the cation	Related pentaborate salt
(10) 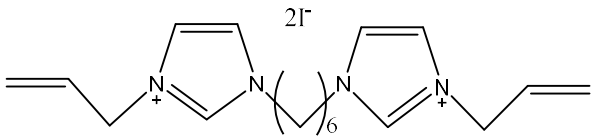	**(10a)** $[CH_2{=}CHCH_2(C_3H_3N_2)(CH_2)_6(C_3H_3N_2)CH_2CH{=}CH_2]\ [B_5O_6(OH)_4]_2$
(11) 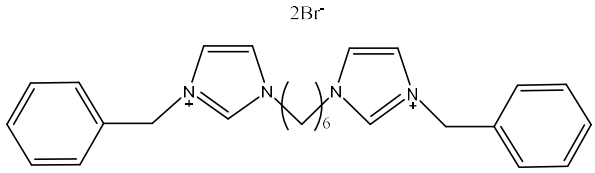	**(11a)** $[(C_6H_5)CH_2(C_3H_3N_2)(CH_2)_6(C_3H_3N_2)CH_2(C_6H_5)]\ [B_5O_6(OH)_4]_2$
(12) 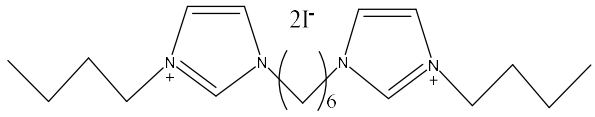	**(12a)** $[C_4H_9(C_3H_3N_2)(CH_2)_6(C_3H_3N_2)C_4H_9]\ [B_5O_6(OH)_4]_2$
(13) 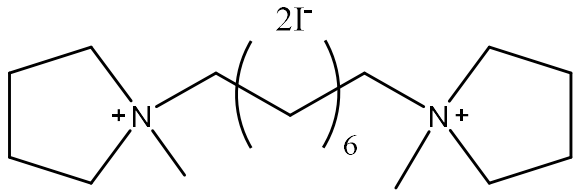	**(13a)** $[CH_3(C_4H_8N)(CH_2)_8(C_4H_8N)CH_3]\ [B_5O_6(OH)_4]_2$
(14) 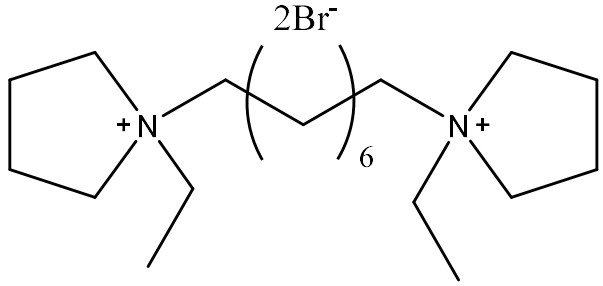	**(14a)** $[C_2H_5(C_4H_8N)(CH_2)_8(C_4H_8N)C_2H_5]\ [B_5O_6(OH)_4]_2$

Table 4.6 (continued): C_n-linked imidazolium and pyrrolidinium cations which formed pentaborate crude products, but did not grow as single crystals.

Structure of the halide salt of the cation	**Related pentaborate salt**
(15) 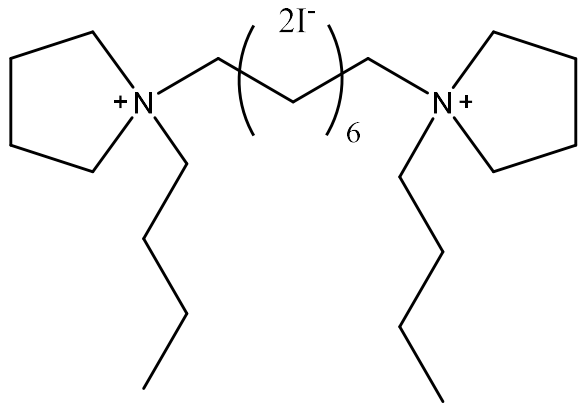	**(15a)** $[C_4H_9(C_4H_8N)(CH_2)_8(C_4H_8N)C_4H_9]$ $[B_5O_6(OH)_4]_2$
(16) 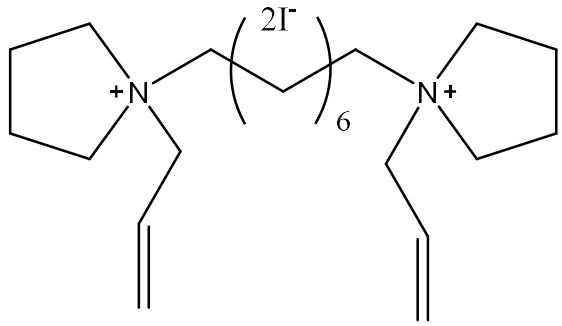	**(16a)** $[CH_2{=}CHCH_2(C_4H_8N)(CH_2)_8(C_4H_8N)$ $CH_2CH{=}CH_2]$ $[B_5O_6(OH)_4]_2$
(17) 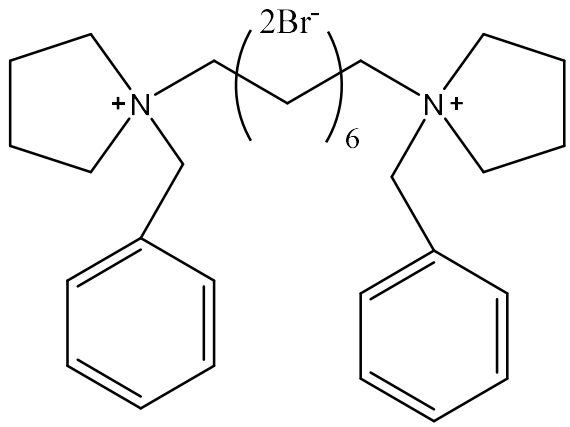	**(17a)** $[(C_6H_5)CH_2(C_4H_8N)(CH_2)_8(C_4H_8N)CH_2(C_6H_5)]$ $[B_5O_6(OH)_4]_2$

Many of these compounds had larger (C_8- or above) linker chains, or excessively bulky side groups, which may have been too large or too flexible to fit within the channels of a typical borate lattice and hence form X-ray quality crystals.

4.2.5: Preparation of polyborates using substituted guanidinium cations

Guanidines are strong, nitrogen-rich bases that could have a good potential to form polyborate salts. Schubert *et al* have previously reported a guanidinium tetraborate and a very unusual guanidinium nonaborate that were obtained at elevated temperatures on a large scale.[275] Utilising the strong basicity of the series, we were particularly interested in expanding this family of compounds by obtaining polyborates of functionalised or methylated guanidines. **Table 4.3** shows a complete list of the substituted guanidine derivatives that were successfully isolated as crystalline pentaborates with crystal structures determined during this stage of the project.

Table 4.7: Guanidinium-based cations successfully used to grow single crystal polyborate salts

Structure of organic starting salt	Notes on crystal structure of the related pentaborate salt
18 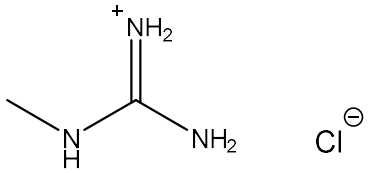	**(18a)** $[MeNHC(NH_2)NH_2][B_5O_6(OH)_4]\cdot H_2O$ Space group $P2_1/c$
19 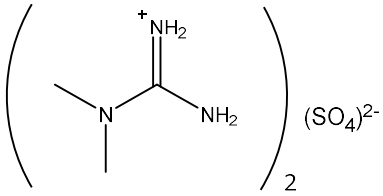	**(19a)** $[Me_2NC(NH_2)NH_2][B_5O_6(OH)_4]$ Space group $P2_1/c$.
20 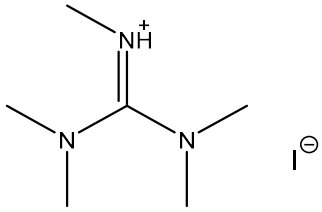	**(20a)** $[Me_2NC(NHMe)N(Me)_2]$ $[B_5O_6(OH)_4]\cdot B(OH)_3$ Space group $P2_1/c$.
21 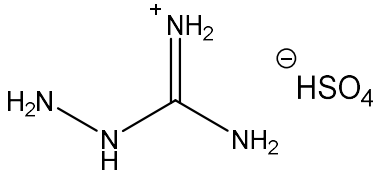	**(21a)** $[NH_2NHC(NH_2)NH_2][B_5O_6(OH)_4]$ Space group P-1.
22 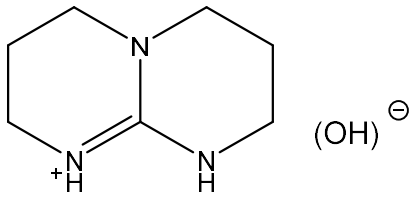	**(22a)** $[C_7H_{14}N_3][B_5O_6(OH)_4]$ Space group P-1.

Compound **18** was obtained as a monohydrochloride salt, and was stirred with a minimum of one equivalent of ion exchange resin ($[OH]^-$ form) for 18 hours prior to addition of 5 equivalents of boric acid using a similar procedure to that for the bivalent imidazolium and pyrrolidinium salts. Compound **19** was obtained as a sulfate salt, **21** was obtained as a hemisulfate salt. The sulfate salts were dissolved in water and exchanged using barium hydroxide solution in a 1:2 stoichiometric ratio of sulfate to barium hydroxide. The mixtures were stirred for 2 hours and the insoluble barium sulphate was removed by filtration to leave the guanidinium hydroxide salts in solution, to which were added 5 equivalents of boric acid. Compound **20** was prepared by reacting tetramethylguanidine with an excess of iodomethane in acetonitrile solvent at reflux temperature to form pentamethylguanidinium iodide as an analytically pure salt (confirmed by ^1H, ^{13}C NMR spectroscopy), which was then exchanged for hydroxide using an exchange resin. The deprotonated amine contained in **22** needed no preliminary treatment and was immediately reacted with 5 equivalents of boric acid in aqueous solution. All solutions containing boric acid and organic cation were stirred for several hours before the solvents were removed using a rotary evaporator to form crude white powders, which were found to be pentaborate salts **(18a-22a)**. This was confirmed by NMR and FTIR spectroscopy.

The crystal structure of the pentaborate **18a** is a typical α,α,α,γ system with some additional hydrogen bonding interactions received from the methylguanidinium cation, which is linked to a water of crystallisation by further H-bonding. Salt **19a** has a similar α,α,α,γ H-bonding environment to **7a**, **9a** and **18a**, but accepts additional hydrogen bonds from the ethylguanidinium cation in a similar way to how **8a** accepted H-bonds from boric acid. Compound **20a** has a unique version of the α,α,α,β system, in which two $R_2^2(8)$ reciprocal-α

interactions occur to adjacent pentaborate anions, and a third occurs to an adjacent molecule of boric acid. An additional boric acid molecule donates two hydrogen bonds to each pentaborate unit at α- and a β–oxygens. Each unit donates its fourth H-bond to a third adjacent pentaborate unit *via* a C(8) β-chain. The only available H-bonding proton on the pentamethylguanidinium cation donates to a molecule of boric acid. Polyborate salt **21a** is a α,α,α,β system, but the β-interaction is an $R_2^2(12)$ reciprocal-β interaction, previously seen in **1b**. Each pentaborate unit also receives a hydrogen bond directly from the cation, at the γ-position. The structure of **22a** has the same α,α,α,β system as **21a** without any further interactions with the cation. The full crystallographic data of **18a**-**22a,** including hydrogen-bonding interactions is presented in the supplementary information, pg 144-201.

The procedures attempted by Schubert to obtain tetraborate and nonaborate salts were attempted using **18**.[275] The hydrochloride salt was added to mixtures of boric acid and sodium tetraborate (borax), totalling 4 and 9 equivalents of boron per cation, and left to crystallise in an oven at 50°C. Crystals obtained from the vessels were found to consist of recrystallized borax with no organic cation, with none of the expected unusual polyborate salts obtained. It is likely that attempted double displacement of the sodium tetraborate and the hydrochloride of the methylguanidine was unsuccessful. The procedures were not repeated on any of the other guanidine derivatives as Schubert's successful syntheses[275] were carried out using carbonate salts as opposed to halides or sulphates.

All borates with resolved crystal structures (excluding **18a**, which was resolved and received after the conclusion of lab-work) were subjected to C, H, N (combustion) elemental analyses, which all provided data consistent with their formulations. All pentaborate salts were also

subjected to DSC/TGA analysis. Polyborates generally decompose in air to form glassy B_2O_3 residues. In the first decomposition step, (between 100°C and 300°C), interstitial H_2O molecules and terminal –OH groups on the borate and interstitial boric acid molecules are lost as water with the formation of a condensed borate. The organic cation is then oxidised in air from 300-650°C to form the fully pyrolysed B_2O_3 glassy solid. **Figure 4.21** shows a typical example of a DSC/TGA curve of one of the products, **2b**.

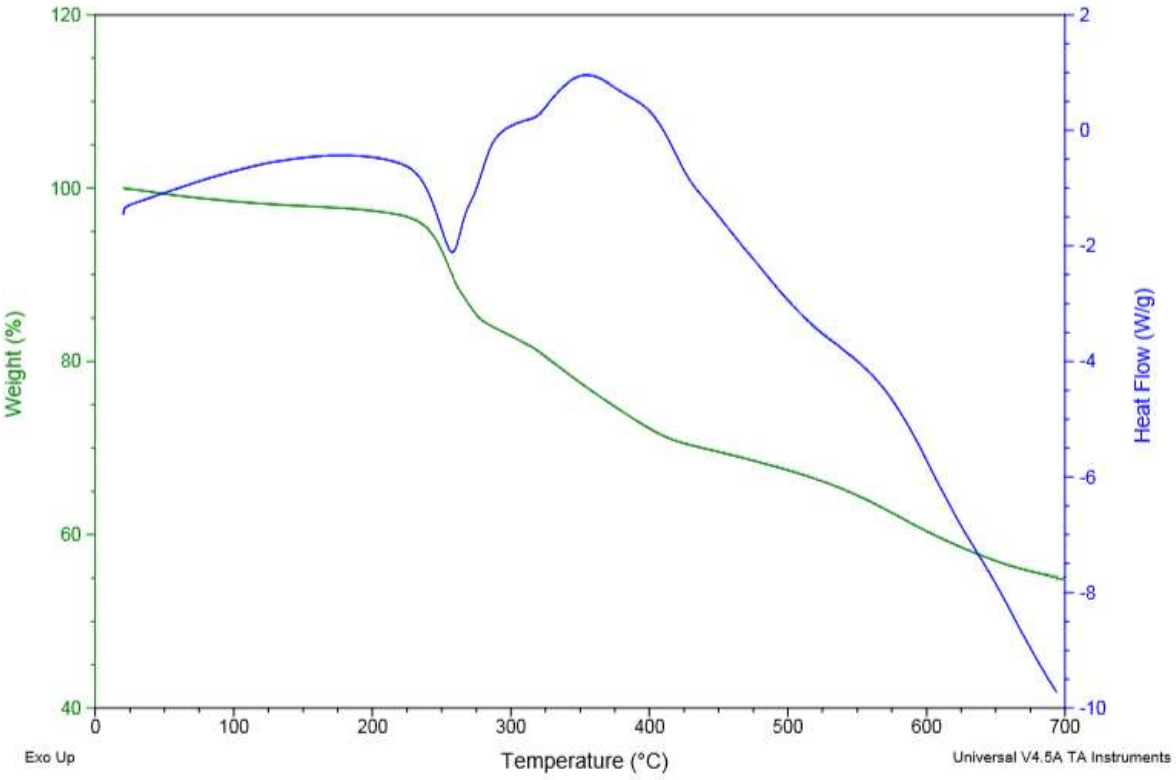

Figure 4.21: Example DSC (blue)/TGA (green) analysis of **2b** showing the stepwise degradation of the polyborate salt to a glassy boron oxide from room temperature to 700°C, in air.

The TGA curve of **2b** shows a 2-step endothermic dehydration of $[Me_3NCH_2CH{=}CH_2][B_5O_6(OH)_4]$ In the first step there is an endothermic dehydration of $[Me_3NCH_2CH{=}CH_2][B_5O_6(OH)_4]$. Two molecules of water are lost from the hydrated borate, equating to 11.3% of the overall weight, to form the condensed borate salt

$[Me_3NCH_2CH=CH_2][B_5O_8]$. In the second step, the organic cation is oxidised exothermically above 300°C to release CO_2 and NO_2 and leave $2.5B_2O_3$ as a glassy solid with 54.7% of the original weight present in the residue. Most products followed a similar pattern, which varied depending on the thermal stability of the cation and the dryness of the starting material.

4.3: Concluding Remarks

Twenty-eight new polyborate salts have been prepared in high yields and successfully characterised using spectroscopic (NMR, IR), elemental analysis and thermal analysis (melting point, DSC/TGA). These products were obtained from four main families of organic ammonium-based cations: C_2- and C_3-linked bis(alkyl ammonium), C_6- and C_8-linked bis(alkyl imidazolium), C_6- and C_8-linked bis(alkyl pyrrolidinium), and guanidinium.

A total of 17 crystal structures were determined with 15 different cations, and of these 16 were pentaborate(1-) salts and one was a tetraborate(2-) salt (**1a**). Of the 16 pentaborate salts, 10 formed the most common α,α,α,β H-bonding configurations, including 2 "herringbone" (**2a**, **3a**), 6 "brickwall" (**1b**, **2b**, **4a**, **5a**, **6a**, **6b**) and two uncategorised configurations featuring reciprocated β interactions (**20a**, **21a**, **22a**). 4 of the pentaborate salts formed α,α,α,γ configurations (**7a**, **9a**, **18a**, **19a**), and compound **8a** formed the particularly rare α,α,β,β configuration, featuring two C(8) β-chains. The size and shape of the cation templates the configuration of the borate lattice and the size of the cavity required to accommodate it. A further eleven cations produced pentaborate salts, but attempts to grow suitable crystals for X-ray structural analysis were unsuccessful.

Chapter 5: Experimental

5.1: General

All chemicals and reagents were purchased from Sigma Aldrich (UK), or Fisher Scientific (UK), and used as supplied without further purification. Halide salts **3**-**17**, used in **Chapter 4**, were kindly provided by Dr. Ahmad Al-Dulayymi, from the School of Natural Science, Bangor, and were also used as obtained.

NMR spectra of all materials in **Chapter 2** and compounds **1-18a** were recorded at room temperature (298K) on a Bruker Ultrashield^{TM} Plus 400, operating at 400 MHz for ^{1}H, 100 MHz for ^{13}C spectra using D_2O solvent as an internal standard; and at 128 MHz for ^{11}B, using $BF_3{\cdot}OEt_2$ as an external standard. ^{29}Si experiments were carried out in D_2O at 80 MHz using TMS as an external standard. Compounds proceeding **18a** were recorded at room temperature (298k) on a UltraShield^{TM} *Plus* 500, operating at 500 MHz for ^{1}H, 125 MHz for ^{13}C and 160 MHz for ^{11}B. All NMR spectra were recorded using the Bruker TopSpin^{TM} 3.2 software package, and were further analysed using MestReNova v14.0.1

Infrared (FTIR) spectra were either obtained as KBr disks on a Perkin-Elmer 100 FTIR spectrometer over 400-4000cm^{-1}, or directly as powders using a Bruker Alpha Platinum ATR FTIR spectrometer over 375-4000cm^{-1}. Both devices ran 32 background and sample scans per experiment. Differential scanning calomimetry (DSC) and thermogravimetric analyses (TGA) were performed from room temperature to 700 ^{o}C (unless otherwise stated) in an air atmosphere on an SDT Q600 V4. Build 59 instrument, using alumina crucibles, with a ramp rate of 10^{o}C min^{-1}. Elemental analyses (C, H and N), were performed externally at OEA Laboratories Ltd. Callington, Cornwall.

Single-crystal X-ray crystallography of the polyborate materials was performed externally by Dr Peter N. Horton as part of the UK National Crystallography Service (NCS), at the University of Southampton.

Flame atomic absorption spectroscopy for silicon determination was carried out on a Varian SpectrAA 220FS Flame AAS using a single-element hollow cathode lamp for silicon. An acetylene flame was utilised with nitrous oxide gas support. The lamp current was set to 10 mA, with a wavelength of 251.6 nm chosen with a slit width of 0.2 nm.

UV-Visible spectroscopy for silicic acid stability studies was carried out using a PerkinElmer Lambda 35 spectrophotometer on aqueous solutions in polystyrene cuvettes, focussing primarily on 400-420 nm wavelength, and 815 nm for extremely dilute samples.

5.2: Preparation of TAA(1)-TAA(7) and related formulations

5.2.1: Preparation of (2,3-Dihydroxypropyl)trimethylammonium hydroxide (TAA(1))

[$Me_3NCH_2CH(OH)CH_2OH$][OH]

Ethanolic trimethylamine solution (23.8 mL, 100 mmol) was cooled on an ice bath. 2,3-Epoxy-1-propanol (8.0 mL, 120 mmol) was added slowly *via* syringe to the amine over 10 mins, while maintaining the solution temperature between 15-25^oC. After 30 mins, H_2O (10 mL) was added and the reaction mixture was stirred overnight. The unreacted glycidol was extracted using $CHCl_3$ (4 x 40 mL), and the aqueous phase was reduced in volume on the rotary exaporator to a yellow solution (28.1 g). An aliquot of the solution (1.0 mL) was titrated against HCl (2.0M) in order to determine the hydroxide concentration, using universal indicator to identify the neutral end point. [OH^-] = 5.93 M. NMR/ppm: δ_H: 2.90 (s, 9H, CH_3), 3.06 (dd, 1H, CH_2N), 3.22 (dd, 1H, CH_2N), 3.37 (dd, 2H, CH_2OH), 3.95 (m, CHOH); δ_C: 53.90 (CH_3N), 53.94 (CH_3N), 53.98 (CH_3N), 64.98 (CH_2N), 69.19 (CHOH), 70.13 (CH_2OH).

5.1.2: Preparation of (2,3-Dihydroxypropyl)ethyldimethylammonium hydroxide (TAA(2))

[$Et_2MeNCH_2CH(OH)CH_2OH$][OH]

N,N-dimethylethylamine (7.3 g, 10.8 mL, 100 mmol) was cooled on an ice bath. 2,3-Epoxy-1-propanol (8.0 mL, 120 mmol) was added slowly *via* syringe to the amine over 10 mins, while maintaining the solution temperature between 15-25^oC. After 30 mins, H_2O (10 mL) was added, and after reducing the temperature to 25^oC a further aliquot of H_2O (20 mL) was added and the reaction mixture was stirred overnight. The unreacted glycidol was extracted using $CHCl_3$ (4 x 40 mL), and unreacted amine was removed by rotary evaporation, while the aqueous phase was reduced in volume to a yellow solution (30.0 g). An aliquot of the solution

(1.0 mL) was titrated against HCl (2.0M) in order to determine the hydroxide concentration, using universal indicator to identify the neutral end point. [OH^-] = 3.70M. NMR/ppm: δ_H: 1.14 (3H, CH_3) 2.90 (6H, 2*CH_3), 3.02 (dd, 1H, CH_2N), 3.17-3.40 (7H, CH_2N, CH_2OH), 3.94 (CHOH); δ_C: 7.47 (CH_3) 50.80 (CH_3N), 50.82(CH_3N), 61.03 (CH_2N), 64.72 (CH_2N) 69.81 (CHOH), 70.42 (CH_2OH).

5.1.3: Preparation of (2,3-Dihydroxypropyl)triethylammonium hydroxide (TAA(3)) [$Et_3NCH_2CH(OH)CH_2OH$][OH]

Triethylamine solution (10.2 g, 14.0 mL, 100 mmol) was cooled on an ice bath. 2,3-Epoxy-1-propanol (8.0 mL, 120 mmol) was added slowly *via* syringe to the amine over 10 mins, while maintaining the solution temperature between 15-25^oC. After 20 mins, H_2O (20 mL) was added, and after cooling the solution to 25^oC, a further aliquot of H_2O (10 mL) was added and the reaction mixture was stirred overnight. The unreacted glycidol was extracted using $CHCl_3$ (4 x 40 mL), and unreacted amine was removed by rotary evaporation, and the aqueous phase was reduced in volume to a pale yellow solution (22.7 g). An aliquot of the solution (1.00 mL) was titrated against HCl (2.00 M) in order to determine the hydroxide concentration, using universal indicator to identify the neutral end point. [OH^-] = 1.8M. NMR/ppm: δ_H: 1.12 (t, 9H, CH_3), 3.06-3.35 (10H, CH_2), 3.60-3.80 (2H, CH_2), 3.98 (1H, CH); δ_C: 6.72 (CH_3), 53.42 (CH_2N), 62.62 (CH_2N), 66.23 (CH_2OH), 70.42 (CHOH).

5.1.4: Preparation of (2,3-Dihydroxypropyl)dimethylethanolammonium hydroxide TAA(4) [$Me_2(CH_2CH_2OH)NCH_2CH(OH)CH_2OH][OH]$

N,N-Dimethylethanolamine (8.9 g, 10.0 mL, 100 mmol) was cooled on an ice bath. 2,3-Epoxy-1-propanol (8.00 mL, 120 mmol) was added dropwise *via* syringe to the amine over 10 minutes, while maintaining the solution temperature below 15°C. The reaction mixture was monitored for the appearance of a yellow colour, and H_2O (25 mL) was added at this point, and left to cool for 20 minutes. A further aliquot of water (10 mL) was added, and left to stir overnight. The unreacted glycidol was extracted using $CHCl_3$ (4 x 40 mL), and unreacted amine was removed by rotary evaporation, and the aqueous phase was reduced in volume to a yellow-orange solution (20.9 g). An aliquot of the solution (1.00 mL) was titrated against HCl (2M) in order to determine the hydroxide concentration, using universal indicator to identify the neutral end point. $[OH^-]$ = 4.2M. NMR/ppm: δ_H: 2.95 (s, 6H, CH_3), 3.15-3.43 (8H, CH_2N), 3.72-3.75 (2H CH_2OH), 3.91-4.05 (1H, CHOH); δ_C: 52.33 (CH_3), 52.37 (CH_3), 55.23 (CH_2N), 64.37 (CH_2N), 66.28 (CHOH), 66.76 (CH_2OH), 68.03 (CH_2OH).

5.1.5: Preparation of (2,3-Dihydroxypropyl)diethylethanolammonium hydroxide TAA(5) [Et2(CH2CH2OH)NCH2CH(OH)CH2OH][OH]

N,N-Diethylethanolamine (11.7 g, 13.3 mL, 100 mmol) was cooled on an ice bath. 2,3-Epoxy-1-propanol (8.0 mL, 120 mmol) was added dropwise *via* syringe to the amine over 10 minutes, while maintaining the solution temperature between 15-25°C. The mixture was left to stand for 20 minutes, and an aliquot of water (20 mL) was added, causing an exothermic reaction. The mixture was left to cool for a further 10 minutes before a further 10 mL of water was added, and left to stir overnight. The unreacted glycidol was extracted using $CHCl_3$ (4 x 40 mL), and unreacted amine was removed by rotary evaporation, and the aqueous phase was

reduced in volume to a yellow solution (23.9 g). An aliquot of the solution (1.0 mL) was titrated against HCl (2.0M) in order to determine the hydroxide concentration, using universal indicator to identify the neutral end point. [OH^-]= 2.6M. NMR/ppm: δ_H: 1.07 (s, 6H, CH_3), 3.18-3.39 (8H, CH_2N), 3.59-3.75 (4H, CH_2OH), 3.88-4.08 (1H, CHOH); δ_C: 6.70 (CH_3), 6.76 (CH_3), 54.16 (CH_2), 54.69 (CH_2), 60.24 (CH_2), 62.53 (CH_2OH), 64.48 (CH_2OH), 66.63 (CHOH).

5.1.6: Preparation of *N,N,N,N',N',N'*-hexamethyl poly(ethylene glycol)-500 diammonium hydroxide TAA(6) [$Me_3N(CH_2CH(OH)(OCH_2CH_2)_nOCH_2CH(OH)CH_2NMe_3]$ [$OH]_2$

Ethanolic trimethylamine (23.8 mL, 80 mmol) was cooled on an ice bath. To this, PEG(500) diglycidyl ether (28.5 g, 25.0 mL, 57 mmol) was added dropwise *via* syringe, maintaining the reaction temperature below 25°C. After 10 minutes, water (15 mL) was added, causing an exothermic reaction. When the temperature dropped below 20°C, a further aliquot of water (15 mL) was added. The resulting product was concentrated under reduced pressure until no further change in weight was observed (34.0 g), yielding a viscous yellow oil. NMR/ppm: δ_H: 3.11 (s, 18H), 3.22-3.28 (t, 2H), 3.35-3.38 (d, 4H), 3.44-3.48, (dq 4H), 3.60 (s, 40H); δ_C: 54.04 (CH_3), 65.01 (CHOH), 69.54 (CH_2), 69.92 (CH_2OH).

5.1.7: Attempted Preparation of TAA(7)

$Me_2(CH_2CH(OH)CH_2OH)N(CH_2)_2N(CH_2CH(OH)CH_2OH)Me_2][OH]_2$

N,N,N',N'-tetramethylethylenediamine (6.0 mL, 7.0 g, 67 mmol) was cooled on an ice bath. 2,3-epoxy-1-propanol (10.0 mL, 150 mmol) was added dropwise *via* syringe to the amine over 10 minutes, while maintaining the solution temperature below 15^{o}C. The reaction mixture was monitored for the appearance of a yellow colour, and H_2O (25 mL) was added at this point, and left to cool for 20 minutes. A further aliquot of water (10 mL) was added, and left to stir overnight. The unreacted glycidol was extracted using $CHCl_3$ (4 x 40 mL), and the aqueous phase was reduced in volume to a yellow-orange solution using a rotary evaporator. An aliquot of the solution (1.0 mL) was titrated against HCl (2.0M) in order to determine the hydroxide concentration, using universal indicator to identify the neutral end point. [OH^-] = 2.45M. NMR/ppm: δ_H: 2.90-2.92 (d, 4H, CH_2N), 3.21-3.27 (m, 12H, CH_3), 3.68-3.80 (m, 4H, CH_2N), 3.92-4.09, (m, 4H, CH_2OH), 4.25-4.38 (m, 2H, CHOH). δ_C: 52.83 (CH_3N) 53.05 (CH_3N), 60.87 (CH_2N), 62.44 (CH_2N), 63.46 (CH_2OH), 66.03 (CHOH).

5.1.8: Determination of silicic acid content in “storage” and “tank” solutions

Silicon content was determined using the silicomolybdate spectrophotometric method, adapted from Preari *et al*,[34] A series of stock solutions were prepared for the spectrophotometric detection test: 10.0 g of ammonium molybdate was dissolved in 100 mL of water, and its pH was adjusted between 7 and 8 using NaOH to prevent precipitation of insoluble ammonium molybdate. A 6M HCl solution was prepared by mixing one volume of 37% HCl solution with one equivalent volume of deionised water. A solution of oxalic acid was prepared by dissolving 8.8 g of oxalic acid in 100 mL of water. Prototype solutions containing stabilised silicic acid at pH = 7 (“tank” solution), and pH = 1 (“storage” solution) were prepared previously and left to stand in poly(ethylene) containers for the desired storage time. Prior to measurement, samples of these solutions were diluted from the previously recorded concentration to approximately 500 ppm “SiO_2” by appropriate dilution using distilled water. From each diluted solution, a 2 mL aliquot was filtered through a 0.45 µm syringe filter, and diluted to 25 mL in a separate container using deionised water. 1 mL of the ammonium molybdate stock solution was added to this solution, followed by 0.5 mL of the 6M HCl solution. The developing solution was then vigorously mixed and left undisturbed for 10 min. Next, 1 mL of the oxalic acid stock solution was added, and the solution was thoroughly mixed. After 2 minutes of standing, the yellow/green solution was pipetted into a polystyrene cuvette to be placed in the test sample holder of the spectrophotometer. A reference solution was prepared containing 25 mL deionised water, 1 mL ammonium molybdate stock, 0.5 mL of 6M HCl and 1 mL of oxalic acid. An aliquot of this solution was added to a polystyrene cuvette, and placed in the reference holder of the spectrophotometer. The absorbance was quanitified at *ca.* 400 nm.

5.2: Shelf-life determination of "storage" formulations

Silicic acid formulations were prepared every 12 months containing 13,000 ppm "SiO_2" in 10 mL batches by firstly acidifying a 34 g batch of concentrated **TAA(1)**, titrated against HCl and found to contain approximately 4.8M $(OH)^-$, with approximately 30 mL 6M HCl solution. This ensured a significant enough excess of acid to prevent a rise in solution pH upon addition of the silicate. To the 10 mL batches of acidified **TAA(1)** was added 0.46 g $Na_2SiO_3.5H_2O$. This equated to approximately 0.13 g "SiO_2" per 10 mL batch.

After the production of the third batch of formulation, aliquots of the three batches were subjected to the silicomolybdate test in section **5.1.8**. In order to reach a concentration suitable to the working range of the spectrophotometer, each batch was diluted as before to approximately 500 ppm "SiO_2". This was achieved by collecting 0.385 mL of the "13,000 ppm" stock solution using a precision pipette and diluting to 10 mL with deionized water.

5.3: Field trials of foliar silicon formulations

5.3.1: *Cultivar swift* potato glasshouse pot trial

5.3.1.1: Preparation of TAA(1) formulations

A **TAA(1)**-stabilised silicic acid formulation (21.5 g, *ca.* 21.5 mL) was produced containing the stabilising ingredient **TAA(1)** (9.6 g), sodium metasilicate (0.9 g, *ca.* 11,500 ppm "SiO_2"), hydrochloric acid (10 mL of 6M) and was found to be pH ~0.5. 1 mL of formulation was diluted to 1 L using standard tap water from the research laboratory at Bangor. In foliar sprays where fulvic acid was used, 0.4 mL of 40% w/v fulvic acid extract was dissolved in 1 L of tap water. For the fulvic/silicic formulation, 0.4 mL of fulvic extract and 1 mL of silicic formulation were diluted to 1 L of spray in the same bottle.

5.3.1.2: Trial procedures

The foliar sprays were applied to run-off. After each application of spray, the plants were re-randomized within the greenhouse growing space. Further sprays were applied once every 8 days (final set once every 16 days), for a total of 6 foliar applications (3 for the final set). The first foliar application used 50 mL of spray across each set of 8 plants. The volume of spray used per set was increased incrementally as the plants matured, eventually reaching 300 mL divided across 8 plants on the final application. Care was taken to prevent the sprays from entering the soil to avoid unwanted uptake through the roots. Foliar sprays were no longer applied after the 56th day. The plants were then left unsprayed with regular watering and feeding until foliar senescence was evident in at least half of the replicates, which was approximately 2 weeks after the final spray.

The plants were randomly numbered, and the tubers were harvested. The fresh weight of the foliage was noted. The foliage was then dried at 80^{o}C for 5 days and the dried weight was recorded. The overall root yield for each set of 8 replicates was also collected. The tubers from each individual plant were segregated into three categories by passing them through a series of riddle sieves: < 25 mm diameter of the narrowest point (defined as too small to go to market), 25-35 mm diameter (baby potatoes) and > 35 mm diameter (marketed as regular potatoes). The number of tubers in each category were also noted, and the number of stems on each potato plant was also recorded.

5.3.2: Paragon spring wheat and winter cabbage glasshouse pot trial

5.3.2.1: Assays of plant material

(a) Attempted determination of plant Si content by colourimetric method

Prior to running AAS for silicon content, 1 mL aliquots of the acid-extracted plant matter were subjected to the molybdenum blue method. Stock solution A, containing 20 g L^{-1} ammonium molybdate tetrahydrate and 60 mL L^{-1} of 12M hydrochloric acid in deionized water, is prepared prior to assays. Stock solution B is also prepared by adding 20 g oxalic acid, 4 methylaminophenol sulphate (6.7 g), anhydrous sodium sulfite (4 g), deionised water (500 mL) and concentrated sulphuric acid (100 mL) in a 1 L volumetric flask and completed with deionised water.

For analysis of the extracts, 1 mL of the diluted extract solution was sampled and diluted to 16 mL with deionised water. To this is added 1.5 mL solution A. After 10 minutes, 7.5 mL solution B is added to the assay solution. The blue colour is left to develop over 2 hours and the optical density is measured at λ = 810 nm. The blue colour remains stable for up to 48

hours, and therefore can be measured at any point in this period. Upon addition of solution B, a faint blue colour was obtained. However, after standing for the required 2-hour development time, this colour faded, due to the removal of phosphate in the solution by the oxalic acid. Absorbances were measured at 810 nm, and the resulting readings showed that there was not any molybdate-active silicon in the test solutions.

(b) Determination of plant Si content by atomic absorption spectroscopy (AAS)

Standards for silicon were produced from a 1,000 mg L^{-1} Si stock solution in 2% NaOH (Sigma Aldrich) ranging from 5 mg L^{-1} to 200 mg L^{-1} to generate a linear calibration. An R^2 value of 0.996 was obtained for the calibrants, with an optimum working range of 3-400 mg L^{-1}. Approximately 1 mL of each sample is drawn into the capillary tube per test, with three sequential readings carried out after a delay of 3 seconds, to generate an average reading. Three digests were prepared for each type of foliar application to produce a total of 9 readings per foliar spray. Readings exceeding +/- 5% of the average absorbance were discounted as experimental errors prior to statistical analysis. The capilliary tube inlet was thoroughly flushed with deionised water between readings, until the colour of the flame returned to normal.

The absorbance reading outputs were converted to concentration in ppm using the equation of the calibration curve. Si content (ppm) for **Cabbage**: Control 19.5 ppm, PEG-Si formulation 21.7 ppm, TAA(1)-Si formulation 20.7 ppm, TAA(1)-SiB formulation 24.3 ppm. Si content (ppm) for **Wheat**: Control 33.3 ppm, PEG-Si formulation 41.1 ppm, TAA(1)-Si formulation 48.3 ppm, TAA(1)-SiB formulation 42.8 ppm.

(c) Total X-Ray Fluorescence (TXRF) elemental analysis of plant material

Total X-Ray Fluorescence spectroscopy (TXRF) analysis was carried out by Sarah Chesworth, technician in the Environment Centre Wales, on an S2 Picofox TXRF (Bruker AXS Microanalysis GmbH, Germany) to determine the element content in powdered foliar samples. The plant samples were finely ground and then passed through a 70 µM sieve. 20 mg of each dried sample was weighed into a centrifuge tube for submission.

The powdered samples were then mixed with 1 ml of 1% Triton-X solution (Sigma). The sample was then internally standardised against 5 µL of gallium 1,000 mg L^{-1} stock solution. The solutions were mixed well using a vortexer, and 10 µL of the sample was pipetted onto the centre of a siliconized disc before settling of any sediments could occur. The disk was then placed on a hotplate and dried at 50^{o}C for 15 minutes. The discs were then fixed onto the sample carrier. Each sample was scanned qualitatively to ensure the absence of gallium prior to internal standardisation.

A gain correction was carried out at the start of each run of (approx. every 20 samples) using an un-siliconised disc carrying 10 µl of Ga 1,000 mg L^{-1}. The disc was prepared in the same manner as the samples, by pipetting 10 µL of mono-element standard onto the unsiliconised disc and dried on a hotplate. The disc was covered with a glass lid to prevent contamination. The gain correction process corrects for any spectroscopic drift, which may occur over time, by reconciling the fluorescence lines of the element used with the software's atomic data library. Each sample disc was analysed for 300 seconds using a calibrated plant method, which is set up to automatically identify the following elements: Al, Si, P, S, Cl, K, Ca, Ti, V, Cr, Mn, Fe, Ni, Cu, Zn, As, Br, Rb, Sr, Y, Ba, and Pb. In this experiment, readings for Al, S and Cl were

deemed unreliable and were omitted from the results. Measurement of Si was not possible using the benchtop TXRF due to the carrier discs being made of quartz.

Wheat control elemental content (mg kg^{-1}): P(2,615), K(23,765), Ca(8,285), Ti(41), V(4.2), Cr(7.1), Mn(117), Fe (549), Ni(3.0), Cu(8.6), Zn(57), As(1.1), Br(38), Rb(15), Sr(19), Y(trace), Ba(37), Pb(5.61). **Wheat PEG-Si** elemental content (mg kg^{-1}): P(3,076), K(28,440), Ca(5,350), Ti(26), V(2.5), Cr(9.2), Mn(139), Fe(551), Ni(4.0), Cu(13), Zn(71), As(1.5), Br(38), RB(17), Sr(14), Y(1.2), Ba(38), Pb(5.0). **Wheat TAA(1)-Si** elemental content (mg kg^{-1}): P(3,358), K(29,214), Ca(5,370), Ti(32), V(2.2), Cr(8.5), Mn(160), Fe(523), Ni(3.2), Cu(14), Zn(76), As(0.4), Br(39), Rb(17), Sr(14), Y(1.7), Ba(29), Pb(8.5). **Wheat TAA(1)-SiB** elemental content (mg kg^{-1}): P(2,522), K(25,622), Ca(4,250), Ti(33), V(2.4), CR(8.3), Mn(132), Fe(445), Ni(3.2), Cu(11), Zn(73), As(1.5), Br(40), Rb(17), Sr(12), Y(1.7), Ba(30), Pb(6.9).

Cabbage control elemental content (mg kg^{-1}): P(1,525), K(16,648), Ca(19,390), Ti(0.0), V(2.4), Cr(trace), Mn(25), Fe(184), Ni(1.3), Cu(3.1), Zn(14), As(0.4), Br(18), Rb(14), Sr(36), Y(1.6), Ba(16), Pb(0.5). **Cabbage PEG-Si** elemental content (mg kg^{-1}): P(1,472), K(16,338), Ca(19,390), Ti(9.0), V(2.4), Cr(4.6), Mn(21), Fe(139), Ni(trace), Cu(3.6), Zn(11), As(trace), Br(17), Rb(14), Sr(37), Y(0.8), Ba(5), Pb(1.4). **Cabbage TAA(1)-Si** elemental content (mg kg^{-1}): P(1,635), K(17,197), Ca(21,326), Ti(4.0), V(trace), Cr(3.1), Mn(24), Fe(99), Ni(0.9), Cu(2.9), Zn(12), As(trace), Br(18), Rb(14), Sr(40), Y(1.5), Ba(14), Pb(1.7). **Cabbage TAA(1)-SiB** elemental content (mg kg^{-1}): P(1,740), K(16,955), Ca(22,890), Ti(7.7), V(3.0), Cr(trace), Mn(25), Fe(114), Ni(0.8), Cu (2.7), Zn(10), As(trace), Br(22), Rb(13), Sr(42), Y(1.2), Ba(14), Pb(0.8).

5.4: Synthesis of NMC borates

5.4.1: Preparation of TAA(1) (2,3-Dihydroxypropyl)trimethylammonium pentaborate [$Me_3NCH_2CH(OH)CH_2(OH)][B_5O_6(OH)_4$]

(2,3-Dihydroxypropyl)trimethylammonium hydroxide solution (1.0 mL, 5.93 mmol) was added to a minimal amount of H_2O and to this boric acid (1.8 g, 29.66 mmol, 5eq.) was added. The pH of the solution was tested and found to be *ca*. 7. The mixture was left in a sample vial for three days, and the solvent was removed by rotary evaporation to yield a crude white powder (2.0 g, 5.68 mmol, 96%), which was set aside for further analysis and recrystallisations. NMR/ppm: δ_H: 3.12 (s, 9H, CH_3), 3.33 (dd, 1H, CH_2N), 3.37 (dd, 1H, CH_2N), 3.48 (dd, 2H, CH_2OH), 4.26 (m, CHOH); δ_B: 1.2 (3%), 6.1 (6%), 10.4 (2%), 13.07 (14%), 19.01 (75%); δ_C: 54.05 (3C, CH_3N), 64.80 (CH_2N). FTIR (KBr, cm^{-1}): 3399 (m), 1643 (m), 1473 (m), 1449 (w), 1346 (s), 1252 (m), 1198 (s), 1103 (m), 1028 (m), 923 (vs), 783 (m), 696 (w).

5.4.2: Preparation of TAA(2) (2,3-Dihydroxypropyl)ethyldimethylammonium pentaborate [$EtMe_2NCH_2CH(OH)CH_2(OH)][B_5O_6(OH)_4$]

(2,3-Dihydroxypropyl)ethyldimethylammonium hydroxide solution (1.0 mL, 3.70 mmol) was added to a minimal amount of H_2O and to this boric acid (1.1 g, 18.5 mmol, 5eq.) was added. The pH of the solution was tested and found to be ~7. The mixture was left in a sample vial for two days, and the solvent was removed by rotary evaporation to yield a thick oil, which was placed in an oven at 80°C for three hours to yield a glassy white solid (1.2 g, 3.38 mmol, 91%), which was set aside for further analysis and recrystallisations. NMR/ppm: δ_H: 1.27 (s, 3H, CH_3), 3.05 (s, 6H, CH_3), 3.26-3.55 (m, 7H, CH_2N, CH_2OH), 3.81 (m, 1H, CHOH); δ_B: 6.3 (%),

10.5 (2%), 13.4 (11%), 18.65 (69%). FTIR (KBr, cm^{-1}): 3398 (w), 1644 (m), 1437 (m), 1362 (s), 1334 (m), 1099 (m), 1024 (m), 922 (vs), 779 (m), 703 (w).

5.4.3: Preparation of TAA(3) (2,3-Dihydroxypropyl)triethylammonium pentaborate $[Et_3NCH_2CH(OH)CH_2(OH)][B_5O_6(OH)_4]$

(2,3-Dihydroxypropyl)triethylammonium hydroxide solution 2.0 mL, (4.0 mmol) was added to a minimal amount of H_2O and to this boric acid (1.2 g, 20 mmol). The pH of the solution was tested and found to be ~7. After several hours of strring, the solvent was removed by rotary evaporation to yield a thick oil, which was placed in an oven at 80^oC for three hours to yield a glassy white solid (1.4 g, 3.4 mmol, 85%), which was set aside for further analysis and recrystallisations. NMR/ppm: δ_H: 1.17 (t, 9H, CH_3) 3.17-3.38 (s, 8H, CH_2N), 3.79-3.96 (m, 2H, CH_2OH), 4.11-4.22 (m, 1H, CHOH); δ_B: 1.2 (4.9%), 5.9 (7.0%), 10.1 (5%), 13.2 (15%), 19.1 (65%).

5.4.4(a): Preparation of *N,N,N,N',N',N'*-hexamethylethanediammonium diiodide (1) $[Me_3N(CH_2)_2NMe_3]I_2$

$Me_2N(CH_2)_2NMe_2$ (3.3 g, 3.0 mL, 20 mmol) was added to acetonitrile (50 ml). MeI (11.4 g, 5 mL, 80 mmol) was added and the resulting solution was heated to reflux for 4 hours. The white solid $[Me_3N(CH_2)_2NMe_3]I_2$ which formed was isolated by filtration and washed with Et_2O (7.0 g, 87%). This was used in the next step without further purification. NMR/ppm: δ_H: 3.34 (t, 18 H); 4.07 (t, 4H); δ_C: 54.02 (CH_3), 59.93 (CH_2). FTIR (KBr/cm^{-1}): 3434 (br), 3012 (s), 3003 (s), 2971 (s), 1487 (s), 1471 (s), 1447 (m), 1403 (s), 1221 (m), 954 (vs), 921 (s), 815 (s).

5.4.4(b): Preparation of *N,N,N,N′,N′,N′*-hexamethylethanediammonium tetraborate (1a)

$[Me_3N(CH_2)_2NMe_3][B_4O_5(OH)_4]\cdot 2H_2O\cdot 2B(OH)_3$

$[Me_3N(CH_2)_2NMe_3]I_2$ (1.1 g, 2.7 mmol) was dissolved in H_2O (20 mL) and stirred with excess (15.0 g) of DOWEX 550A ion-exchange resin (OH^- form) for 24 h. The slurry was filtered and $B(OH)_3$ (0.5 g, 8.1 mmol) was added to the filtrate. The solution was left stand for 4 h and concentrated to ca. 7 mL under reduced pressure. The solution was left to stand in a small sample vial for 7 days to yield a crystalline product (0.3 g, 0.6 mmol, 22%). These crystals were suitable for sc-XRD studies. $C_8H_{36}B_6N_2O_{17}$. Anal. Calc.: C = 19.3%, H = 7.3%, N = 5.6%. Found: C = 20.6%, H = 7.3%, N = 5.7%. TGA: 100–200 °C, condensation of tetraborate/$B(OH)_3$ units and loss of 2 interstitial H_2O (total $7H_2O$) 25.7% (25.3% calc.); 200–800 °C, oxidation of organic cation to leave residual $3B_2O_3$ 32.3% (29.0% calc.). NMR/ppm: δ_H: 3.00 (18H, s, CH_3), 3.85 (4H, m, CH_2); δ_B: 1.3 (5%), 7.4 (43%), 11.7 (52%); δ_C: 53.82 (CH_3) 57.77 (CH_2). FTIR (KBr, cm^{-1}): 3435 (s), 1638 (m), 1481 (s), 1418 (s), 1385 (m), 1352 (m), 1070 (m), 958 (s), 927 (m). XRD crystallographic data: $C_8H_{36}B_6N_2O_{17}$, *M*r = 497.25, monoclinic, $P2_1$, a = 9.0242(2) Å, b = 12.0350(3) Å, c = 11.1688(4) Å, α = γ = 90°, β = 109.811(3)°, V = 1141.21(6) $Å^3$, T = 100(2) K, Z = 2, Z' = 1, μ(MoKα) = 0.131 mm^{-1}, 24237 reflections measured, 5229 unique (R_{int} = 0.0265) which were used in calculations. The final wR_2 was 0.0802 (all data) and R_1 was 0.0303 (I > 2σ(I)).

5.4.4(c): Preparation of *N,N,N,N′,N′,N′*-hexamethylethanediammonium bis(pentaborate) (1b) $[Me_3NCH_2CH_2NMe_3][B_5O_6(OH)_4]_2$

$[Me_3NCH_2CH_2NMe_3]I_2$ (0.7 g, 1.62 mmol), prepared as described for **1**, was dissolved in H_2O (20 ml), and stirred with excess Dowex 550 A monosphere ion exchange resin (OH^- form, 15 g) for 24 h. The slurry was filtered and $B(OH)_3$ (1.0 g, 16.2 mmol) was added to the filtrate, which was allowed to stand for 4 h and then reduced to dryness to yield the crude product (1b) (0.8 g, 80%). A 0.2 g sample of the crude product was redissolved in 20 mL H_2O and left to stand for 7 days to form a few white crystals. These crystals were suitable for sc-XRD studies. $C_8H_{30}B_{10}N_2O_{20}$. Anal. Calc.: C = 16.5%, H = 5.2%, N = 4.8%. Found: C = 16.8%, H = 5.2%, N = 4.8%. M.p. >250 °C. TGA: 100-250 °C, condensation of pentaborate with loss of four H_2O 12.0% (12.4% calc.); 150-700 °C, oxidation of organic residue leaving residual B_2O_3 61.8% (59.8% calc.). NMR/ppm: δ_H: 3.20 (t, 18H, CH_3); 3.92 (t, 4H, CH_2); δ_B: 13.2 (16%), 17.1 (84%); δ_C: 53.77 (CH_3), 57.82 (CH_2). FTIR (KBr, cm^{-1}): 3437 (br), 3052 (m), 1651 (m), 1434 (m), 1361 (m), 1252 (s), 1103 (s), 1020 (s), 925 (vs), 782 (vs), 696 (s), 591 (m), 509 (m), 455 (s). XRD Crystallographic data: $C_8H_{30}B_{10}N_2O_{20}$, *Mr* = 582.44, triclinic, P-1 (No. 2), *a* = 8.5098(2) Å, *b* = 9.3293(2) Å, *c* = 16.7816(5) Å, *α* = 88.937(2)°, *β* = 78.940(2)°, *γ* = 80.430(2)°, *V* = 1289.24(6) $Å^3$, *T* = 100(2) K, *Z* = 2, *Z′* = 1, μ(MoK_α) = 0.134 mm^{-1}, 26740 reflections measured, 5854 unique (R_{int} = 0.0493) which were used in all calculations. The final wR_2 was 0.1145 (all data) and R_1 was 0.0438 (I > 2σ(I)).

5.4.5(a): Preparation of *N,N,N,N′,N′,N′*-1,3-propanediammonium iodide $[Me_3N(CH_2)_3NMe_3]I_2$ (2)

$Me_2N(CH_2)_3NMe_2$ (2.6 g, 20 mmol) dissolved in CH_3CN (50 mL) was refluxed with MeI (11.4 g, 80 mmol) for 4 h. The white solid formed, $[Me_3N(CH_2)_3NMe_3]I_2$ (8.3 g, 100%) was isolated by filtration, washed with Et_2O and used without further purification. NMR/ppm: δ_H: 2.31 (2H, quin., CH_2), 3.13 (18H, s, CH_3), 3.37 (4H, t, CH_2N); δ_C: 17.41 (CH_2), 53.25 (CH_3), 62.39 (CH_2). FTIR (KBr, cm^{-1}): 3447 (s), 3011 (s), 2957 (m), 1624 (m), 1486 (s), 1475 (s), 1408 (m), 1244 (m), 1054 (m), 973 (s), 944 (s), 901 (s), 762 (m), 545 (m).

5.4.5(b): Preparation of *N,N,N,N′,N′,N′*-1,3-propanediammonium bis(pentaborate) $[Me_3N(CH_2)_3NMe_3]\ [B_5O_6(OH)_4]_2{\cdot}0.5H_2O$ (2a)

$[Me_3N(CH_2)_3NMe_3]I_2$ (0.4 g, 0.97 mmol), prepared as described in section **5.4.5(a)**, was dissolved in H_2O (20 mL) and stirred with excess (8.0 g) of DOWEX 550A ion-exchange resin (OH^- form) for 24 h. The slurry was filtered and $B(OH)_3$ (0.6 g, 9.7 mmol) was added to the filtrate. Partial evaporation of the solution afforded a white crystalline solid (0.6 g, 96%), separated by filtration. These crystals were suitable for sc-XRD studies. $C_9H_{33}B_{10}N_2O_{20.5}$. Anal. Calc.: C = 17.9%, H = 5.5%, N = 4.6%. Found: C = 18.2%, H = 5.4%, N = 4.6%. TGA: 250–300 °C, condensation of pentaborate units with loss of $4.5H_2O$ 13.0% (13.4% calc.); 300–700 °C, oxidation of organic cation to leave residual $5B_2O_3$ 57.3% (57.5% calc.). NMR /ppm: δ_H: 2.29 (2H, quint., CH_2), 3.11 (18H, s, CH_3), 3.33 (4H, t, CH_2N); δ_B: 1.1 (3%), 13.1 (35%), 18.0 (62%); δ_C: 17.28 (CH_2), 53.15 (CH_3), 62.37 (CH_2). FTIR (KBr, cm^{-1}): 3437 (s), 3082 (s), 1638 (m), 1438 (m), 1359 (s), 1251 (m), 1102 (s), 1026 (m), 926 (s), 782 (m), 696 (m). XRD crystallographic data: $C_9H_{33}B_{10}N_2O_{20.5}$. *Mr* = 605.47, monoclinic, *C*2/*c*, *a* = 26.8754(5) Å, *b* = 11.5269(2) Å, *c* =

17.9383(4) Å, $\alpha = \gamma = 90^{o}$, β =103.154(2)^{o}, V = 5411.30(19) Å^3, T = 100(2) K, Z = 8, Z' = 1, μ(MoKα) = 0.132 mm^{-1}, 31515 reflections measured, 6191 unique (R_{int} = 0.0294) which were used in calculations. The final wR_2 was 0.0919 (all data) and R_1 was 0.0351 (I > 2σ(I)).

5.4.6: Preparation of *N,N,N,*trimethylallylammonium pentaborate

$[Me_3NCH_2CH{=}CH_2][B_5O_6(OH)_4]$ (2b)

$[Me_3N(CH_2)_3NMe_3]I_2$ (0.7 g, 1.62 mmol) was dissolved in H_2O (20 mL) and stirred with excess (13.5 g) of DOWEX 550A ion-exchange resin (OH^- form) for 24 h. The slurry was filtered and $B(OH)_3$ (1.0 g, 16.2 mmol) was added to the filtrate. The solution was left for 4 h before removal of solvent under reduced pressure at 85 °C to yield a 'damp' solid which was dried in an oven at 75 °C for 3 h to yield a white solid (0.93 g). ^{1}H NMR analysis showed this to be a ~ 2:1 mixture of **2a** and **2b**. Recrystallization of 0.2 g of this solid resulted in 0.1 g of **2b** with crystals suitable for sc-XRD analysis. $C_6H_{18}B_5NO_{10}$. Anal. Calc.: C = 22.6%, H = 5.7%, N = 4.4%. Found: C = 23.0%, H = 5.7%, N = 4.4%. TGA: 100–285 °C, condensation of pentaborate units with loss of $2H_2O$ 11.7% (11.3% calc.); 285–700 °C, oxidation of organic cation to leave residual $2.5B_2O_3$ 55.2% (54.7% calc.). NMR/ppm: δ_H: 3.00 (9H, s, CH_3), 3.85 (2H, d, CH_2N), 5.63 (2H, dd, CH_2=C), 5.96 (1H, m, CH=C); δ_B: 1.1 (1%), 13.4 (17%), 17.1 (82%); δ_C: 52.30 (CH_3), 68.39 (CH_2), 124.43 (CH), 129.14 (CH_2). FTIR (KBr, cm^{-1}): 3437 (s), 3262 (m), 1471 (m), 1427 (s), 1414 (s), 1389 (s), 1311 (s), 1168 (m), 1105 (s), 1012 (s), 921 (s), 777 (s), 724 (m), 708 (s). XRD crystallographic data: $C_6H_{18}B_5NO_{10}$, Mr = 318.26, monoclinic, $P2_1/c$, a = 9.54050(10) Å, b = 16.1031(2) Å, c = 9.43280(10) Å, $\alpha = \gamma = 90^{o}$, β = 90.1710(10)^{o}, V = 1449.17(3) Å^3, T = 100(2) K, Z = 4, Z' = 1, μ(CuKα) = 1.096 mm^{-1}, 13531 reflections measured, 2661 unique (R_{int} = 0.0236) which were used in calculations. The final wR_2 was 0.0845 (all data) and R_1 was 0.0314 (I > 2σ(I)).

5.4.7: Preparation of 1,1'-(1,6-hexanediyl)bis(3-methyl-1H-imidazol-3-ium) bispentaborate $[CH_3(C_3H_3N_2)(CH_2)_6(C_3H_3N_2)CH_3][B_5O_6(OH)_4]_2$ (3a)

1,1'-(1,6-hexanediyl)bis(3-methyl-1H-imidazol-3-ium diiodide (1.0 g, 1.99 mmol) was added to 16 g of DOWEX 550A ion exchange resin (OH^- form) and stirred for 18 hours. The DOWEX was removed by vacuum filtration and the filtrate was added to 1.2 g (20 mmol) boric acid. The aqueous solution was stirred for 3 hours and then evaporated under reduced pressure to yield a crude white solid (1.4 g, 2.0 mmol, 100%). 0.3 g of this solid was redissolved in 15 mL deionised water and recrystallized to yield a few white crystals within 5 days, suitable for X-ray diffraction studies. $C_{14}H_{32}B_{10}N_4O_{20}$. Anal. Calc.: C = 24.5 %, H = 4.7 %, N = 8.2 %. Found C = 24.9 %, H = 4.7 %, N = 8.1 %. TGA: 250–400 °C, condensation of pentaborate units with loss of $4H_2O$ 11.3% (10.5% calc.); 400–800 °C, oxidation of organic cation to leave residual $5B_2O_3$ 48.7% (50.8% calc.). NMR/ppm: δ_H: 1.24 (4H, t, CH_2); 1.76, (4H, t, CH_2), 3.79 (6H, s, CH_3), 4.08 (4H, t, CH_2N), 4.70 (HOD), 7.36 (4H, d, CH); δ_B: 17.9 (77%), 13.2 (20%), 1.2 (3%); δ_C: 24.81 (CH_2), 28.99 (CH_2), 35.34 (CH_3), 49.29 (CH_2), 122.06 (CH), 123.45 (CH). FTIR (ATR, neat solid state, cm^{-1}): 3437 (w), 3235 (w), 3156 (w), 3125 (w), 3094 (w), 2941 (w), 2869 (w), 1575 (m), 1472 (w), 1388 (s), 1304 (s), 1171 (s), 1156 (s), 1094 (w), 1074 (m), 1012 (s), 914 (vs), 871 (w), 857 (w), 835 (m), 772 (s), 721 (m), 705 (s), 652 (m), 624 (m), 576 (vw), 523 (w), 473 (s), 456 (w). XRD crystallographic data: $C_{14}H_{32}B_{10}N_4O_{20}$, *M*r = 684.53, monoclinic, $P2_1/c$, a = 9.6754(2) Å, b = 16.7781(3) Å, c = 9.1677(2) Å, $\alpha = \gamma = 90^o$, β = 92.680(2)^o, V = 1486.61(5) Å^3, T = 100(2) K, Z = 2, Z'= 0.5 μ(MoKα) = 0.131, 20877 reflections measured, 3403 unique (R_{int} = 0.0339) which were used in calculations. The final ωR_2 was 0.0851 (all data) and R_1 was 0.0335 (I > 2σ(I)).

5.4.8: Preparation of 1,1′-(1,6-hexanediyl)bis(3-ethyl-1H-imidazol-3-ium) bispentaborate $[C_2H_5(C_3H_3N_2)(CH_2)_6(C_3H_3N_2)C_2H_5][B_5O_6(OH)_4]_2{\cdot}3H_2O$ (4a)

1,1′-(1,6-hexanediyl)bis(3-ethyl-1H-imidazol-3-ium) dibromide (1.0 g, 2.29 mmol) was added to 20 g of DOWEX 550A ion exchange resin (OH^- form) and stirred for 18 hours. The DOWEX removed by vacuum filtration and the filtrate was added to 1.4 g (22.9 mmol) boric acid. The solution was stirred for 2 hours, and then evaporated under reduced pressure to yield a crude powder (1.5 g, 2.0 mmol, 85%), which was subjected to FTIR and NMR studies. Recrystallation of 0.3 g of the crude product in water yielded a few white crystals within 14 days, suitable for single crystal XRD studies. $C_{16}H_{42}B_{10}N_4O_{23}$. Anal. Calc.: C = 25.1 %, H = 5.5 %, N = 7.3 %. Found C = 25.5 %, H = 5.0 %, N = 7.3 %. TGA: 270–390 °C, condensation of pentaborate units and 2 lattice H_2O with total loss of $6H_2O$ 13.9% (14.1% calc.); 390–800 °C, oxidation of organic cation to leave residual $5B_2O_3$ 43.3% (45.4% calc.). NMR/ppm: δ_H: 1.24 (4H, m, CH_2); 1.41, (6H, t, CH_3), 1.78 (4H, m, CH_2), 4.12 (8H, dt, CH_2N), 4.70 (HOD), 7.39 (4H, m, CH); δ_B: 13.2 (7%), 17.2 (93%); δ_C: 14.36 (CH_3), 24.85 (CH_2), 28.99 (CH_2), 44.74 (CH_2), 49.32 (CH_2), 121.93 (CH), 122.13 (CH). FTIR (neat solid state, cm^{-1}): 3217 (br), 3152 (w), 3091 (w), 2950 (w), 2870 (w), 2863 (w), 1569 (w), 1397 (w), 1380 (m), 1299 (s), 1169 (m), 1148 (w), 1076 (m), 1013 (s), 912 (m), 817 (m), 802 (m), 771 (w), 741 (m), 722 (w), 705 (w), 642 (w), 547 (w), 524 (w), 475 (m), 460 (w), 413 (w). XRD crystallographic data: $C_{16}H_{42}B_{10}N_4O_{23}$, *M*r = 766.63, triclinic, *P*-1, a = 9.4616(4) Å, b = 9.4780(3) Å, c = 19.8856(8) Å, α = 86.483(3)°, β = 81.244(3)°, γ = 75.624(3)°, V = 1706.79(12) $Å^3$, T = 100(2) K, Z = 2, Z' = 1, μ(MoKα) = 0.129 mm^{-1}, 38202 reflections measured, 7820 unique (R_{int} = 0.0424) which were used in calculations. The final ωR_2 was 0.1431 (all data) and R_1 was 0.0457 ($I > 2\sigma(I)$).

5.4.9: Preparation of 1,1'-[1,4-Phenylenebis(methylene)]bis(2-methyl-1H-imidazol-3-ium) bispentaborate $[CH_3(C_3H_3N_2)CH_2(C_6H_4)CH_2(C_3H_3N_2)CH_3][B_5O_6(OH)_4]_2$ (5a)

1,1'-[1,4-Phenylenebis(methylene)]bis(2-methyl-1H-imidazol-3-ium) diiodide (1.0 g, 1.91 mmol) was added to DOWEX 550A monosphere $(OH)^-$ (15 g), and stirred for 18 hours. The DOWEX was removed by vacuum filtration and the filtrate was added to boric acid (1.2 g, 19.1 mmol). The aqueous solution was stirred for 3 hours and then evaporated under reduced pressure to yield a crude white solid (1.3 g, 1.8 mmol, 97%). 0.3 g of this solid was redissolved in 15 mL deionised water and recrystallized to yield a few white crystals within 7 days, suitable for X-ray diffraction studies. $C_{16}H_{28}B_{10}N_4O_{20}$. Anal. Calc.: C = 27.3 %, H = 4.0 %, N = 8.0 %. Found C = 27.5 %, H = 4.0 %, N = 7.9 %. NMR: δ_H/ppm: 3.79 (6H, s, CH_3N), 4.70 (HOD), 5.32 (4H, s, CH_2N), 7.36 (8H, m, CH); δ_B: 1.2 (6.6%) 13.1 (29%), 18.1 (64%); δ_C: 35.68 (CH_3), 52.24 (CH_2), 122.22 (CH), 123.82 (CH), 129.21 (CH), 134.57 (C (quat). FTIR (KBr, cm^{-1}): 3439 (s), 3379 (s), 3142 (m), 3074 (m), 1647 (m), 1562 (m), 1575 (w), 1435 (s), 1360 (s), 1252 (m), 1162 (s), 1103 (s), 1025 (s), 925 (vs), 841 (w), 782 (m), 765 (w), 732 (w), 698 (m), 651 (vw), 622 (w), 594 (vw). XRD crystallographic data: $C_{16}H_{28}B_{10}N_4O_{20}$, *M*r = 704.52, triclinic, *P*-1, a = 9.0501(2) Å, b = 9.1652(2) Å, c = 9.95476(2) Å, α = 104.254(2)°, β = 94.968(2)°, γ = 103.538(2)°, V = 737.43(3) Å^3, T = 100(2) K, Z = 1, Z' = 0.5, μ(MoKα) = 0.135 mm^{-1}, 44644 reflections measured, 4490 unique (R_{int} = 0.0242) which were used in calculations. The final ωR_2 was 0.0890 (all data) and R_1 was 0.0312 (I > 2σ(I)).

5.4.10: Preparation of 1,1'-(1,6-hexanediyl)bis(1-methylpyrrolidin-1-ium) bispentaborate $[CH_3(C_4H_8N)(CH_2)_6(C_4H_8N)CH_3][B_5O_6(OH)_4]_2$ (6a and 6b) (two polymorphs)

1,1'-(1,6-hexanediyl)bis(1-methylpyrrolidin-1-ium) diiodide (1.0 g, 1.9 mmol) was added to DOWEX 550A monosphere $(OH)^-$ (17 g), and stirred for 24 hours. The aqueous solution was collected and added to boric acid (1.2 g, 19 mmol). The solution was stirred for 2 hours, and then the solution was evaporated under reduced pressure to yield a crude powder (1.3 g, 1.9 mmol, 99%), which was subjected to FTIR and NMR studies. Recrystallisation of 0.3 g of the crude product in water yielded a few white crystals after 7 days, suitable for XRD studies. $C_{16}H_{42}B_{10}N_2O_{20}$. Anal. Calc.: C = 27.8 %, H = 6.1 %, N = 4.0 %. Found C = 28.1 %, H = 6.1 %, N = 4.0 %. TGA: 100–285 °C, condensation of pentaborate units with loss of $4H_2O$ 10.5% (10.4% calc.); 285–800 °C, oxidation of organic cation to leave residual $5B_2O_3$ 53.0% (50.4% calc.). NMR/ppm: δ_H: 1.35 (4H, m, CH_2); 1.74, (4H, t, CH_2), 2.12 (8H, s, CH_2), 2.95 (6H, s, CH_3N), 3.24 (4H, m, CH_2N), 3.42 (8H, m, CH_2N), 4.70 (HOD); δ_B: 1.1 (1 %), 14.1 (13 %), 17.3 (85 %); δ_C: 21.20 (CH_2), 22.94 (CH_2), 25.26 (CH_2), 47.91 (CH_3), 63.95 (CH_2), 64.20 (CH_2). FTIR (KBr, cm^{-1}): 3233 (w), 1387 (m), 1297 (s), 1132 (m), 1068 (w), 1009 (s), 908 (vs), 820 (m), 770 (s), 740 (w), 722 (m), 705 (s), 579 (vw), 566 (vw), 521 (vw), 471 (m), 459 (m). XRD crystallographic data: **(a)** $C_{16}H_{42}B_{10}N_2O_{20}$, M_r = 690.61, triclinic, *P*-1, a = 9.05340(10) Å, b = 11.9367(2) Å, c = 14.5824(2) Å, α = 94.1950(10)°, β = 104.1560(10)°, γ = 94.8550(10)°, V = 1515.35(4) $Å^3$, T = 100(2) K, Z = 2, Z' = 1, $\mu(MoK_\alpha)$ = 0.127 mm^{-1}, 69149 reflections measured, 6954 unique (R_{int} = 0.0243) which were used in all calculations. The final wR_2 was 0.0906 (all data) and R_1 was 0.0314 (I > 2(I)). **(b)** $C_{16}H_{42}B_{10}N_2O_{20}$, M_r = 690.61, triclinic, *P*-1 (No. 2), a = 9.6641(4) Å, b = 12.7484(4) Å, c = 13.0913(4) Å, α = 84.415(3)°, β = 84.541(3)°, γ = 75.872(3)°, V = 1552.40(10) $Å^3$, T = 100(2) K, Z = 2, Z' = 1, $\mu(MoK_\alpha)$ = 0.124 mm^{-1}, 35495 reflections measured,

7118 unique (R_{int} = 0.0398) which were used in all calculations. The final wR_2 was 0.0929 (all data) and R_1 was 0.0358 (I > 2(I)).

5.4.11: Preparation of 1,1'-(1,6-hexanediyl)bis(1-ethylpyrrolidin-1-ium) bispentaborate $[C_2H_5(C_4H_8N)(CH_2)_6(C_4H_8N)C_2H_5][B_5O_6(OH)_4]_2$ (7a)

1,1'-(1,6-hexanediyl)bis(1-ethylpyrrolidin-1-ium) dibromide (0.9 g, 2.0 mmol) was added to DOWEX 550A monosphere $(OH)^-$ (18 g), and stirred for 18 hours. The DOWEX was removed by vacuum filtration and the filtrate was added to boric acid (1.3 g, 20 mmol). The aqueous solution was stirred for 3 hours and then evaporated under reduced pressure to yield a crude white solid (1.5 g, 2.0 mmol, 100%). 0.3 g of this solid was redissolved in 15 mL deionised water and recrystallized to yield a few white crystals suitable for X-ray diffraction studies within 10 days. $C_{18}H_{46}B_{10}N_2O_{20}$. Anal. Calc.: C = 30.1 %, H = 6.45 %, N = 3.9 %. Found C = 28.1 %, H = 6.2 %, N = 3.6 %. TGA: 100–800 °C, simultaneous condensation of pentaborate units with loss of $4H_2O$ and oxidation of organic cation to leave residual $5B_2O_3$ 52.9% (48.4% calc.) NMR/ppm: δ_H: 1.20 (6H, t, CH_3), 1.31 (4H, m, CH_2), 1.63 (4H, m, CH_2), 2.05 (8H, s, CH_2), 3.11 (4H, m, CH_2N), 3.24, (4H, q, CH_2N), 3.37 (8H, m, CH_2N); 4.70 (HOD); δ_B: 13.1 (9%), 17.4 (91%); δ_C: 7.91 (CH_3), 21.39 (CH_2), 22.38 (CH_2), 25.26 (CH_2), 54.76 (CH_2), 58.68 (CH_2), 62.24 (CH_2). FTIR (ATR, solid state, cm^{-1}): 3363 (br), 1395 (m), 1297 (m), 1141 (w), 1104 (m), 1046 (vw), 1020 (m), 920 (s), 907 (s), 802 (w), 767 (s), 720 (m), 704 (vs), 647 (vw), 592 (vw), 457 (m). XRD crystallographic data: $C_{18}H_{46}B_{10}N_2O_{20}$, M_r = 718.67, monoclinic, $P2_1/c$, a = 10.06420(10) Å, b = 11.55510(10) Å, c = 15.7004(2) Å, β = 107.6290(10)°, α = γ = 90°, V = 1740.10(3) $Å^3$, T = 100(2) K, Z = 2, Z' = 0.5, $\mu(CuK_\alpha)$ = 0.976 mm^{-1}, 25011 reflections measured, 3183 unique (R_{int} = 0.0306) which were used in all calculations. The final wR_2 was 0.1290 (all data) and R_1 was 0.0417 (I > 2(I)).

5.4.12: Preparation of 1,1'-(1,6-hexanediyl)bis(1-butylpyrrolidin-1-ium) bispentaborate $[C_4H_9(C_4H_8N)(CH_2)_6(C_4H_8N)C_4H_9]\ [B_5O_6(OH)_4]_2{\cdot}4B(OH)_3$ (8a)

1,1'-(1,6-hexanediyl)bis(1-butylpyrrolidin-1-ium) diiodide (1.0 g, 1.7 mmol) was added to DOWEX 550A monosphere $(OH)^-$ (14 g), and stirred for 18 hours. The DOWEX was removed by vacuum filtration and the filtrate was added to boric acid (1.0 g, 16.9 mmol). The aqueous solution was stirred for 3 hours and then evaporated under reduced pressure to yield a crude white solid (1.7 g, 1.7 mmol, 98%). 0.3 g of this solid was redissolved in 15 mL deionised water and recrystallized to yield a few white crystals within 7 days, suitable for X-ray diffraction studies. $C_{20}H_{46}B_{10}N_2O_{20}$. Anal. Calc.: C = 25.9 %, H = 6.5 %, N = 2.7 %. Found C = 26.5 %, H = 6.5 %, N = 2.8 %. NMR/ppm: δ_H: 0.83 (6H, t, CH_3); 1.27 (8H, m, CH_2), 1.58 (8H, s, CH_2), 2.05 (8H, s, CH_2), 3.11 (8H, t, CH_2N), 3.38 (8H, m, CH_2N), 4.70 (HOD); δ_B: 1.4 (<1%), 13.1 (14%), 18.0 (86%); δ_C: 12.74 (CH_3), 19.12 (CH_2), 21.40 (CH_2), 22.47 (CH_2), 24.53 (CH_2), 25.23 (CH_2), 59.36 (CH_2), 62.74 (CH_2). FTIR (ATR, solid state, cm^{-1}): 3312 (br), 1404 (m), 1306 (vs), 1225 (m), 1158 (m), 1128 (w), 1031 (m), 923 (s), 872 (w), 824 (w), 781 (m), 745 (w), 717 (w), 701 (m), 669 (m), 520 (w), 462 (m), 409 (w) $C_{22}H_{66}B_{14}N_2O_{32}$, M_r = 1022.10, monoclinic, *Cc*, a = 9.7545(3) Å, b = 15.4363(4) Å, c = 17.0325(5) Å, β = 101.851(3)°, $\alpha = \gamma = 90°$, V = 2509.98(13) $Å^3$, T = 100(2) K, Z = 2, Z' = 0.5, $\mu(MoK_\alpha)$ = 0.117, 9481 reflections measured, 9481 unique (R_{int} = .) which were used in all calculations. The final wR_2 was 0.1483 (all data) and R_1 was 0.0532 (I > 2(I)).

5.4.13: Preparation of 1,1'-(1,6-hexanediyl)bis(1-allylpyrrolidin-1-ium) bispentaborate) $[C_3H_5(C_4H_8N)(CH_2)_6(C_4H_8N)C_3H_5][B_5O_6(OH)_4]_2$ (9a)

1,1'-(1,6-hexanediyl)bis(1-allylpyrrolidin-1-ium) diiodide (1.0 g, 1.8 mmol) was added to DOWEX 550A monosphere $(OH)^-$ (16 g), and stirred for 18 hours. The DOWEX was removed by vacuum filtration and the filtrate was added to boric acid (1.1 g, 18 mmol). The aqueous solution was stirred for 3 hours and then evaporated under reduced pressure to yield a crude white solid (1.3 g, 1.8 mmol, 100%). 0.3 g of this solid was redissolved in 15 mL deionised water and recrystallized to yield a few white crystals within 7 days, suitable for X-ray diffraction studies. $C_{20}H_{46}B_{10}N_2O_{20}$. Anal. Calc.: C = 32.3%, H = 6.2%, N = 3.8%. Found C = 29.7 %, H = 5.9 %, N = 3.3 %. TGA: 110–800 °C simultaneous condensation of pentaborate units with loss of $4H_2O$ and oxidation of organic cation to leave residual $5B_2O_3$ 45.7% (46.9% calc.). NMR/ppm: δ_H: 1.32 (4H, m, CH_2); 1.71, (4H, t, CH_2), 2.10 (8H, s, CH_2), 3.17 (4H, s, CH_2N), 3.36 (4H, m, CH_2N), 3.47 (4H, m, CH_2N), 3.82 (4H, m CH_2N), 4.70 (HOD), 5.61 (4H, m, CH_2=C), 5.89 (2H, t, CH=C); δ_B: 1.2 (1%), 13.0 (20%), 17.3 (79%); δ_C: 21.39 (CH_2), 22.37 (CH_2), 25.20 (CH_2), 59.91 (CH_2), 61.41 (CH_2), 61.97 (CH_2), 125.07 (CH), 127.59 (CH_2). FTIR (KBr, cm^{-1}): 3270 (w), 1407 (s), 1393 (m), 1296 (s), 1137 (w), 1090 (m), 1056 (vw), 1018 (s), 975 (w), 953 (vw), 909 (vs), 813 (vw), 804 (vw), 769 (vs), 747 (vw), 722 (m), 706 (s), 676 (w), 658 (w), 638 (w), 623 (w), 616 (w), 593 (w), 583 (w), 553 (w), 505 (w), 494 (w), 471 (w), 457 (s). $C_{20}H_{46}B_{10}N_2O_{20}$, M_r = 742.69, monoclinic, $P2_1/c$, a = 10.0823(5) Å, b = 11.6950(4) Å, c = 15.7836(6) Å, β = 105.717(5)°, $\alpha = \gamma = 90°$, V = 1791.50(13) $Å^3$, T = 100(2) K, Z = 2, Z' = 0.5, $\mu(MoK_\alpha)$ = 0.113 mm^{-1}, 22100 reflections measured, 4090 unique (R_{int} = 0.0653) which were used in all calculations. The final wR_2 was 0.1324 (all data) and R_1 was 0.0449 (I > 2(I)).

5.4.14: Preparation of 1,1′-(1,6-hexanediyl)bis(3-allyl-1H-imidazol-3-ium) bispentaborate [$(CH_2{=}CHCH_2(C_3H_3N_2)(CH_2)_6(C_3H_3N_2)CH_2CH{=}CH_2)][B_5O_6(OH)_4]_2$ (10a)

1,1′-(1,6-hexanediyl)bis(3-allyl-1H-imidazol-3-ium) diiodide (1.0 g, 1.8 mmol) was added to DOWEX 550A monosphere $(OH)^-$ (14 g), and stirred for 18 hours. The DOWEX was removed by vacuum filtration and the filtrate was added to boric acid (1.1 g, 18 mmol). The aqueous solution was stirred for 3 hours and then evaporated under reduced pressure to yield a crude white solid (0.7 g, 0.9 mmol, 52%). 0.3 g of this solid was redissolved in 15 mL deionised water, and left to crystallise to form a few white crystals, but these were unsuitable for XRD studies. FTIR (KBr, cm^{-1}) 3437 (s), 3390 (s), 3140 (m), 3091 (m), 2863 (w), 1647 (m), 1563 (m), 1434 (s), 1361 (s), 1252 (m), 1160 (w), 1103 (s), 1026 (s), 944 (w), 926 (s), 782 (m), 696 (m).

5.4.15: Preparation of 1,1′-(1,6-hexanediyl)bis(3-benzyl-1H-imidazol-3-ium) bispentaborate $[PhCH_2(C_3H_3N_2)(CH_2)_6(C_3H_3N_2)CH_2Ph][B_5O_6(OH)_4]_2$ (11a)

1,1′-(1,6-hexanediyl)bis(3-benzyl-1H-imidazol-3-ium) diiodide (1.0 g, 1.8 mmol) was added to DOWEX 550A monosphere $(OH)^-$ (14 g), and stirred for 18 hours. The DOWEX was removed by vacuum filtration and the filtrate was added to boric acid (1.1 g, 18 mmol). The aqueous solution was stirred for 3 hours and then evaporated under reduced pressure to yield a crude white solid (0.9 g, 1.1 mmol, 60%). 0.3 g of this solid was redissolved in 15 mL deionised water and recrystallised to form a few white crystals, but these were unsuitable for XRD studies. These crystals were subjected to FTIR and NMR studies. FTIR (KBr, cm^{-1}) 3445 (s), 3437 (s), 3135 (w), 3067 (m), 2864 (w), 1651 (m), 1562 (m), 1434 (s), 1361 (s), 1252 (m), 1193 (w), 1154 (w), 1103 (s), 1027 (s), 926 (s), 782 (s), 697 (m). NMR/ppm: δ_H: 1.16 (4H, t (CH_2), 1.72 (4H, t, CH_2), 4.05 (4H, t CH_2N), 5.29 (4H, s, $PhCH_2N$), 7.31-7.4 (14H, m, CH); δ_B: 13.5 (13%), 16.7 (87%); δ_C: 24.64 (CH_2), 28.83 (CH_2), 49.40 (CH_2) 52.83 (CH_2), 122.45 (CH), 128.46 (CH), 129.26 (CH), 129.33 (C).

5.4.16: Preparation of 1,1'-(1,6-hexanediyl)bis(3-butyl-1H-imidazol-3-ium) bispentaborate $[C_4H_9(C_3H_3N_2)(CH_2)_6(C_3H_3N_2)C_4H_9][B_5O_6(OH)_4]_2$ (12a)

1,1'-(1,6-hexanediyl)bis(3-butyl-1H-imidazol-3-ium) diiodide (1.0 g, 1.7 mmol) was added to DOWEX 550A monosphere $(OH)^-$ (14 g), and stirred for 24 hours. The aqueous solution was collected and added to boric acid (1.1 g, 17.1 mmol). The aqueous solution was stirred for 3 hours and then evaporated under reduced pressure to yield a crude white solid (1.1 g, 1.4 mmol, 84%). 0.3 g of this solid was redissolved in 15 mL deionized water and left to evaporate to yield a few white crystals, but these were unsuitable for XRD studies. FTIR (ATR, solid state,

cm^{-1}): 3296 (w), 3152 (w), 2960 (w), 2875 (w), 1567 (w), 1397 (s), 1294 (s), 1195 (vw), 1166 (vw), 1146 (m), 1089 (m), 1016 (m), 919 (s), 905 (s), 810 (w), 770 (vs), 742 (w), 722 (m), 705 (vs), 674 (vw), 632 (w), 589 (w), 551 (w), 524 (w), 469 (m), 456 (w), 415 (vw). NMR/ppm: δ_H: 0.90 (6H, t, CH_3), 1.22 (8H, m, CH_2) 1.74 (8H, m, CH_2), 4.07 (8H, q, CH_2N), 4.70 (HOD), 7.38 (4H, d, CH); δ_B: 13.7 (15 %), 17.1 (85 %); δ_C: 12.51 (CH_3), 18.67 (CH_2), 24.79 (CH_2), 28.97 (CH_2), 31.13 (CH_2), 49.22 (CH_2), 49.28 (CH_2), 122.15 (CH), 122.27 (CH).

5.4.17: Preparation of 1,1'-(1,8-octanediyl)bis(1-methylpyrrolidin-1-ium) bispentaborate $[Me(C_4H_8N)(CH_2)_8(C_4H_8N)Me][B_5O_6(OH)_4]_2$ (13a)

1,1'-(1,8-octanediyl)bis(1-methylpyrrolidin-1-ium) diiodide (1.0 g, 1.9 mmol) was dissolved in 20 mL water and stirred with excess (15 g) of DOWEX 550A ion-exchange resin (OH^- form) for 24 h. the slurry was filtered under reduced pressure and $B(OH)_3$ (1.2 g, 19 mmol) was added to the filtrate. The solution was left to stand for 4 hours, and then evaporated to dryness using a rotary evaporator. The crude white product was left to dry in an oven at 50^oC for 2 h to yield. (1.0 g, 1.4 mmol, 73%). 0.3 g of this solid was redissolved in 15 mL deionized water and left to evaporate to yield a few white crystals, but these were unsuitable for XRD studies. FTIR (KBr, cm^{-1}) 3437 (s), 3379 (s), 3061 (m), 2933 (w), 2857 (w), 1647 (m), 1433 (s), 1361 (s), 1253 (m), 1103 (s), 1027 (s), 927 (s), 782 (m), 698 (m). NMR/ppm: δ_H: 1.29 (8H, m, CH_2), 2.12-2.14 (12H, m, CH_2), 2.94 (6H, s, CH_3N), 3.96 (4H, m, CH_2N), 3.41 (8H, m, CH_2N); δ_B: 13.1(10%), 16.6 (90%); δ_C: 21.24 (CH_2), 23.00 (CH_2), 25.52 (CH_2), 27.96 (CH_2), 47.96 (CH_3), 64.19 (CH_2), 64.21 (CH_2).

5.4.18: Preparation of 1,1'-(1,8-octanediyl)bis(1-ethylpyrrolidin-1-ium) bispentaborate $[Et(C_4H_8N)(CH_2)_8(C_4H_8N)Et][B_5O_6(OH)_4]_2$ (14a)

1,1'-(1,8-octanediyl)bis(1-ethylpyrrolidin-1-ium) dibromide (1.0 g, 2.13 mmol) was dissolved in 20 mL water and stirred with excess (18 g) DOWEX 550A ion-exchange resin (OH^- form) for 24 h. The slurry was filtered under reduced pressure and $B(OH)_3$ (1.3 g, 21.3 mmol) was added to the filtrate. The solution was left to stand for 4 hours, and then evaporated to dryness using a rotary evaporator. The crude white product was left to dry in an oven at 50°C for 2 h to yield (1.5 g, 2.0 mmol, 94%). 0.3 g of this solid was redissolved in 15 mL deionized water and left to evaporate to yield a few white crystals, but these were unsuitable for XRD studies. NMR/ppm: δ_H: 1.18 (6H, t, CH_3), 1.24 (8H, m, CH_2), 1.59 (4H, m, CH_2), 2.03 (8H, m, CH_2), 3.08-3.13 (4H, t, CH_2N), 3.18-3.24 (4H, q, CH_2N), 3.35 (8H, m, CH_2N); δ_B: 1.2 (2%), 13.3 (15%), 18.2 (82%); δ_C: 7.91 (CH_3), 21.37 (CH_2), 22.38 (CH_2), 25.47 (CH_2), 28.00 (CH_2), 54.73 (CH_2), 58.90 (CH_2), 62.17 (CH_2). FTIR (KBr, cm^{-1}): 3436 (s), 3379 (s), 3061 (m), 2949 (m), 2861 (w), 1648 (m), 1428 (s), 1363 (s), 1253 (m), 1103 (s), 1027 (s), 926 (s), 781 (m), 702 (m).

5.4.19: Preparation of 1,1'-(1,8-octanediyl)bis(1-butylpyrrolidin-1-ium) bispentaborate $[Bu(C_4H_8N)(CH_2)_8(C_4H_8N)Bu][B_5O_6(OH)_4]_2$ (15a)

1,1'-(1,8-octanediyl)bis(1-butylpyrrolidin-1-ium) diiodide (1.0 g, 1.6 mmol) was dissolved in 20 mL water and stirred with excess (14 g) of DOWEX 550A ion-exchange resin (OH^- form) for 24 h. The slurry was filtered under reduced pressure and $B(OH)_3$ (1.0 g, 16 mmol) was added to the filtrate. The solution was left to stand for 4 hours, and then evaporated to dryness using a rotary evaporator. The crude white product was left to dry in an oven at 50°C for 2 h to yield (1.2 g, 1.5 mmol, 94%). 0.3 g of this solid was redissolved in 15 mL deionized water and left to evaporate to yield a few white crystals, but these were unsuitable for XRD studies. NMR/ppm: δ_H: (ppm): 0.82 (6H, t, CH_3), 1.24 (12H, m, CH_2), 1.57 (8H, m, CH_2), 2.03 (8H, m, CH_2), 3.12 (8H, m, CH_2N), 3.37 (8H, m, CH_2N); δ_B: 12.8 (5%), 17.3 (95%); δ_C: 12.74 (CH_3), 19.11 (CH_2), 21.37 (CH_2), 22.46 (CH_2), 24.53 (CH_2), 25.43 (CH_2), 27.98 (CH_2), 59.33 (CH_2), 59.45 (CH_2), 62.68 (CH_2). FTIR (KBr, cm^{-1}) 3427 (s), 3390 (s), 2960 (m), 2940 (m), 1637 (m), 1432 (s), 1343 (s), 1253 (w), 1228 (w), 1103 (m), 1028 (m), 925 (s), 782 (m), 702 (m).

5.4.20: Preparation of 1,1'-(1,8-octanediyl)bis(1-allylpyrrolidin-1-ium) bispentaborate $[CH_2{=}CHCH_2(C_4H_8N)(CH_2)_8(C_4H_8N)CH_2CH{=}CH_2][B_5O_6(OH)_4]_2$ (16a)

1,1'-(1,8-octanediyl)bis(1-allylpyrrolidin-1-ium) diiodide (1.0 g, 1.7 mmol) was dissolved in 20 mL water and stirred with excess (14 g) DOWEX 550A ion-exchange resin (OH^- form) for 24 h. The slurry was filtered under reduced pressure and $B(OH)_3$ (1.1 g, 17 mmol) was added to the filtrate. The solution was left to stand for 4 hours, and then evaporated to dryness using a rotary evaporator. The crude white product was left to dry in an oven at 50°C for 2 h to yield (0.9 g, 1.2 mmol, 69%). 0.3 g of this solid was redissolved in 15 mL deionized water and left to

evaporate to yield a few white crystals, but these were unsuitable for XRD studies. NMR/ppm: δ_H: 1.23 (8H, m, CH_2), 1.64 (4H, m, CH_2), 2.04 (8H, m, CH_2), 3.09-3.13 (4H, m, CH_2N), 3.34 (4H, m, CH_2N), 3.43 (4H, m, CH_2N), 3.76-3.77 (4H, m, CH_2N), 5.52-5.56 (4H, m, CH_2=C), 5.84-5.90 (2H, m, CH=C); δ_B: 1.1 (4%), 13.2 (17%), 17.8 (79%); δ_C: 21.33 (CH_2), 22.35 (CH_2), 25.41 (CH_2), 27.92 (CH_2), 60.09 (CH_2), 61.33 (CH_2), 61.86 (CH_2), 125.07 (CH), 127.49 (CH_2). FTIR (KBr, cm^{-1}) 3436 (s), 3379 (s), 3056 (m), 2938 (w), 2862 (w), 1648 (m), 1431 (s), 1362 (s), 1253 (m), 1103 (s), 1027 (s), 926 (s), 782 (m), 699 (m).

5.4.21: Preparation of 1,1'-(1,8-octanediyl)bis(1-benzylpyrrolidin-1-ium) bispentaborate $[PhCH_2(C_4H_8N)(CH_2)_8(C_4H_8N)CH_2Ph][B_5O_6(OH)_4]_2$ (17a)

1,1'-(1,8-octanediyl)bis(1-benzylpyrrolidin-1-ium) dibromide (1.0 g, 1.6 mmol) was dissolved in 20 mL water and stirred with excess (14 g) DOWEX 550A ion-exchange resin (OH^- form) for 24 h. The slurry was filtered under reduced pressure and $B(OH)_3$ (1.0 g, 16.0 mmol) was added to the filtrate. The solution was left to stand for 4 hours, and then evaporated to dryness using a rotary evaporator. The crude white product was left to dry in an oven at 50°C for 2 h to yield (1.2 g, 1.4 mmol, 86%). 0.3 g of this solid was redissolved in 15 mL deionized water and left to evaporate to yield a few white crystals, but these were unsuitable for XRD studies. NMR/ppm: δ_H: 1.29 (8H, m, CH_2), 1.82 (4H, m, CH_2), 2.12 (8H, m, CH_2), 3.04 (4H, m, CH_2N), 3.39 (4H, m, CH_2N), 3.51 (4H, m, CH_2N), 7.28-7.46 (10H, m, CH); δ_B: 13.3 (13%), 18.0 (87%); δ_C: 20.78 (CH_2), 22.49 (CH_2), 25.40 (CH_2), 27.98 (CH_2), 58.81 (CH_2), 61.21 (CH_2), 61.95 (CH_2), 129.24 (CH), 130.58 (CH), 132.14 (CH). FTIR (KBr, cm^{-1}): 3377 (s), 2933 (m), 2859 (w), 1648 (m), 1429 (s), 1362 (s), 1315 (s), 1252 (m), 1104 (m), 1029 (m), 926 (s), 828 (w), 782 (m), 702 (m).

5.4.22: Preparation of methylguanidinium pentaborate

$[MeNHC(NH_2)NH_2][B_5O_6(OH)_4]\cdot H_2O$ (18a)

Methylguanidine hydrochloride (0.5 g, 4.6 mmol) was added to 25 mL deionised water and to this was added DOWEX 550A $(OH)^-$ ion exchange resin (18 g), and stirred for 18 hours. The resin was removed under reduced pressure and the filtrate was added to boric acid (1.4 g, 23 mmol). The solution was stirred for 2 hours, and evaporated under reduced pressure to yield a crude white powder (1.1 g, 3.5 mmol, 77%). 0.3 g of crude powder was redissolved in warm deionized water and left to recrystallize to yield a few white single crystals suitable for XRD studies. TGA: 100-275 °C, condensation of pentaborate with loss of $3H_2O$ 17.4% (17.4% calc.); 275-700 °C, oxidation of organic residue leaving residual $2.5B_2O_3$ 55.9% (56.1% calc.). NMR/ppm: δ_H: 2.69 (s, CH_3) 4.70 (HOD); δ_B: 1.1 (3%), 13.2 (24 %), 18.1 (73%); δ_C: 36.98 (CH_3) {no quaternaries}. FTIR (KBr, cm^{-1}): 3435 (s), 3400 (s), 2958 (m), 2924 (m), 2854 (w), 1664 (s), 1439 (m), 1347 (m), 1252 (w), 1103 (m), 1025 (m), 925 (s), 782 (m), 696 (m). XRD crystallographic data: $C_2H_{14}B_5N_3O_{11}$, M_r = 310.21, monoclinic, $P2_1/c$ (No. 14), a = 9.9962(2) Å, b = 10.9047(2) Å, c = 11.7215(2) Å, β = 96.101(2)°, $\alpha = \gamma$ = 90°, V = 1270.47(4) $Å^3$, T = 100(2) K, Z = 4, Z' = 1, $\mu(MoK_\alpha)$ = 0.151 mm^{-1}, 17592 reflections measured, 2893 unique (R_{int} = 0.0115) which were used in all calculations. The final wR_2 was 0.0743 (all data) and R_1 was 0.0267 (I > 2(I)).

5.4.23: Preparation of dimethylguanidinium pentaborate $[Me_2NC(NH_2)NH_2]$ $[B_5O_6(OH)_4]$ (19a)

1,1-dimethylguanidine sulfate (1.0 g, 3.7 mmol) was dissolved in water and to this barium hydroxide (1.2 g, 3.7 mmol) was added. The mixture was stirred for 1 hour and the barium sulphate was removed from solution by gravity filtration and washed with a little water. To the filtrate was added boric acid (1.1 g, 18 mmol) and the solution was stirred under gentle warming for 1 hour. The solvent was removed under reduced pressure to yield a crude white powder (1.2 g, 3.7 mmol, 100%), which was characterised by FT-IR and NMR (^{1}H, ^{11}B, ^{13}C) studies. 0.3 g of crude powder was redissolved in warm deionized water and left to recrystallize to yield a few white single crystals suitable for XRD studies. $C_3H_{14}B_5N_3O_{10}$. Anal. Calc.: C = 11.8%, H = 4.6%, N = 13.8%. Found C = 11.9 %, H = 4.6 %, N = 13.5 %. TGA: 240-275 °C, condensation of pentaborate with loss of $2xH_2O$ 12.3% (11.8% calc.); 275-700 °C, oxidation of organic residue leaving residual $2.5B_2O_3$ 53.3% (56.8% calc.). NMR/ppm δ_H: 2.87 (1H, s), 2.89 (6H, s, CH_3N), 4.70 (HOD); δ_B: 1.0 (13%), 13.2 (11%), 18.3 (77%); δ_C: 37.34 (CH_3) {no quaternaries}. FTIR (KBr, cm^{-1}): 3370 (s), 3249 (m), 3200 (m), 2959 (w), 2924 (w), 2855 (w), 1688 (m), 1671 (s), 1634 (s), 1552 (vw), 1435 (vs), 1393 (s), 1364 (s), 1313 (s), 1150 (w), 1114 (s), 1058 (w), 1033 (s), 926 (vs), 780 (s), 699 (m), 619 (vw). XRD crystallographic data: $C_3H_{14}B_5N_3O_{10}$, *M*r = 306.22, monoclinic, $P2_{1/c}$, a = 9.9747(2) Å, b = 11.2563(3) Å, c = 11.6174(3) Å, $\alpha = \gamma = 90^{o}$, β = 96.084(2)°, V = 1297.03(5) $Å^3$, T = 100(2) K, Z = 4, Z' = 1, 18168 reflections measured, 2969 unique (R_{int} = 0.0191) which were used in calculations. The final ωR_2 was 0.0811 (all data) and R_1 was 0.0280 ($I > 2\sigma(I)$).

5.4.24(a): Preparation of pentamethylguanidinium iodide [$Me_2NC(NHMe)N(Me)_2$]I (20)

Tetramethylguanidine (2.1 g, 2.3 mL, 20 mmol) was added to an Ar charged two necked flask, and to this 10 mL of acetonitrile was added. The sealed vessel was then cooled to 0°C using an ice bath. Methyl iodide (2.9 g, 20 mmol) was then added to 8 mL of acetonitrile and this solution was added dropwise to the cold solution of tetramethyl guanidine. The mixture was then stirred for 12 hours and left to slowly equilibrate to room temperature. The solvents were then removed via rotary evaporation. The resulting oil was then washed with ethyl acetate (3 x 25 mL) and dried under vacuum at room temperature to yield a white crystalline product *N,N,N',N'',N''*-pentamethylguanidine hydroiodide (3.2 g, 12.6 mmol, 63 %). NMR/ppm: δ_H: 2.73 (3H, s, CH_3N), 2.80 (12H, s, CH_3N); δ_C: 38.91 (CH_3)

5.4.24(b): Preparation of pentamethylguanidinium pentaborate [$Me_2NC(NHMe)N(Me)_2$] [$B_5O_6(OH)_4$]·$B(OH)_3$ (20a)

Pentamethyl guanidine hydroiodide (1.0 g, 4.0 mmol) was dissolved in 25 mL deionised water and to this was added DOWEX 550A $(OH)^-$ ion exchange resin (18 g), and stirred for 18 hours. The resin was removed by filtration under reduced pressure and the filtrate was added to boric acid (1.3 g, 20 mmol). The solution was stirred for 2 hours, and evaporated under reduced pressure to yield a crude white powder (1.6 g, 3.9 mmol, 98%). 0.3 g of this solid was redissolved in 15 mL deionised water and recrystallized to yield white crystals within 10 days, suitable for X-ray diffraction studies. $C_6H_{23}B_6N_3O_{13}$. Anal. Calc.: C = 17.6%, H = 5.7%, N = 10.2%. Found C = 17.7 %, H = 5.5 %, N = 10.1 %. TGA: 240-275 °C, condensation of pentaborate with loss of $2H_2O$ 12.3% (11.8% calc.); 275-700 °C, oxidation of organic residue leaving residual $2.5B_2O_3$ 53.3% (56.8% calc.). NMR/ppm: δ_H: 2.73 (3H, s, CH_3N), 2.80 (12H, s, CH_3N), 2.82 (1H, s), 4.70 (HOD); δ_B: 1.1 (9%), 13.2 (13%), 18.8 (78%); δ_C: 38.89 (CH_3). FTIR (KBr, cm^{-1}): 3370 (s),

3236 (s), 2955 (w), 2935 (w), 1625 (s), 1592 (m), 1426 (s), 1398 (m), 1367 (s), 1324 (m), 1235 (w), 1211 (w), 1182 (w), 1156 (m), 1139 (w), 1107 (w), 1087 (w), 1065 (w), 1022 (m), 922 (vs), 832 (w), 803 (w), 779 (m), 722 (w), 709 (m), 696 (w), 672 (w). {no quaternaries}. XRD crystallographic data: $C_6H_{23}B_6N_3O_{13}$, M_r = 410.13, monoclinic, $P2_1/c$ (No. 14), a = 9.49570(10) Å, b = 11.44900(10) Å, c = 16.84590(10) Å, β = 98.0710(10)°, $\alpha = \gamma$ = 90°, V = 1813.28(3) Å^3, T = 100(2) K, Z = 4, Z' = 1, μ(CuK$_\alpha$) = 1.164 mm^{-1}, 20493 reflections measured, 3281 unique (R_{int} = 0.0196) which were used in all calculations. The final wR_2 was 0.0674 (all data) and R_1 was 0.0263 (I > 2(I)).

5.4.25: Preparation of aminoguanidinium pentaborate $[NH_2NHC(NH_2)NH_2][B_5O_6(OH)_4]$ (21a)

Aminoguanidine hemisulphate (1 g, 7.6 mol) was dissolved in x water and to this was added barium hydroxide (1.3 g, 7.6 mol). The resulting cloudy solution was stirred for 1 hour and the solid barium sulphate was filtered from the solution. Boric acid (2.3 g, 37 mmol, 5 eq) was added to the clear solution, and stirred with gentle heating for 3 hours. The solution was then evaporated under reduced pressure and dried in an oven to yield a crude white powder (2.1 g, 7.16 mmol, 94%). 0.3 g of this solid was redissolved in 10 mL deionised water and left to crystallise over a few days to yield a few crystals suitable for sc-XRD studies. $CH_{11}B_5N_4O_{10}$. Anal. Calc.: C = 4.1%, H = 3.8%, N = 19.1%. Found C = 4.2 %, H = 3.7 %, N = 18.7 %. TGA: 240-320 °C, condensation of pentaborate with loss of 2 x H_2O 11.9% (12.3% calc.); 320-700 °C, oxidation of organic residue leaving residual $2.5B_2O_3$ 59.3% (59.3% calc.). NMR/ppm: δ_B: 1.2 (10 %), 13.3 (9%), 19.2 (81%); δ_H, δ_C: not available. FTIR (KBr, cm^{-1}) 3451 (s), 3372 (s), 3295 (s), 3235 (m), 1672 (s), 1657 (s), 1437 (s), 1361 (s), 1252 (m), 1196 (m), 1103 (s), 1026 (s), 925 (s), 782 (s), 735 (w), 698 (s). XRD crystallographic data: $CH_{11}B_5N_4O_{10}$, M_r = 293.19, triclinic, P-1

(No. 2), a = 7.4870(2) Å, b = 8.5076(2) Å, c = 9.6502(2) Å, α = 93.906(2)°, β = 98.470(2)°, γ = 96.457(2)°, V = 601.88(3) Å^3, T = 100(2) K, Z = 2, Z' = 1, μ(CuK$_\alpha$) = 1.341 mm^{-1}, 11885 reflections measured, 2142 unique (R_{int} = 0.0404) which were used in all calculations. The final wR_2 was 0.0827 (all data) and R_1 was 0.0294 (I > 2(I)).

5.4.26: Preparation of 1,5,7-Triazabicyclo[4.4.0]dec-5-ene pentaborate [C7H14N3][B5O6(OH)4] (22a)

1,5,7-Triazabicyclo[4.4.0]dec-5-ene (1.0 g, 7.2 mmol) was dissolved in deionised water (20 mL) and to this was added boric acid (2.2 g, 36 mmol, 5 eq.). The resulting solution was stirred under gentle heating to fully dissolve the boric acid, and left for 3 hours. The solution was then evaporated under reduced pressure to yield a crude white powder (2.4 g, 6.7 mmol, 93%). 0.3 g of this solid was redissolved in 20 mL deionised water and left to recrystallize over 7 days to yield a small number of white crystals, suitable for X-ray diffraction studies.

$C_7H_{18}B_5N_3O_{10}$. Anal. Calc.: C = 23.5%, H = 5.1%, N = 11.7%. Found C = 23.7 %, H = 5.0 %, N = 11.5 %., TGA: 245-295 °C, condensation of pentaborate with loss of $2H_2O$ 13.0% (10.0% calc.); 295-700 °C, oxidation of organic residue leaving residual $2.5B_2O_3$ 49.0% (48.6% calc.). NMR/ppm: δ_H: 1.84 (4H, quin, CH_2), 3.12 (4H, t, CH_2N), 3.20 (4H, t, CH_2N), 4.70 (HOD); δ_C: 20.12 (CH_2), 37.71 (CH_2), 46.38 (CH_2); δ_B: 0.8 (1%), 13.0 (29%), 17.7 (70%). FTIR (ATR, solid state/cm^{-1}): 3391 (w), 3238 (m), 1630 (m), 1509 (w), 1408 (m), 1375 (w), 1294 (s), 1201 (w), 1144 (m), 1086 (m), 1015 (m), 910 (vs), 816 (m), 772 (s), 723 (m), 706 (s). XRD crystallographic data: $C_7H_{18}B_5N_3O_{10}$, M_r = 358.29, triclinic, *P*-1 (No. 2), a = 9.3096(6) Å, b = 9.3175(3) Å, c = 9.3733(6) Å, α = 76.598(5)°, β = 85.611(5)°, γ = 79.947(4)°, V = 778.22(8) $Å^3$, T = 100(2) K, Z = 2, Z' = 1, $\mu(CuK_\alpha)$ = 1.133 mm^{-1}, 13382 reflections measured, 2836 unique (R_{int} = 0.0443) which were used in all calculations. The final wR_2 was 0.1899 (all data) and R_1 was 0.0598 (I > 2(I)).

References

1 M. Berzelius, *Philos. Mag.*, 1825, **65**, 254–267.

2 H. S.-C. Deville, *Comptes rendus*, 1854, **39**, 321–326.

3 L. C. Andreani, A. Bozzola, P. Kowalczewski, M. Liscidini and L. Redorici, *Adv. Phys. X*, 2019, **4**, 1548305.

4 M. Gul, Y. Kotak and T. Muneer, *Energy Explor. Exploit.*, 2016, **34**, 485–526.

5 F. Shimura, in *Springer Handbook of Electronic and Photonic Materials*, Springer International Publishing, Cham, 2017, pp. 1–1.

6 G. Fisher, M. R. Seacrist and R. W. Standley, *Proc. IEEE*, 2012, **100**, 1454–1474.

7 J. W. Mellor, *A comprehensive treatise on inorganic and theoretical chemistry*, Longmans, Green and Co., London, Vol. 6., 1947.

8 C. Winkler, *Berichte der Dtsch. Chem. Gesellschaft*, 1890, **23**, 2642–2668.

9 J. A. Del Alamo, *Nature*, 2011, **479**, 317–323.

10 R. B. Bergmann, *Appl. Phys. A Mater. Sci. Process.*, 1999, **69**, 187–194.

11 A. G. Aberle, *Prog. Photovoltaics Res. Appl.*, 2000, **8**, 473–487.

12 W. A. Deer, R. A. Howie and J. Zussman., *An Introduction to the Rock Forming Minerals. Eighth edition. London, Longmans. p.1-528.*, Longman, London, 2nd edn., 1975.

13 J. Pinkas, *Ceram. - Silikaty*, 2005, 49, 287–298.

14 E. Lippmaa, A. Samoson and M. Mägi, *J. Am. Chem. Soc.*, 1986, **108**, 1730–1735.

15 B. Boddenberg, *Appl. Catal.*, 1988, **42**, 187–188.

16 Iler, in *The Chemistry of Silica: Solubility, Polymerization, Colloid and Surface Properties and Biochemistry of Silica*, John Wiley & Sons, Ltd., New York, 1979, pp. 3–104.

17 K. B. Krauskopf, *Geochim. Cosmochim. Acta*, 1956, **10**, 1–26.

18 N. N. Greenwood and A. Earnshaw, *Chemistry of the Elements*, Elsevier, Amsterdam, 2nd edn., 1997.

19 M. Hasanuzzaman, A. Rafferty, M. Sajjia and A.-G. Olabi, in *Reference Module in Materials Science and Materials Engineering*, Elsevier, 2016.

20 I. N. Levine, *Physical Chemistry*, McGraw-Hill, Boston, 5th edn., 2001.

21 S. A. Greenberg, *J. Chem. Educ.*, 1959, 36, 218–219.

22 T. Tarutani, *Anal. Sci.*, 1989, **5**, 245–252.

23 L. M. Jurkić, I. Cepanec, S. K. Pavelić and K. Pavelić, *Nutr. Metab.*, 2013, **10**, 2.

24 R. K. Harris, C. T. G. Knight and D. N. Smith, *J. Chem. Soc. Chem. Commun.*, 1980, 726.

25 G. B. Alexander, *J. Am. Chem. Soc.*, 1954, **76**, 2094–2096.

26 K. D. Demadis and A. Stathoulopoulou, *Ind. Eng. Chem. Res.*, 2006, **45**, 4436–4440.

27 S. A. Greenberg and D. Sinclair, *J. Phys. Chem.*, 1955, **59**, 435–440.

28 D. J. Belton, O. Deschaume and C. C. Perry, *FEBS J.*, 2012, **279**, 1710–1720.

29 P. Taylor, *Adv. Colloid Interface Sci.*, 1998, **75**, 107–163.

30 P. W. Voorhees, *J. Stat. Phys.*, 1985, **38**, 231–252.

31 K. D. Demadis, A. Ketsetzi, K. Pachis and V. M. Ramos, *Biomacromolecules*, 2008, **9**, 3288–3293.

32 K. D. Demadis and E. Mavredaki, *Environ. Chem. Lett.*, 2005, **3**, 127–131.

33 E. Neofotistou and K. D. Demadis, *Colloids Surfaces A Physicochem. Eng. Asp.*, 2004, **242**, 213–216.

34 M. Preari, K. Spinde, J. Lazic, E. Brunner and K. D. Demadis, *J. Am. Chem. Soc.*, 2014, **136**, 4236–4244.

35 E. Mavredaki, E. Neofotistou and K. D. Demadis, *Ind. Eng. Chem. Res.*, 2005, **44**, 7019–7026.

36 K. D. Demadis, A. Tsistraki, A. Popa, G. Ilia and A. Visa, *RSC Adv.*, 2012, **2**, 631–641.

37 V. V. Annenkov, E. N. Danilovtseva, Y. V. Likhoshway, S. V. Patwardhan and C. C. Perry, *J. Mater. Chem.*, 2008, **18**, 553–559.

38 H. M. Laane, *Plants*, 2018, **7**, 45.

39 A. I. Vogel, *Vogel's textbook of quantitative chemical analysis*, Wiley, New York, 5th edn., 1989.

40 M. Greger, T. Landberg and M. Vaculík, *Plants*, 2018, **7**, 41.

41 P. Li, Y. Du, L. Huang, N. Mitter and Z. P. Xu, *RSC Adv.*, 2016, **6**, 69465–69478.

42 J. W. Robinson, *Anal. Chem.*, 1960, **32**, 17A-29A.

43 J. Sucharová and I. Suchara, *Anal. Chim. Acta*, 2006, **576**, 163–176.

44 S. Hauptkorn, J. Pavel and H. Seltner, *Anal. Bioanal. Chem.*, 2001, **370**, 246–250.

45 F. Guntzer, C. Keller and J. D. Meunier, *New Phytol.*, 2010, **188**, 902–906.

46 A. A. Ammann, *J. Mass Spectrom.*, 2007, **42**, 419–427.

47 S. H. J. M. Van Den Boorn, P. Z. Vroon, C. C. Van Belle, B. Van Der Wagt, J. Schwieters and M. J. Van Bergen, *J. Anal. At. Spectrom.*, 2006, **21**, 734–742.

48 J. Keeler, *Understanding NMR Spectroscopy*, Wiley-VCH, Chichester, 2nd edn., 2010.

49 K. M. Itoh, J. Kato, M. Uemura, A. K. Kaliteevskii, O. N. Godisov, G. G. Devyatych, A. D. Bulanov, A. V. Gusev, I. D. Kovalev, P. G. Sennikov, H. J. Pohl, N. V. Abrosimov and H. Riemann, *Japanese J. Appl. Physics, Part 1 Regul. Pap. Short Notes Rev. Pap.*, 2003, **42**, 6248–6251.

50 S. D. Kinrade, A. M. E. Gillson and C. T. G. Knight, *J. Chem. Soc. Dalt. Trans.*, 2002, **3**, 307–309.

51 C. T. G. Knight, R. J. Kirkpatrick and E. Oldfield, *J. Magn. Reson.*, 1988, **78**, 31–40.

52 M. Mägi, E. Lippmaa, A. Samoson, G. Engelhardt and A. R. Grimmer, *J. Phys. Chem.*,

1984, **88**, 1518–1522.

53 E. Lippmaa, M. Magi, A. Samoson, G. Engelhard and A. R. Grimmer, *J. Am. Chem. Soc.*, 1980, **102**, 4889–4893.

54 J. L. Bass and G. L. Turner, *J. Phys. Chem. B*, 1997, **101**, 10638–10644.

55 H. C. Marsmann, in *Encyclopedia of Magnetic Resonance*, John Wiley & Sons, Ltd, Chichester, UK, 2011.

56 K. Spinde, K. Pachis, I. Antonakaki, S. Paasch, E. Brunner and K. D. Demadis, *Chem. Mater.*, 2011, **23**, 4676–4687.

57 H. Guenter, *NMR Spectroscopy: Basic Principles, Concepts and Applications in Chemistry, 3rd Edition*, Wiley-VCH Verlag GmbH & Co. KGaA, 2013.

58 R. K. Harris and C. T. G. Knight, *J. Chem. Soc. Faraday Trans. 2 Mol. Chem. Phys.*, 1983, **79**, 1525–1538.

59 R. K. Harris and C. T. G. Knight, *J. Chem. Soc. Faraday Trans. 2 Mol. Chem. Phys.*, 1983, **79**, 1539–1561.

60 B. C. Smith, *Fundamentals of Fourier transform infrared spectroscopy*, CRC Press, Boca Raton, 2nd edn., 2011.

61 H. Elimelech and D. Avnir, *Chem. Mater.*, 2008, **20**, 2224–2227.

62 D. Skoog, D. West and J. Holler, *Fundamentals of Analytical Chemistry*, Brooks-Cole, New York, 9E edn., 2013.

63 H. W. Knudson, C. Juday and V. W. Meloche, *Ind. Eng. Chem. - Anal. Ed.*, 1940, **12**, 270–273.

64 V. W. Truesdale, P. J. Smith and C. J. Smith, *Analyst*, 1979, **104**, 897–918.

65 A. W. Morris and J. P. Riley, *Anal. Chim. Acta*, 1963, **29**, 272–279.

66 H. Yang, C. Li, C. Wei, M. Li, X. Li, Z. Deng and G. Fan, *Anal. Methods*, 2015, **7**, 5462–

5467.

67 P. Wobrauschek, *X-Ray Spectrom.*, 2007, **36**, 289–300.

68 G. Li and S. Fan, *J. Geochemical Explor.*, 1995, **55**, 75–80.

69 S. Reidinger, M. H. Ramsey and S. E. Hartley, *New Phytol.*, 2012, **195**, 699–706.

70 F. Chainet, C.-P. Lienemann, M. Courtiade, J. Ponthus and O. F. Xavier Donard, *J. Anal. At. Spectrom.*, 2011, **26**, 30–51.

71 L. H. P. Jones and K. A. Handreck, in *Advances in Agronomy*, 1967, vol. 19, pp. 107–149.

72 E. Trembath-Reichert, J. P. Wilson, S. E. McGlynn and W. W. Fischer, *Proc. Natl. Acad. Sci. U. S. A.*, 2015, **112**, 5449–5454.

73 P. J. Tréguer and C. L. De La Rocha, *Ann. Rev. Mar. Sci.*, 2013, **5**, 477–501.

74 E. Struyf, A. Smis, S. van Damme, P. Meire and D. J. Conley, *Silicon*, 2009, **1**, 207–213.

75 F. A. Street-Perrott and P. A. Barker, *Earth Surf. Process. Landforms*, 2008, **33**, 1436–1457.

76 P. C. Bennett, J. R. Rogers, W. J. Choi and F. K. Hiebert, *Geomicrobiol. J.*, 2001, **18**, 3–19.

77 R. D. Schuiling, S. A. Wilson and L. M. Power, *Proc. Natl. Acad. Sci.*, 2011, **108**, E41–E41.

78 P. V. Brady and S. A. Carroll, *Geochim. Cosmochim. Acta*, 1994, **58**, 1853–1856.

79 A. F. White and H. L. Buss, in *Treatise on Geochemistry: Second Edition*, 2013, vol. 7, pp. 115–155.

80 J. Gaillardet, B. Dupré, P. Louvat and C. J. Allègre, *Chem. Geol.*, 1999, **159**, 3–30.

81 K. Matsumoto, J. L. Sarmiento and M. A. Brzezinski, *Global Biogeochem. Cycles*, 2002, **16**, 5-1-5–23.

82 C. C. Perry, in *Progress in molecular and subcellular biology*, Springer Berlin Heidelberg, Berlin, Heidelberg, 2009, vol. 47, pp. 295–313.

83 G. Sarthou, K. R. Timmermans, S. Blain and P. Tréguer, *J. Sea Res.*, 2005, **53**, 25–42.

84 P. Curnow, L. Senior, M. J. Knight, K. Thamatrakoln, M. Hildebrand and P. J. Booth, *Biochemistry*, 2012, **51**, 3776–3785.

85 K. Thamatrakoln and M. Hildebrand, *Plant Physiol.*, 2008, **146**, 1397–1407.

86 E. G. Vrieling, W. W. C. Gieskes and T. P. M. Beelen, *J. Phycol.*, 1999, **35**, 548–559.

87 A. Chiovitti, R. E. Harper, A. Willis, A. Bacic, P. Mulvaney and R. Wetherbee, *J. Phycol.*, 2005, **41**, 1154–1161.

88 M. Sumper and E. Brunner, *ChemBioChem*, 2008, **9**, 1187–1194.

89 S. Wenzl, R. Hett, P. Richthammer and M. Sumper, *Angew. Chemie Int. Ed.*, 2008, **47**, 1729–1732.

90 P. Richthammer, M. Börmel, E. Brunner and K. H. Van Pée, *ChemBioChem*, 2011, **12**, 1362–1366.

91 V. V. Annenkov, T. N. Basharina, E. N. Danilovtseva and M. A. Grachev, *Protoplasma*, 2013, **250**, 1147–1155.

92 W. E. G. Müller, M. Rothenberger, A. Boreiko, W. Tremel, A. Reiber and H. C. Schröder, *Cell Tissue Res.*, 2005, **321**, 285–297.

93 C. Gröger, M. Sumper and E. Brunner, *J. Struct. Biol.*, 2008, **161**, 55–63.

94 E. Brunner, P. Richthammer, H. Ehrlich, S. Paasch, P. Simon, S. Ueberlein and K. H. Van Pée, *Angew. Chemie - Int. Ed.*, 2009, **48**, 9724–9727.

95 B. Tesson, S. Masse, G. Laurent, J. Maquet, J. Livage, V. Martin-Jézéquel and T. Coradin, *Anal. Bioanal. Chem.*, 2008, **390**, 1889–1898.

96 F. Azam, *Planta*, 1974, **121**, 205–212.

97 H. M. Laane, *Silicon*, 2017, **9**, 803–807.

98 N. B. Prakash, N. Chandrashekar, C. Mahendra, S. U. Patil, G. N. Thippeshappa and H. M. Laane, *J. Plant Nutr.*, 2011, **34**, 1883–1893.

99 A. Nikpay and H. M. Laane, in *Proceedings of the 7th International Conference on Silicon in Agriculture*, Bengaluru, India, 2017, p. 95.

100 G. C. Satisha and A. K. Saxena, in *Proceedings of the 7th International Conference on Silicon in Agriculture*, Bengaluru, India, 2017.

101 FAO and World Health Organization, *World Heal. Organ.*, 1998, 1–20.

102 P. J. White and P. H. Brown, *Ann. Bot.*, 2010, **105**, 1073–1080.

103 S. R. Noack, T. M. McBeath and M. J. McLaughlin, *Crop Pasture Sci.*, 2010, **61**, 659.

104 R. D. Macnicol and P. H. T. Beckett, *Plant Soil*, 1985, **85**, 107–129.

105 P. H. Brown, R. M. Welch and E. E. Cary, *Plant Physiol.*, 1987, **85**, 801–803.

106 H. Marschner, *Mineral Nutrition of Higher Plants*, Elsevier, London, 2nd edn., 1995.

107 K. Mengel, E. A. Kirby, H. Kosegarten and T. Appel, *Principales of Plants Nutrition*, Springer-Science+Business Media, 2001.

108 P. J. White, *J. Exp. Bot.*, 2004, **55**, 1927–1937.

109 E. A. Pilon-Smits, C. F. Quinn, W. Tapken, M. Malagoli and M. Schiavon, *Curr. Opin. Plant Biol.*, 2009, **12**, 267–274.

110 M. J. Hodson, P. J. White, A. Mead and M. R. Broadley, *Ann. Bot.*, 2005, **96**, 1027–1046.

111 K. E. Richmond and M. Sussman, *Curr. Opin. Plant Biol.*, 2003, **6**, 268–272.

112 Y. Liang, in *Plant Membrane and Vacuolar Transporters*, 2008, pp. 205–212.

113 N. Mitani and F. M. Jian, *J. Exp. Bot.*, 2005, **56**, 1255–1261.

114 H. A. Currie and C. C. Perry, *Ann. Bot.*, 2007, **100**, 1383–1389.

115 M. H. Guével, J. G. Menzies and R. R. Bélanger, *Eur. J. Plant Pathol.*, 2007, **119**, 429–436.

116 D. Sun, H. I. Hussain, Z. Yi, R. Siegele, T. Cresswell, L. Kong and D. M. Cahill, *Plant Cell Rep.*, 2014, **33**, 1389–1402.

117 M. Z. Islam, M. A. Mele, K.-Y. Choi and H.-M. Kang, *Zemdirbyste-Agriculture*, 2018, **105**, 159–164.

118 US7915198 B2, 2011.

119 A. H. Hanafy Ahmed, E. M. Harb, M. A. Higazy and S. H. Morgan, *Int. J. Agric. Res.*, 2008, **3**, 1–26.

120 K. Warington, *Ann. Bot.*, 1923, **os**-**37**, 629–672.

121 I. A. Jehangir, S. H. Wani, M. Anwar Bhat, A. Hussain, W. Raja and A. Haribhushan, *Int. J. Curr. Microbiol. Appl. Sci.*, 2017, **6**, 5347–5353.

122 J. J. Camacho-cristóbal, J. Rexach and A. González-Fontes, *J. Integr. Plant Biol.*, 2008, 50, 1247–1255.

123 A. W. Laubengayer, D. T. Hurd, A. E. Newkirk and J. L. Hoard, *J. Am. Chem. Soc.*, 1943, **65**, 1924–1931.

124 A. W. Adamson, *Inorg. Chem.*, 1963, **2**, 665–665.

125 K. Nedunchezhian, *J. Clin. Diagnostic Res.*, 2016, **10**, ZE01–ZE04.

126 J. A. Coderre and G. M. Morris, *Radiat. Res.*, 1999, **151**, 1.

127 M. F. Hawthorne, *Angew. Chemie Int. Ed. English*, 1993, **32**, 950–984.

128 R. F. Barth, Mg. H Vicente, O. K. Harling, W. Kiger, K. J. Riley, P. J. Binns, F. M. Wagner, M. Suzuki, T. Aihara, I. Kato and S. Kawabata, *Radiat. Oncol.*, 2012, **7**, 146.

129 A. H. Soloway, W. Tjarks, B. A. Barnum, F.-G. Rong, R. F. Barth, I. M. Codogni and J. G. Wilson, *Chem. Rev.*, 1998, **98**, 1515–1562.

130 R. F. Barth, *Clin. Cancer Res.*, 2005, **11**, 3987–4002.

131 M. A. Beckett, *Coord. Chem. Rev.*, 2016, **323**, 2–14.

132 P. T. Corbett, J. Leclaire, L. Vial, K. R. West, J.-L. L. Wietor, J. K. M. M. Sanders and S. Otto, *Chem. Rev.*, 2006, **106**, 3652–3711.

133 J. L. Andersen, E. M. Eyring and M. P. Whittaker, *J. Phys. Chem.*, 1964, **68**, 1128–1132.

134 J. Neeru, C. Shaliesh, T. Vaishali, S. Purav and R. Manoherlal, *Silicon*, 2019, **11**, 2407–2411.

135 WO2012035364 A1, 2012.

136 E. Epstein, *Stud. Plant Sci.*, 2001, **8**, 1–15.

137 B. S. Tubana, T. Babu and L. E. Datnoff, *Soil Sci.*, 2016, **181**, 393–411.

138 D. J. Conley and C. L. Schelske, 2002, pp. 281–293.

139 L. E. Datnoff, C. W. Deren and G. H. Snyder, *Crop Prot.*, 1997, **16**, 525–531.

140 W. D. Keller, *Sci. Mon.*, 1948, **66**, 122–130.

141 B. Hogan, F. McDermott and O. Schmidt, *J. Soils Sediments*, 2019, **19**, 1272–1285.

142 B. Hogan, F. McDermott and O. Schmidt, *Scand. J. For. Res.*, 2018, **33**, 550–559.

143 E. K. Dann and S. Muir, *Australas. Plant Pathol.*, 2002, **31**, 9–13.

144 R. Crooks and P. Prentice, *Silicon*, 2017, **9**, 301–304.

145 S. L. Lim, T. Y. Wu, E. Y. S. Sim, P. N. Lim and C. Clarke, *Ecol. Eng.*, 2012, **41**, 60–64.

146 N. Escobar, J. Espejo and L. Rodríguez, *WIT Trans. Ecol. Environ.*, 2014, **181**, 409–420.

147 V. Martin-Jézéquel, M. Hildebrand and M. A. Brzezinski, *J. Phycol.*, 2000, **36**, 821–840.

148 M. Hildebrand, in *Biomineralization*, Wiley-VCH Verlag GmbH & Co. KGaA, Weinheim, FRG, 2005, pp. 159–176.

149 B. S. Tubaña and J. R. Heckman, in *Silicon and Plant Diseases*, Springer International Publishing, Cham, 2015, pp. 7–51.

150 S. M. Bokhtiar, H.-R. Huang, Y.-R. Li and V. A. Dalvi, *J. Plant Nutr.*, 2012, **35**, 1255–1275.

151 V. D. Meena, M. L. Dotaniya, V. Coumar, S. Rajendiran, Ajay, S. Kundu and A. Subba Rao, *Proc. Natl. Acad. Sci. India Sect. B - Biol. Sci.*, 2014, 84, 505–518.

152 F. A. Rodrigues, H. S. S. Duarte, G. P. Domiciano, C. A. Souza, G. H. Korndrfer and L. Zambolim, in *Australasian Plant Pathology*, 2009, vol. 38, pp. 366–372.

153 S. Y. Wang and G. J. Galletta, *J. Plant Nutr.*, 1998, **21**, 157–167.

154 G. B. Buck, G. H. Korndörfer, A. Nolla and L. Coelho, *J. Plant Nutr.*, 2008, **31**, 231–237.

155 L. J. Dallagnol, F. A. Rodrigues, S. F. Pascholati, A. A. Fortunato and L. E. A. Camargo, *Plant Pathol.*, 2015, **64**, 1085–1093.

156 J. Menzies, P. Bowen, D. Ehret and A. D. M. Glass, *J. Am. Soc. Hortic. Sci.*, 2019, **117**, 902–905.

157 F. Á. Rodrigues, H. S. S. Duarte, D. C. Rezende, J. A. Wordell Filho, G. H. Korndö rfer and L. Zambolim, *J. Plant Nutr.*, 2010, **33**, 2082–2093.

158 F. Abed-Ashtiani, J. Bin Kadir, A. Bin Selamat, A. H. B. M. Hanif and A. Nasehi, *Plant Pathol. J.*, 2012, **28**, 164–171.

159 M. Garbuzov, S. Reidinger and S. E. Hartley, *Ann. Bot.*, 2011, **108**, 1355–1363.

160 A. Yassen, E. Abdallah, M. Gaballah and S. Zaghloul, *Int. J. Agric. Res.*, 2017, **12**, 130–135.

161 P. Overton, E. Danilovtseva, E. Karjalainen, M. Karesoja, V. Annenkov, H. Tenhu and V. Aseyev, *Polymers (Basel).*, 2016, **8**, 96.

162 M. Janmohammadi, T. Amanzadeh, N. Sabaghnia and V. Ion, *Bot. Lith.*, 2016, **22**, 53–64.

163 R. Suriyaprabha, G. Karunakaran, R. Yuvakkumar, V. Rajendran and N. Kannan, *Synth.*

React. Inorganic, Met. Nano-Metal Chem., 2014, **44**, 1128–1131.

164 J. Schaller, C. Brackhage, S. Paasch, E. Brunner, E. Bäucker and E. G. Dudel, *Sci. Total Environ.*, 2013, **442**, 6–9.

165 R. Suriyaprabha, G. Karunakaran, R. Yuvakkumar, V. Rajendran and N. Kannan, *Curr. Nanosci.*, 2012, **8**, 902–908.

166 D. L. Slomberg and M. H. Schoenfisch, *Environ. Sci. Technol.*, 2012, **46**, 10247–10254.

167 US20060165815A1, 2003.

168 R. P. Soratto, C. A. C. Crusciol, G. S. A. Castro, C. H. M. da Costa and J. F. Neto, *Rev. Bras. Cienc. do Solo*, 2012, **36**, 1538–1544.

169 C. Pilon, R. P. Soratto and L. A. Moreno, *Crop Sci.*, 2013, **53**, 1605–1614.

170 G. A. Icopini, S. L. Brantley and P. J. Heaney, *Geochim. Cosmochim. Acta*, 2005, **69**, 293–303.

171 S. A. Wolff, I. Karoliussen, J. Rohloff and R. Strimbeck, *J. Food, Agric. Environ.*, 2012, **10**, 355–359.

172 J. F. Ma, *Soil Sci. Plant Nutr.*, 2004, **50**, 11–18.

173 M. Luyckx, J.-F. Hausman, S. Lutts and G. Guerriero, *Front. Plant Sci.*, 2017, **8**, 411.

174 S. Wang, F. Wang and S. Gao, *Environ. Sci. Pollut. Res.*, 2015, **22**, 2837–2845.

175 M. Igarashi, T. Matsumoto, F. Yagihashi, H. Yamashita, T. Ohhara, T. Hanashima, A. Nakao, T. Moyoshi, K. Sato and S. Shimada, *Nat. Commun.*, 2017, **8**, 140.

176 T. Kleiber, M. Calomme and K. Borowiak, *Plant Physiol. Biochem.*, 2015, **96**, 180–188.

177 K. Maghsoudi, Y. Emam and M. Ashraf, *Turk. J. Botany*, 2015, **39**, 625–634.

178 C. Côté-Beaulieu, F. Chain, J. G. Menzies, S. D. Kinrade and R. R. Bélanger, *Environ. Exp. Bot.*, 2009, **65**, 155–161.

179 A. Spinthaki, C. Zerfaß, H. Paulsen, S. Hobe and K. D. Demadis, *ChemistrySelect*, 2017,

2, 6–17.

180 R. R. Wickett, E. Kossmann, A. Barel, N. Demeester, P. Clarys, D. Vanden Berghe and M. Calomme, *Arch. Dermatol. Res.*, 2007, **299**, 499–505.

181 L. N. Niu, K. Jiao, Y. P. Qi, C. K. Y. Yiu, H. Ryou, D. D. Arola, J. H. Chen, L. Breschi, D. H. Pashley and F. R. Tay, *Angew. Chemie - Int. Ed.*, 2011, **50**, 11688–11691.

182 K. D. Demadis, K. Pachis, A. Ketsetzi and A. Stathoulopoulou, *Adv. Colloid Interface Sci.*, 2009, **151**, 33–48.

183 K. D. Demadis, M. Preari and I. Antonakaki, *Pure Appl. Chem.*, 2014, **86**, 1663–1674.

184 M. Calomme, P. Geusens, N. Demeester, G. J. Behets, P. D. Haese, J. B. Sindambiwe, V. Van Hoof and D. Vanden Berghe, *Calcif. Tissue Int.*, 2006, **78**, 227–232.

185 F. Aguilar, *EFSA J.*, 2009, **7**, 948.

186 C. C. Bland, Bangor University, 2007.

187 B. M. Stiefwater-Thomas, Bangor University, 2005.

188 R. Burger and P. Bigler, *J. Magn. Reson.*, 1998, 135, 529–534.

189 A. B. Tourky and D. H. Bangham, *Nature*, 1936, **138**, 587–588.

190 A. Ahmad, M. Afzal, A. U. H. Ahmad and M. Tahir, *Cercet. Agron. Mold.*, 2013, **46**, 21–28.

191 L. A. Zanão Júnior, R. L. F. Fontes, J. C. L. Neves, G. H. Korndörfer and V. T. de Ávila, *Rev. Bras. Ciência do Solo*, 2010, **34**, 1629–1639.

192 H. K. Bhavya, in *Proc. 5th Int. Conf. on Silicon in Agriculture*, Beijing, 2011, pp. 7–8.

193 O. H. Realpe and H. M. Laane, in *Proceedings of the 4th International Conference on Silicon in Argriculture*, Natal, South Africa, 2008, p. 88.

194 R. K. . Kedarnath, N. . Prakash and R. Achari, in *Proceedings of the 7th International Conference on Silicon in Agriculture*, Bengaluru, India, 2017, p. 92.

195 T. S. Sandhya, N. B. Prakash, A. Nagaraja and Y. A. Nanja Reddy, in *Proceedings of the 5th International Conference on Silicon in Agriculture*, Beijing, China, 2011, pp. 183–184.

196 B. Ahmad, *J. Integr. Agric.*, 2014, **13**, 1889–1899.

197 D. Birkhaeuser, R. E. Evenson and G. Feder, *Econ. Dev. Cult. Change*, 1991, **39**, 607–650.

198 H. Valin, R. D. Sands, D. van der Mensbrugghe, G. C. Nelson, H. Ahammad, E. Blanc, B. Bodirsky, S. Fujimori, T. Hasegawa, P. Havlik, E. Heyhoe, P. Kyle, D. Mason-D'Croz, S. Paltsev, S. Rolinski, A. Tabeau, H. van Meijl, M. von Lampe and D. Willenbockel, *Agric. Econ. (United Kingdom)*, 2014, **45**, 51–67.

199 A. Dai, *Wiley Interdiscip. Rev. Clim. Chang.*, 2011, **2**, 45–65.

200 A. Dai, *Nat. Clim. Chang.*, 2013, **3**, 52–58.

201 K. E. Trenberth, A. Dai, G. van der Schrier, P. D. Jones, J. Barichivich, K. R. Briffa and J. Sheffield, *Nat. Clim. Chang.*, 2014, **4**, 17–22.

202 K. E. Trenberth, *Clim. Res.*, 2011, **47**, 123–138.

203 R. N. Strange and P. R. Scott, *Annu. Rev. Phytopathol.*, 2005, **43**, 83–116.

204 K. Parris, *Int. J. Water Resour. Dev.*, 2011, **27**, 33–52.

205 N. Donley, *Environ. Heal. A Glob. Access Sci. Source*, 2019, **18**, 44.

206 V. Pelaez, L. R. da Silva and E. B. Araújo, *Sci. Public Policy*, 2013, **40**, 644–656.

207 F. Snyder and L. Ni, *Eur. J. Risk Regul.*, 2017, **8**, 469–505.

208 P. Treguer, D. M. Nelson, A. J. Van Bennekom, D. J. DeMaster, A. Leynaert and B. Queguiner, *Science*, 1995, **268**, 375–379.

209 M. Gocke, W. Liang, M. Sommer and Y. Kuzyakov, *J. Plant Nutr. Soil Sci.*, 2013, **176**, 551–560.

210 P. Zuccarini, *Biol. Plant.*, 2008, **52**, 157–160.

211 A. L. Tuna, C. Kaya, D. Higgs, B. Murillo-Amador, S. Aydemir and A. R. Girgin, *Environ. Exp. Bot.*, 2008, **62**, 10–16.

212 Z. Stoyanova, E. Zozikova, C. Poschenrieder, J. Barcelo and S. Doncheva, *Acta Biol. Hung.*, 2008, **59**, 479–487.

213 H. J. Gong, K. M. Chen, G. C. Chen, S. M. Wang and C. L. Zhang, *J. Plant Nutr.*, 2003, **26**, 1055–1063.

214 C. C. Ma, Y. B. Gao, T. R. Xin, C. C. Ma and Q. F. Li, *Soil Sci. Plant Nutr.*, 2004, **50**, 623–632.

215 H. Gong, X. Zhu, K. Chen, S. Wang and C. Zhang, *Plant Sci.*, 2005, **169**, 313–321.

216 E. Sacała, *J. Elem.*, 2012, **14**, 619–630.

217 D. Savvas and G. Ntatsi, *Sci. Hortic. (Amsterdam).*, 2015, **196**, 66–81.

218 J. F. Ma and N. Yamaji, *Trends Plant Sci.*, 2006, **11**, 392–397.

219 Y. C. Liang, W. C. Sun, J. Si and V. Romheld, *Plant Pathol.*, 2005, **54**, 678–685.

220 P. Bowen, J. Menzies, D. Ehret, L. Samuels and A. D. M. Glass, *J. Am. Soc. Hortic. Sci.*, 1992, **117**, 906–912.

221 B. S. Rodgers-Gray and M. W. Shaw, *Plant Pathol.*, 2004, **53**, 733–740.

222 Y. Liang, M. Nikolic, R. Bélanger, H. Gong, A. Song, Y. Liang, M. Nikolic, R. Bélanger, H. Gong and A. Song, in *Silicon in Agriculture*, Springer Netherlands, Dordrecht, 2015, pp. 69–82.

223 D. C. Rezende, F. Á. Rodrigues, V. Carŕ-Missio, D. A. Schurt, I. K. Kawamura and G. H. Korndrfer, *Australas. Plant Pathol.*, 2009, **38**, 67–73.

224 G. Lu, W. Jian, J. Zhang, Y. Zhou and J. Cao, *HortScience*, 2008, **43**, 811–817.

225 V. F. da Silva, J. C. Moraes and B. A. Melo, *Ciência e Agrotecnologia*, 2010, **34**, 1465–

1469.

226 M. J. Van Oosten, O. Pepe, S. De Pascale, S. Silletti and A. Maggio, *Chem. Biol. Technol. Agric.*, 2017, **4**, 5.

227 P. Calvo, L. Nelson and J. W. Kloepper, *Plant Soil*, 2014, **383**, 3–41.

228 L. P. Canellas, F. L. Olivares, N. O. Aguiar, D. L. Jones, A. Nebbioso, P. Mazzei and A. Piccolo, *Sci. Hortic. (Amsterdam).*, 2015, **196**, 15–27.

229 H. Kaur and M. Greger, *Plants*, 2019, **8**, 81.

230 M. A. Beckett, B. I. Meena, T. A. Rixon, S. J. Coles and P. N. Horton, *Molecules*, 2019, **25**, 53.

231 M. A. Beckett, S. J. Coles, P. N. Horton and T. A. Rixon, *Phosphorus. Sulfur. Silicon Relat. Elem.*, 2019, **194**, 952–955.

232 D. Schubert, in *Kirk-Othmer Encyclopedia of Chemical Technology*, John Wiley & Sons, Inc., Hoboken, NJ, USA, 2011, pp. 1–68.

233 Q. Wang, J. P. Undrell, Y. Gao, G. Cai, J. C. Buffet, C. A. Wilkie and D. O'Hare, *Macromolecules*, 2013, **46**, 6145–6150.

234 J. Liang, Y. G. Wang, Y. X. Wang, F. H. Liao and J. H. Lin, *J. Solid State Chem.*, 2013, **200**, 99–104.

235 Q. Meng, G. M. Wang, H. He, B. F. Yang and G. Y. Yang, *J. Clust. Sci.*, 2014, **25**, 1295–1305.

236 W. Luo, Y. Wang, T. Wen, H. Zhang, X. Lin, Y. Wang, F. Liao and J. Lin, *J. Mol. Struct.*, 2013, **1048**, 1–5.

237 C.-Y. Pan, L.-J. Zhong, J. Lu, D.-G. Li, F.-H. Zhao and H.-M. Yang, *Zeitschrift für Anorg. und Allg. Chemie*, 2014, **640**, 352–356.

238 P. Becker, *Adv. Mater.*, 1998, **10**, 979–992.

239 L. Wei, B. F. Yang, H. He and G. Y. Yang, *J. Clust. Sci.*, 2014, **25**, 617–626.

240 D. M. Schubert, F. Alam, M. Z. Visi and C. B. Knobler, *Chem. Mater.*, 2003, **15**, 866–871.

241 M. A. Altahan, M. A. Beckett, S. J. Coles and P. N. Horton, *Phosphorus, Sulfur Silicon Relat. Elem.*, 2016, **191**, 572–575.

242 D. Lin, X. You and L. Zhu, *Chinese J. Chem.*, 2011, **29**, 463–467.

243 M. A. Altahan, M. A. Beckett, S. J. Coles and P. N. Horton, *Inorg. Chem. Commun.*, 2015, **59**, 95–98.

244 M. A. Altahan, M. A. Beckett, S. J. Coles and P. N. Horton, *J. Clust. Sci.*, 2019, **30**, 599–605.

245 A. Choudhury, S. Neeraj, S. Natarajan and C. N. R. Rao, *J. Chem. Soc. Dalt. Trans.*, 2002, 1535–1538.

246 H. Taube, *Chem. Rev.*, 1952, **50**, 69–126.

247 M. A. Beckett, S. J. Coles, P. N. Horton and C. L. Jones, *Eur. J. Inorg. Chem.*, 2017, **2017**, 4510–4518.

248 M. Z. Visi, C. B. Knobler, J. J. Owen, M. I. Khan and D. M. Schubert, *Cryst. Growth Des.*, 2006, **6**, 538–545.

249 C. G. Salentine, *Inorg. Chem.*, 1983, **22**, 3920–3924.

250 C. L. Christ and J. R. Clark, *Phys. Chem. Miner.*, 1977, **2**, 59–87.

251 P. C. Burns, J. D. Grice and F. C. Hawthorne, *Can. Mineral.*, 1995, **33**, 1131–1151.

252 J. D. Grice, P. C. Burns and F. C. Hawthorne, *Can. Mineral.*

253 Q. Li, F. Xue and T. C. W. Mak, *Inorg. Chem.*, 1999, **38**, 4142–4145.

254 M. A. Beckett, P. N. Horton, M. B. Hursthouse and J. L. Timmis, *RSC Adv.*, 2013, **3**, 15185–15191.

255 D. M. Schubert, M. Z. Visi and C. B. Knobler, *Inorg. Chem.*, 2008, **47**, 2017–2023.

256 M. A. Beckett, P. N. Horton, S. J. Coles and D. W. Martin, *Inorg. Chem.*, 2011, **50**, 12215–12218.

257 G. M. Wang, Y. Q. Sun and G. Y. Yang, *J. Solid State Chem.*, 2004, **177**, 4648–4654.

258 M. A. Beckett, P. N. Horton, M. B. Hursthouse, D. A. Knox and J. L. Timmis, *Dalt. Trans.*, 2010, **39**, 3944–3951.

259 M. A. Beckett, P. N. Horton, S. J. Coles, D. A. Kose and A.-M. M. Kreuziger, *Polyhedron*, 2012, **38**, 157–161.

260 M. A. Beckett, S. J. Coles, R. A. Davies, P. N. Horton and C. L. Jones, *Dalt. Trans.*, 2015, **44**, 7032–7040.

261 H. X. Zhang, S. T. Zheng and G. Y. Yang, *Acta Crystallogr. Sect. C Cryst. Struct. Commun.*, 2004, **60**, m241–m243.

262 M. A. Beckett, C. C. Bland, P. N. Horton, M. B. Hursthouse and K. S. Varma, *J. Organomet. Chem.*, 2007, **692**, 2832–2838.

263 D. M. Schubert, C. B. Knobler and M. Z. Visi, *Main Gr. Chem.*, 2012, **11**, 69–88.

264 U. Sizir, D. A. Kose and O. Yurdakul, *Hittite J. Sci. Eng.*, 2015, **2**, 91–96.

265 G. M. Wang, Y. Q. Sun and G. Y. Yang, *J. Solid State Chem.*, 2005, **178**, 729–735.

266 M. A. Beckett, P. N. Horton, M. B. Hursthouse and J. L. Timmis, *Polyhedron*, 2014, **77**, 96–102.

267 R. C. Petersen, M. Finkelstein and S. D. Ross, *J. Am. Chem. Soc.*, 1959, **81**, 3264–3267.

268 G. Huang, R. Pan, H. He, B. F. Yang and G. Y. Yang, *J. Clust. Sci.*, 2015, **26**, 2023–2032.

269 H. X. Yang, W. J. Zhang, X. L. Liu and Z. H. Liu, *Acta Crystallogr. Sect. E Struct. Reports Online*, 2006, **62**, o4877–o4879.

270 M. A. Altahan, M. A. Beckett, S. J. Coles and P. N. Horton, *Inorg. Chem.*, 2015, **54**,

412–414.

271 Z.-H. Liu, L.-Q. Li, W.-J. Zhang, * Zhi-Hong Liu, A. Lian-Qing Li and W.-J. Zhang, *Inorg. Chem.*, 2006, **45**, 1430–2.

272 N. Jemai, M. Rzaigui and S. Akriche, *J. Clust. Sci.*, 2015, **26**, 2051–2064.

273 C. Y. Pan, G. M. Wang, S. T. Zheng and G. Y. Yang, *Zeitschrift fur Anorg. und Allg. Chemie*, 2007, **633**, 336–340.

274 D. M. Schubert, M. Z. Visi, S. Khan and C. B. Knobler, *Inorg. Chem.*, 2008, **47**, 4740–4745.

275 D. M. Schubert, M. Z. Visi and C. B. Knobler, *Inorg. Chem.*, 2000, **39**, 2250–2251.

276 D. M. Schubert, R. A. Smith and M. Z. Visi, *Glas. Technol.*, 2003, **44**, 63–70.

277 G. M. Wang, Y. Q. Sun, S. T. Zheng and G. Y. Yang, *Zeitschrift fur Anorg. und Allg. Chemie*, 2006, **632**, 1586–1590.

278 S. Merlino and F. Sartori, *Science*, 1971, **171**, 377–379.

279 J. E. Anderson, R. S. Bubnova, S. K. Filatov, V. L. Ugolkov and S. N. Britvin, *Glas. Phys. Chem.*, 2009, **35**, 191–198.

280 L. Zheng, J. Zhang and Z. Liu, *Chinese J. Chem.*, 2009, **27**, 494–500.

281 W.-J. Zhang and Z.-H. Liu, *Zeitschrift für Krist. - New Cryst. Struct.*, 2006, **221**, 189–190.

282 A. K. Paul, K. Sachidananda and S. Natarajan, *Cryst. Growth Des.*, 2010, **10**, 456–464.

283 G. M. Wang, C. Y. Pan, S. T. Zheng and G. Y. Yang, *Acta Crystallogr. Sect. E Struct. Reports Online*, 2007, **63**, o1101–o1103.

284 Z. H. Liu, J. J. Zhang and W. J. Zhang, *Inorganica Chim. Acta*, 2006, **359**, 519–524.

285 M. A. Beckett, P. N. Horton, M. B. Hursthouse, J. L. Timmis and K. S. Varma, *Dalt. Trans.*, 2012, **41**, 4396–4403.

286 J. M. Coddington and M. J. Taylor, *J. Coord. Chem.*, 1989, **20**, 27–38.

287 M. Li, J. Chang, Z. Wang and H. Shi, *J. Solid State Chem.*, 2006, **179**, 3265–3269.

288 H. Z. Sommer, H. I. Lipp and L. L. Jackson, *J. Org. Chem.*, 1971, **36**, 824–828.

289 M. C. Etter, *Acc. Chem. Res.*, 1990, **23**, 120–126.

290 A. C. Cope, N. A. LeBel, P. T. Moore and W. R. Moore, *J. Am. Chem. Soc.*, 1961, **83**, 3861–3865.

291 A. W. von Hofmann, *Justus Liebigs Ann. Chem.*, 1851, **78**, 253–286.

292 S. Zhang, H. Yan, M. Zhao and L. Zheng, *J. Colloid Interface Sci.*, 2012, **372**, 52–57.

293 M. J. Saif, J. Anwar, A. Munawar, M. Kashif and M. I. Asghar, *Arkivoc*, 2010, **2010**, 133.

294 J. Z. Vlahakis, S. Mitu, G. Roman, E. P. Rodriguez, I. E. Crandall and W. A. Szarek, *Bioorganic Med. Chem.*, 2011, **19**, 6525–6542.

295 C. L. Jones, M. A. Beckett, S. J. Coles, R. A. Davies and P. N. Horton, *Phosphorus, Sulfur Silicon Relat. Elem.*, 2016, **191**, 628–630.